(2)

PL-TR-93-2181

TARGET GLOW ANALYSIS PROGRAM FOR AIR FORCE MAUI OPTICAL STATION

A. L. Broadfoot

University of Arizona
Lunar and Planetary Laboratory
Tucson, Arizona 85721

15 June 1993

Final Report
August 1989-November 1992

Approved for public release; distribution unlimited

PHILLIPS LABORATORY
AIR FORCE MATERIEL COMMAND
HANSCOM AFB, MA 01731-3010

This technical report has been reviewed and is approved for publication.

DAVID J. KNECHT
Contract Manager

CHARLES P. PIKE, Chief
Spacecraft Interactions Branch

This report has been reviewed by the ESC Public Affairs Office (PA) and is releasable to the National Technical Information Service (NTIS).

Qualified requesters may obtain additional copies from the Defense Technical Information Center. All others should apply to the National Technical Information Service.

If your address has changed, or if you wish to be removed from the mailing list, or if the addressee is no longer employed by your organization, please notify PL/TSI, Hanscom AFB, MA 01731-3010. This will assist us in maintaining a current mailing list.

Do not return copies of this report unless contractual obligations or notices on a specific document requires that it be returned.

REPORT DOCUMENTATION PAGE

Form Approved
OMB No. 0704-0188

1. AGENCY USE ONLY (Leave blank)	2. REPORT DATE	3. REPORT TYPE AND DATES COVERED
	15 Jun 1993	Final (August 1989-November 1992)

4. TITLE AND SUBTITLE
Target Glow Analysis Program for Air Force Maui Optical Station

5. FUNDING NUMBERS
PE 63214C
PR 7601 - TA 30 - WU CB

Contract F19628-89-K-0039

6. AUTHOR(S)
A. L. Broadfoot

7. PERFORMING ORGANIZATION NAME(S) AND ADDRESS(ES)
University of Arizona
Lunar and PLanetary Laboratory
Tucson, Arizona 85721

8. PERFORMING ORGANIZATION REPORT NUMBER

9. SPONSORING/MONITORING AGENCY NAME(S) AND ADDRESS(ES)
Phillips Laboratory
29 Randolph Road
Hanscom AFB, MA 01731-3010

Contract Manager: David J. Knecht/WSSI

10. SPONSORING/MONITORING AGENCY REPORT NUMBER
PL-TR-93-2181

11. SUPPLEMENTARY NOTES

12a. DISTRIBUTION/AVAILABILITY STATEMENT
Approved for public release;
Distribution unlimited

12b. DISTRIBUTION CODE

13. ABSTRACT *(Maximum 200 words)*

The experimental program was directoed toward the Space Systems Environmental Interactions Technology research to observe and analyze the glow surrounding spacecraft using the AMOS ground-based telescope facility. This unique optical facility was used for acquisition and tracking of the Space Shuttle during overflights of the site. The imager/spectrograph which was used for the data acquisition was similar in design and operation to the AIS instrument described in the earlier report.

14. SUBJECT TERMS			15. NUMBER OF PAGES
Spectrometer	Visible	Space flight	80
Ultraviolet	Infrared		16. PRICE CODE

17. SECURITY CLASSIFICATION OF REPORT	18. SECURITY CLASSIFICATION OF THIS PAGE	19. SECURITY CLASSIFICATION OF ABSTRACT	20. LIMITATION OF ABSTRACT
Unclassified	Unclassified	Unclassified	SAR

CONTENTS

AMOS/Shuttle Program

Summary

The AMOS program to date has involved seven expeditions to AMOS. We obtained observations of Shuttle thruster firings during six overflights. A special effort was made to observe the STRYPI rocket flight. All of the observations added to our knowledge, each observation defining questions to be answered at the next opportunity. The experimental techniques were changed and improved to address the new questions. It is noteworthy that this program complements observational programs which observe the thruster firings from the Shuttle, the Shuttle Glow Experiment (GLO).

The first observation, STS-41 (AMOS-06), resulted in a low resolution spectrum of the thruster plume. Strong features were detected in the 3400-Å region and the 6300-Å region with varying intensity of continua across the whole spectral range from 3000 Å to 8000 Å.

The objective for the second opportunity, STS-38, was to improve the spectral resolution on these unknown emissions to determine the source of the emission. We were successful in identifying the 3370-Å emission as NH but the emission at 6300 Å was still in question. The weather was poor and we did not obtain sufficient night sky spectra to verify that the 6300, 6364-Å emission detected during the thruster firing was not due just to the nocturnal emission.

The instrumentation developed for the Shuttle observations was appropriate for the coordinated observational program organized to observe the STRYPI rocket experiment. Although the trajectory was low, we were able to acquire the target with the AMOS 1.6 meter tracking telescope. We recorded the spectrum of the rocket plume which resembled a blackbody emission. The related atmospheric emissions were detected.

The observations during the overflight of STS-43 (AMOS-09) verified the identification of the O [6300, 6364 Å] with the thruster plume. It had become clear also that the emission had a substantial lifetime compared to the NH emission at 3370 Å. We made our first attempt to use the 6-channel monochromatic imager during this experiment. Results were encouraging.

The last set of observations was made in conjunction with the overflight of STS-44 (AMOS-11). For this opportunity, we had spectrographs and imagers on both the 1.6-meter and BDT tracking telescopes. We recorded excellent spectra and images of the thruster plume at 0.5-sec intervals. This was a very successful experiment from our systems point of view and demonstrated the utility of the program and its logical development to a powerful observational capability.

AMOS/Shuttle Program

1. Introduction

The AMOS program was developed to observe the thruster firings of the Shuttle and study the interaction of the thruster gases with the atmosphere. A large plume, related to thruster firings, several kilometers across, had been detected with the intensified video cameras on the AMOS telescopes (Figure 1.0). Since the thruster event was large compared to the field of view of the AMOS telescopes and their associated instrumentation, we proposed to use auxiliary experiments carried by the telescopes to investigate the emission.

This program is a companion to the Shuttle Glow Experiment (GLO) which is flown on the Shuttle to observe this interaction. The rationale is that measurements from inside the Shuttle environment and outside are important. The ground-based program is cost effective in building up our knowledge of this important interaction question.

This report will follow the development of the program. We describe the experiments, the results and the objective for the next opportunity.

2. Shuttle Mission, STS-41 (October 7, 1990)

We prepared experiments for both the Beam Director/Tracker (BDT) and 1.6-meter telescopes. The instrumental problem was to provide a high-throughput spectrographic instrument to allow both spectral and spatial examination of the thruster plume from the Shuttle. The BDT field of view (using coudé path) was narrow but satisfactory for probing the close environment about the Shuttle. The 1.6-meter telescope had a bracket that would support extra equipment. In that case, a Newtonian telescope and spectrograph were prepared.

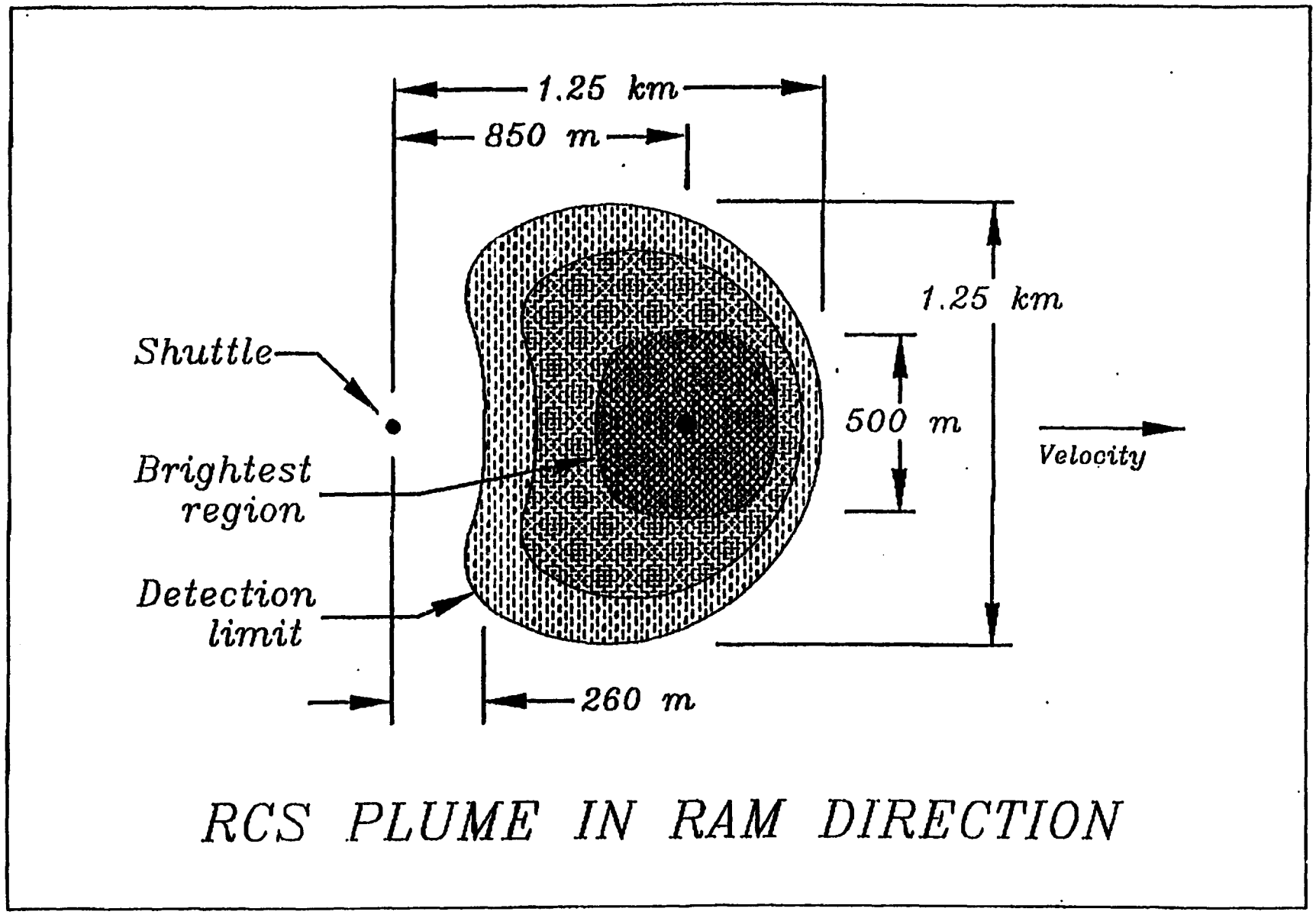
1.25 km
850 m
1.25 km
Shuttle
500 m
Velocity
Brightest region
Detection limit
260 m
RCS PLUME IN RAM DIRECTION

Figure 1

2.1 BDT - Coudé Feed Experiment

The beam down the coudé light path is afocal, having been converted from a 32-inch to a 6-inch diameter beam. The distance from the secondary to the coudé table is 37.4 feet. The field of view of the BDT is limited by vignetting at the coudé end of the light path. Vignetting begins when the 6-inch beam begins to move off the 8-inch adapting telescope on the coudé table. This has to be taken into account in calibration of the spectrograph. The usable beam angular width was about 0.02 radians (0.5°).

We were not able to find an optically fast CCD spectrograph commercially. However, JY (Jobin Yvon) had a grating on the shelf which met our requirements. It has an f-ratio of 1.2, a focal length of 35 mm and dispersed the wavelength range from 3000 Å to 8000 Å across our standard detector. A spectrograph was designed around this grating. Figure 2 was prepared from the AutoCAD mechanical assembly drawing. Figure 3 is a more schematic representation of the important elements. In order that the spectrograph be properly matched to the telescope, the foreoptics were arranged to have an image of the entrance "stop" at the matching lens of Figure 3 where the beam became f/1.2.

A problem associated with the BDT was the fact that the sky rotates in the image plane as the telescope points in different directions. To correct this, the spectrographs were placed on a rotary table which would allow the orientation of the slit to be adjusted to be tangent to the trajectory of the orbiter. The entrance beam was split with an aluminized "roof" prism to feed two spectrographs. This was to give us flexibility in future experiments.

An 8-inch Newtonian telescope was used on the BDT coudé table to collect the coudé beam. The setup is shown in Figure 4. The 6-inch focal beam is collected by the 8-inch paraboloid and brought to a focus in 48 inches resulting in an f/8 system. The beam is turned by a flat mirror and comes to a focus at the roof prism, as shown in the series of drawings, Figures 5 and 6. The spectrograph slits are perpendicular to the paper. The spectrographs have independent fields of view separated by a few minutes of arc.

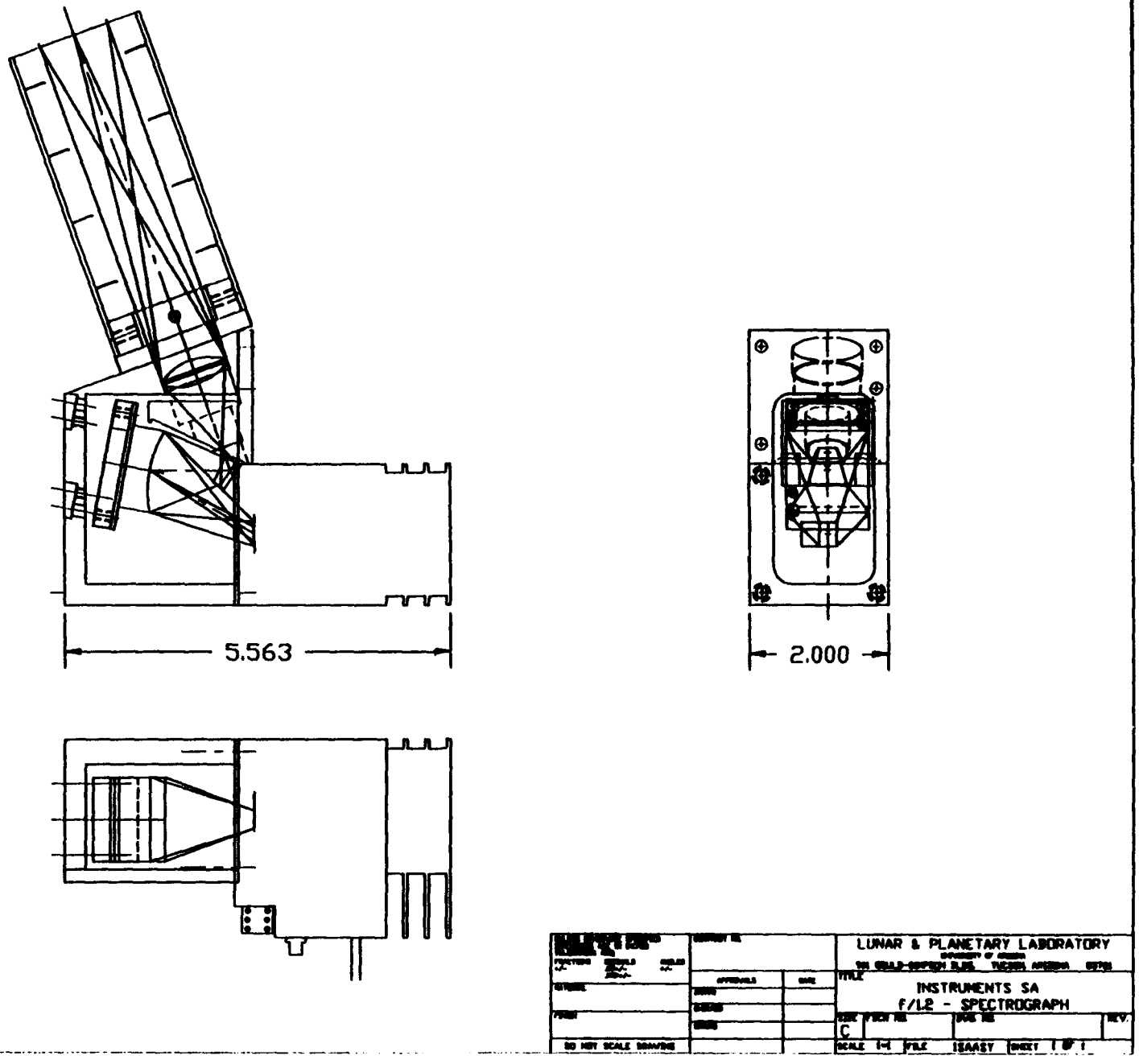
5.563
2.000
LUNAR & PLANETARY LABORATORY
INSTRUMENTS SA
F/L2 - SPECTROGRAPH
C
SCALE 1=1
ISAASY

Figure 2

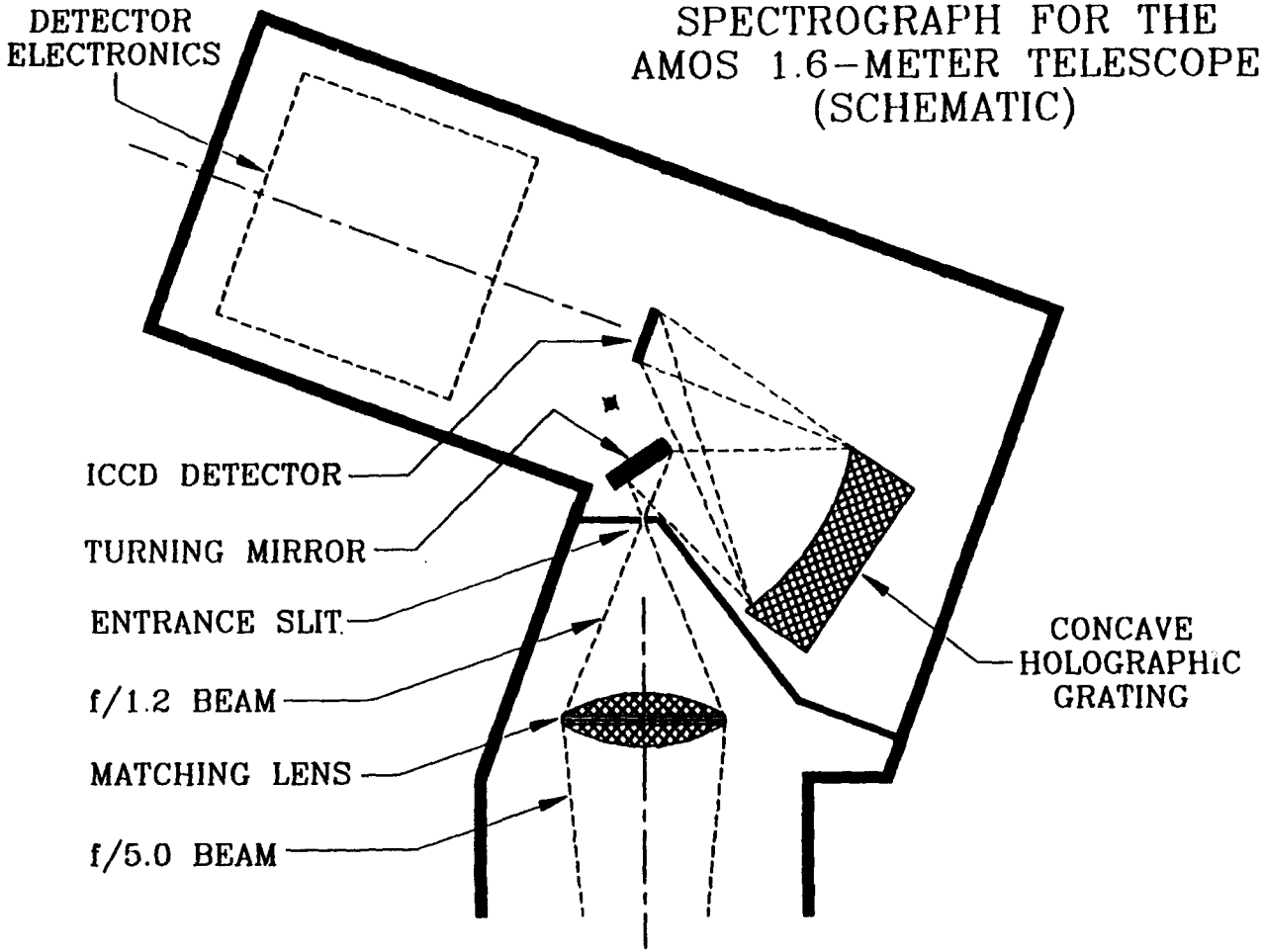
SPECTROGRAPH FOR THE
AMOS 1.6-METER TELESCOPE
(SCHEMATIC)
DETECTOR
ELECTRONICS
ICCD DETECTOR
TURNING MIRROR
ENTRANCE SLIT
f/1.2 BEAM
MATCHING LENS
f/5.0 BEAM
CONCAVE
HOLOGRAPHIC
GRATING

Figure 3

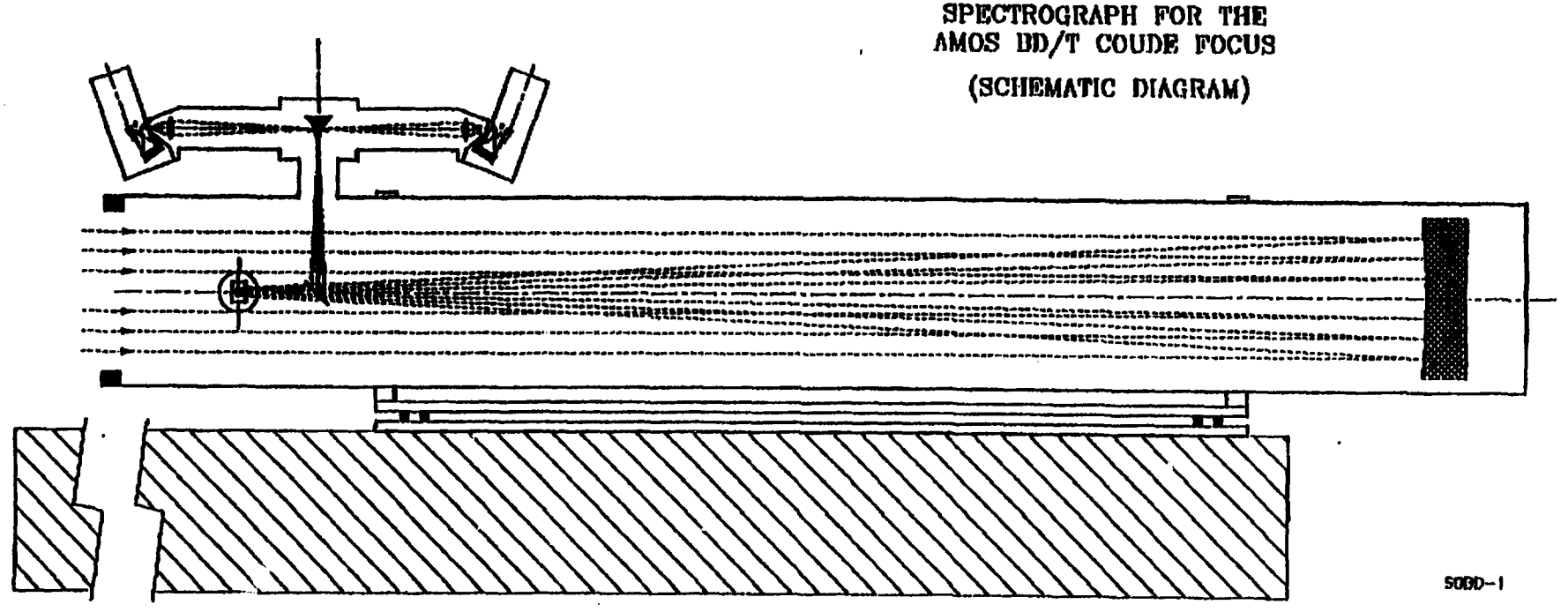
SPECTROGRAPH FOR THE
AMOS BD/T COUDE FOCUS
(SCHEMATIC DIAGRAM)
5080-1

Figure 4

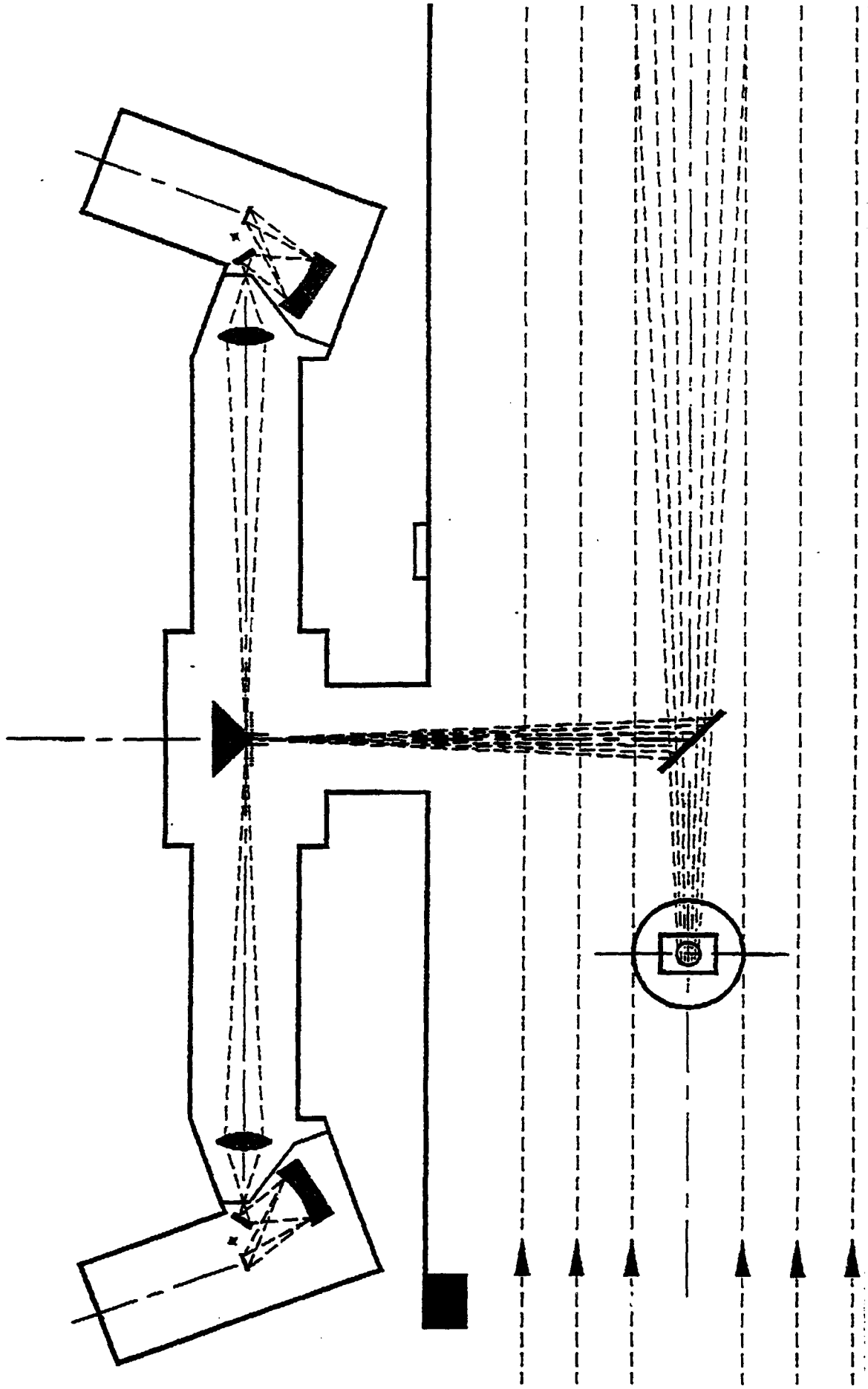

Figure 5

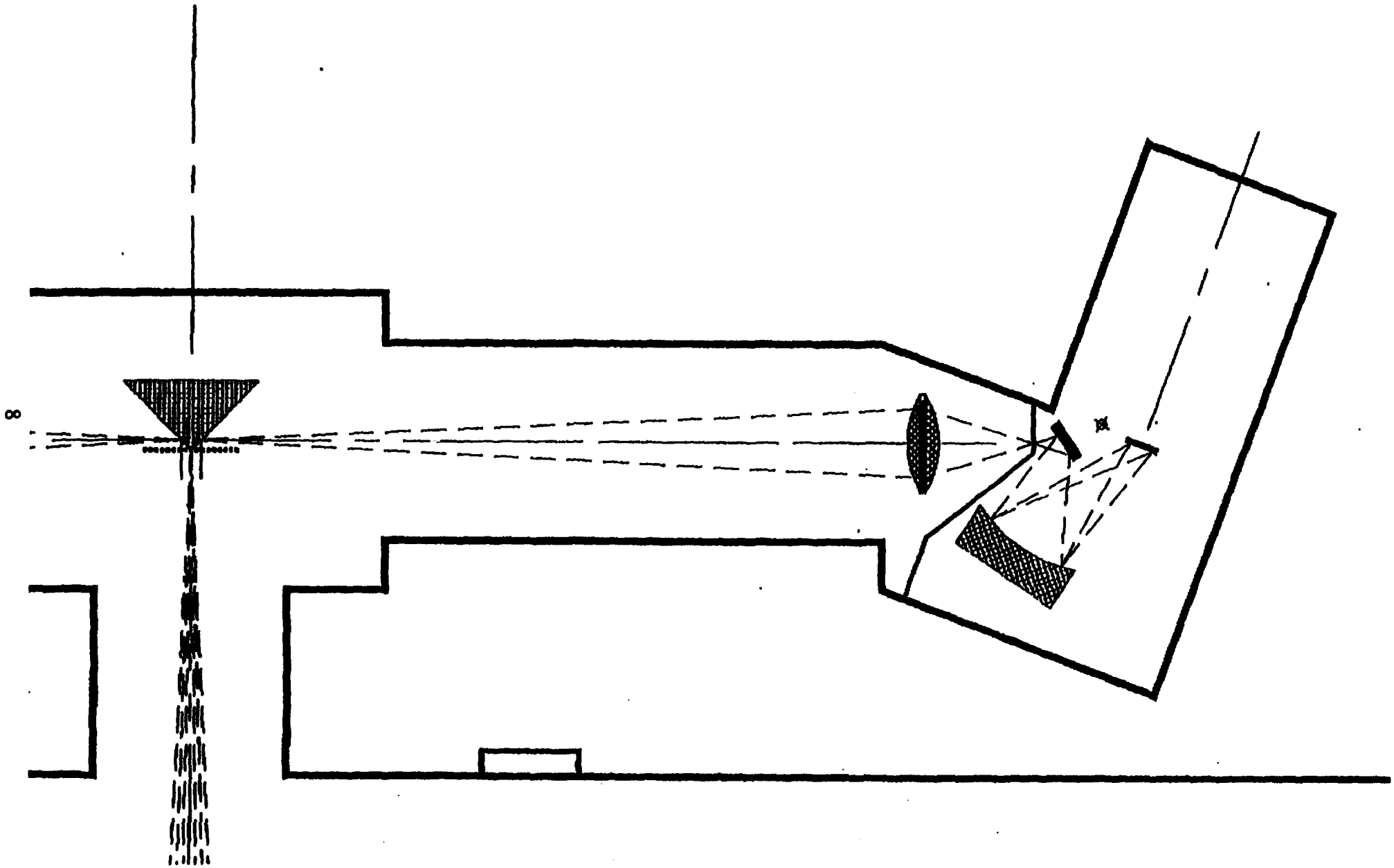

Figure 6

2.2 1.6-Meter Telescope Experiment

An identical spectrograph was used on the 1.6-meter mount telescope. A bracket on the side of the telescope was used to support an 8-inch f/5 Newtonian telescope and the spectrograph. The telescope arrangement is shown in Figure 7, with details in Figure 8. A single spectrograph was used on this telescope.

2.3 Operations

A considerable amount of work had to be done to instrument the 1.6-meter telescope. Both wires and freon cooling lines had to be taken out onto the mount through the cable wrap up.

The telescope and spectrograph slits had to be boresighted to their respective tracking telescopes. This was done using stars prior to the flight.

The STS-41 flight was scrubbed twice before it was launched in October 1990.

2.4 Results

Good data was recorded from both systems. The spectrum, Figure 9, was obtained with the f/5 telescope system on the 1.6-meter mount and shows the presence of strong emission in the 3300-Å region. There is a broad continuum between 3000 Å and 4600 Å. There is strong emission near 6300 Å and, at the longer wavelength around 6600 Å, the emission is contaminated by a second order emission. Figure 10 shows the time sequence of spectra with respect to the burn. Notice the 3300-Å feature intensifies quickly while the 6300-Å feature is slower rising and falling. Figure 11 is the spectral image with dispersion along the page abscissa and spatial position in the ordinate direction. The Shuttle travel distance between spectra was 4.3 km. The spectrum in Figure 12 was obtained with the f/8 telescope system on the BDT. The emission near 6300 Å was detected and some broad features in the longer wavelength region appear to be significant. The second spectrograph for the blue wavelength on the BDT did not record the emission at 3300 Å. It was found later that the telescope transmission was poor at short wavelengths.

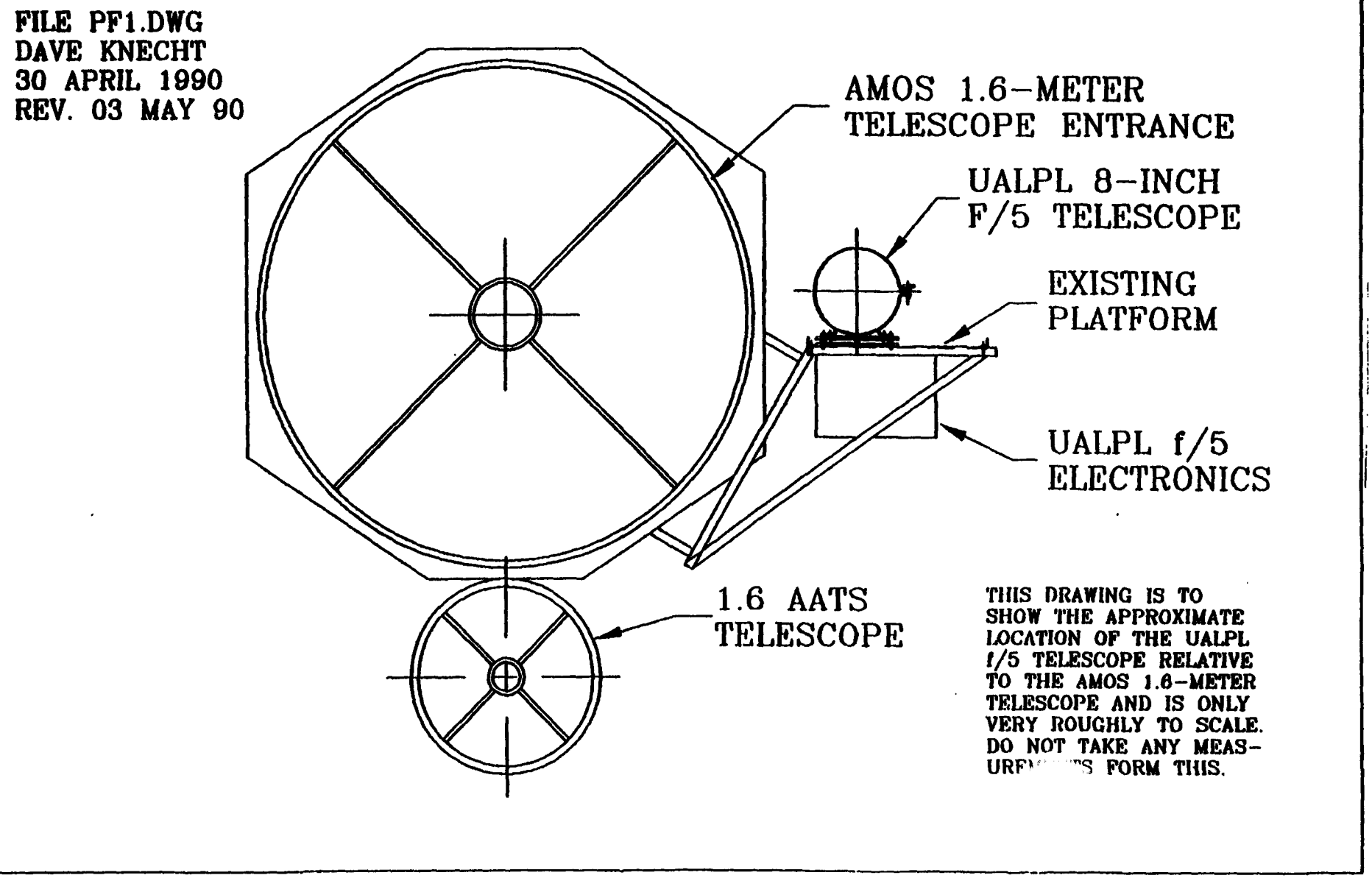
FILE PF1.DWG
DAVE KNECHT
30 APRIL 1990
REV. 03 MAY 90
AMOS 1.6-METER
TELESCOPE ENTRANCE
UALPL 8-INCH
F/5 TELESCOPE
EXISTING
PLATFORM
UALPL f/5
ELECTRONICS
1.6 AATS
TELESCOPE
THIS DRAWING IS TO SHOW THE APPROXIMATE LOCATION OF THE UALPL f/5 TELESCOPE RELATIVE TO THE AMOS 1.6-METER TELESCOPE AND IS ONLY VERY ROUGHLY TO SCALE. DO NOT TAKE ANY MEAS-
URE
S FORM THIS.

Figure 7

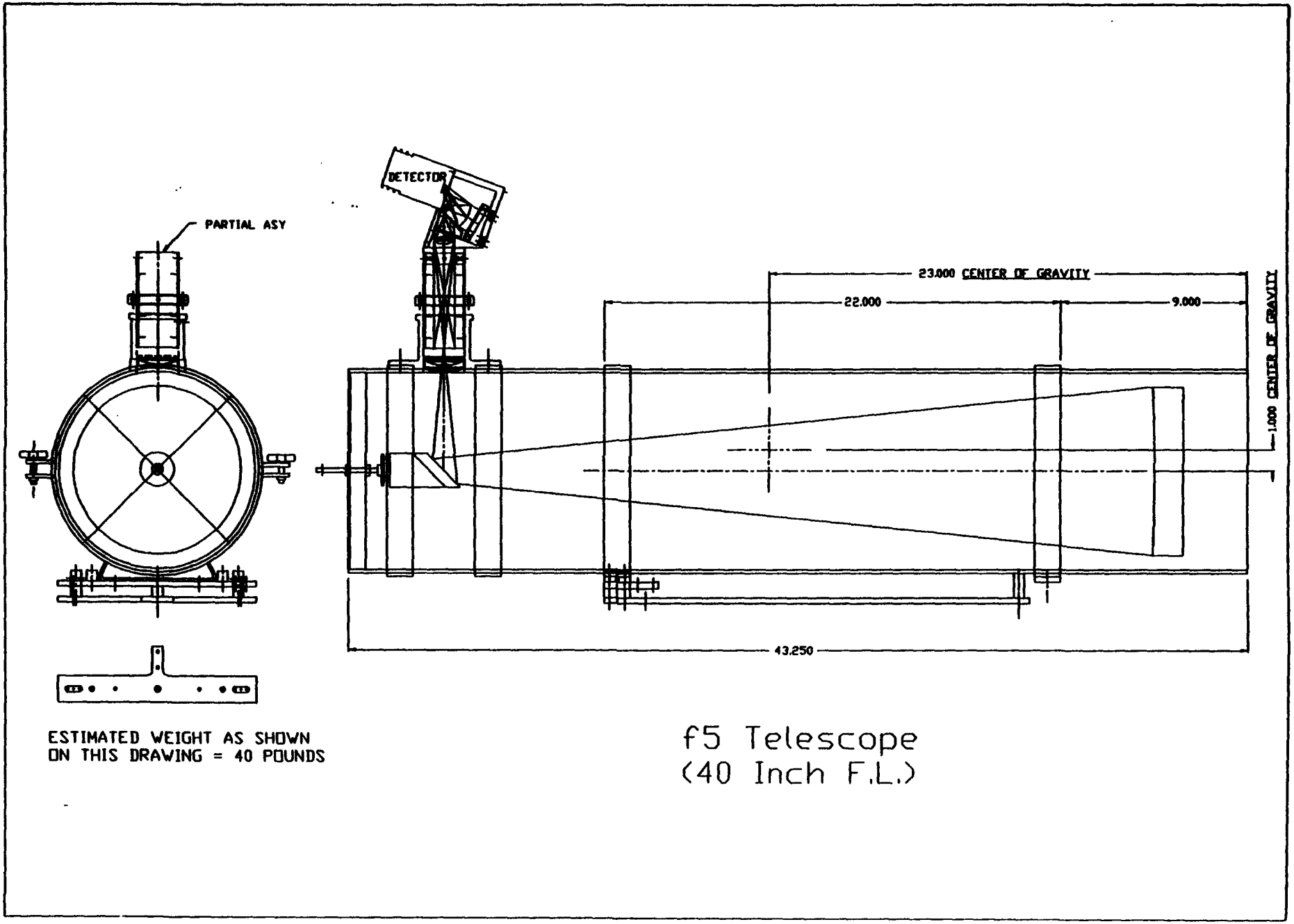
DETECTOR
PARTIAL ASY
23.000 CENTER OF GRAVITY
22.000
9.000
1.000 CENTER OF GRAVITY
43.250
ESTIMATED WEIGHT AS SHOWN
ON THIS DRAWING = 40 POUNDS
f5 Telescope
(40 Inch F.L.)

Figure 8

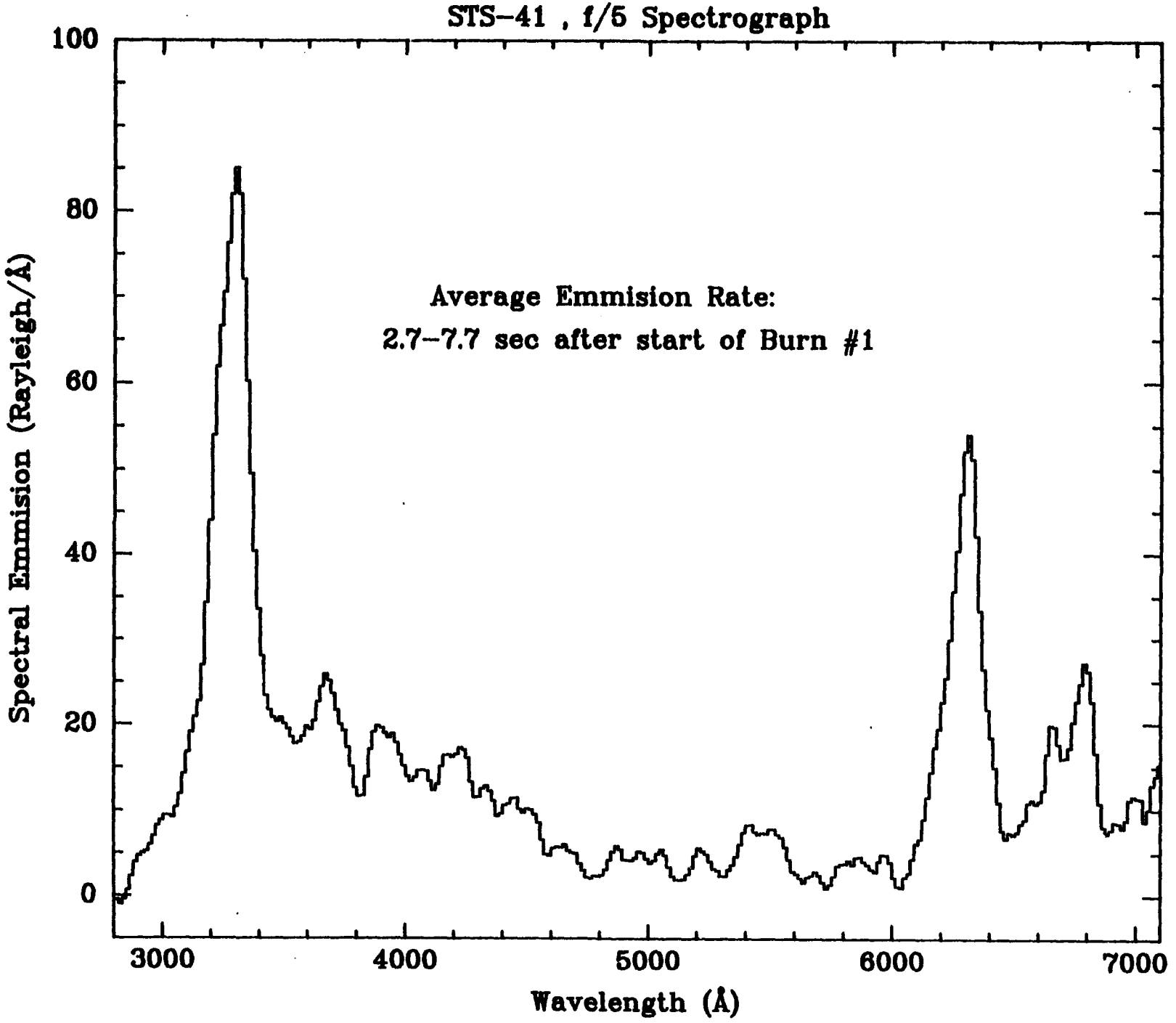
STS-41 , f/5 Spectrograph
Average Emmision Rate:
2.7-7.7 sec after start of Burn #1
Spectral Emmision (Rayleigh/Å)
Wavelength (Å)
100
80
60
40
20
0
3000
4000
5000
6000
7000

Figure 9

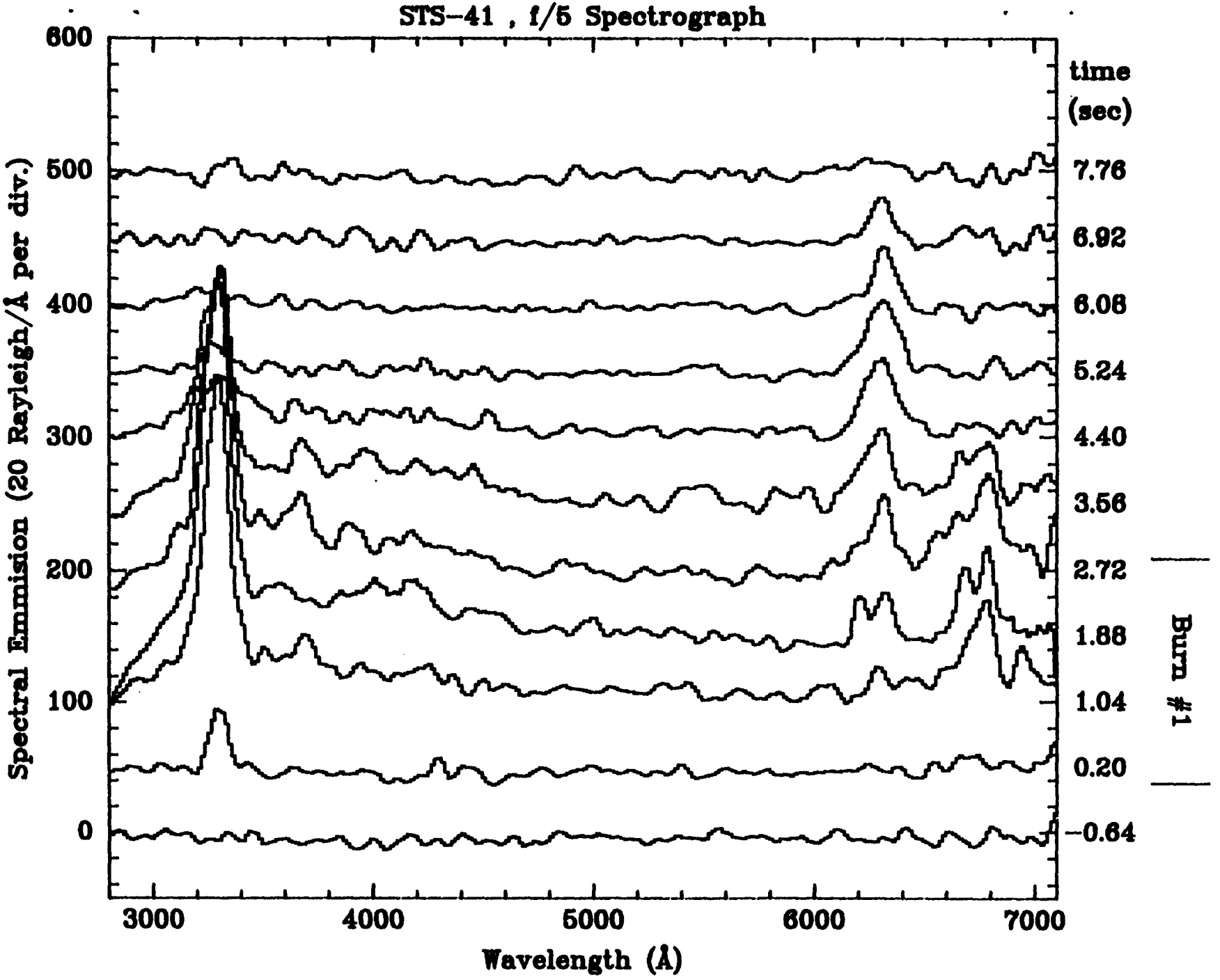
STS-41 , f/5 Spectrograph
Spectral Emmision (20 Rayleigh/Å per div.)
600
500
400
300
200
100
0
3000
4000
5000
6000
7000
Wavelength (Å)
time
(sec)
7.76
6.92
6.08
5.24
4.40
3.56
2.72
1.88
1.04
0.20
-0.64
Burn #1

Figure 10

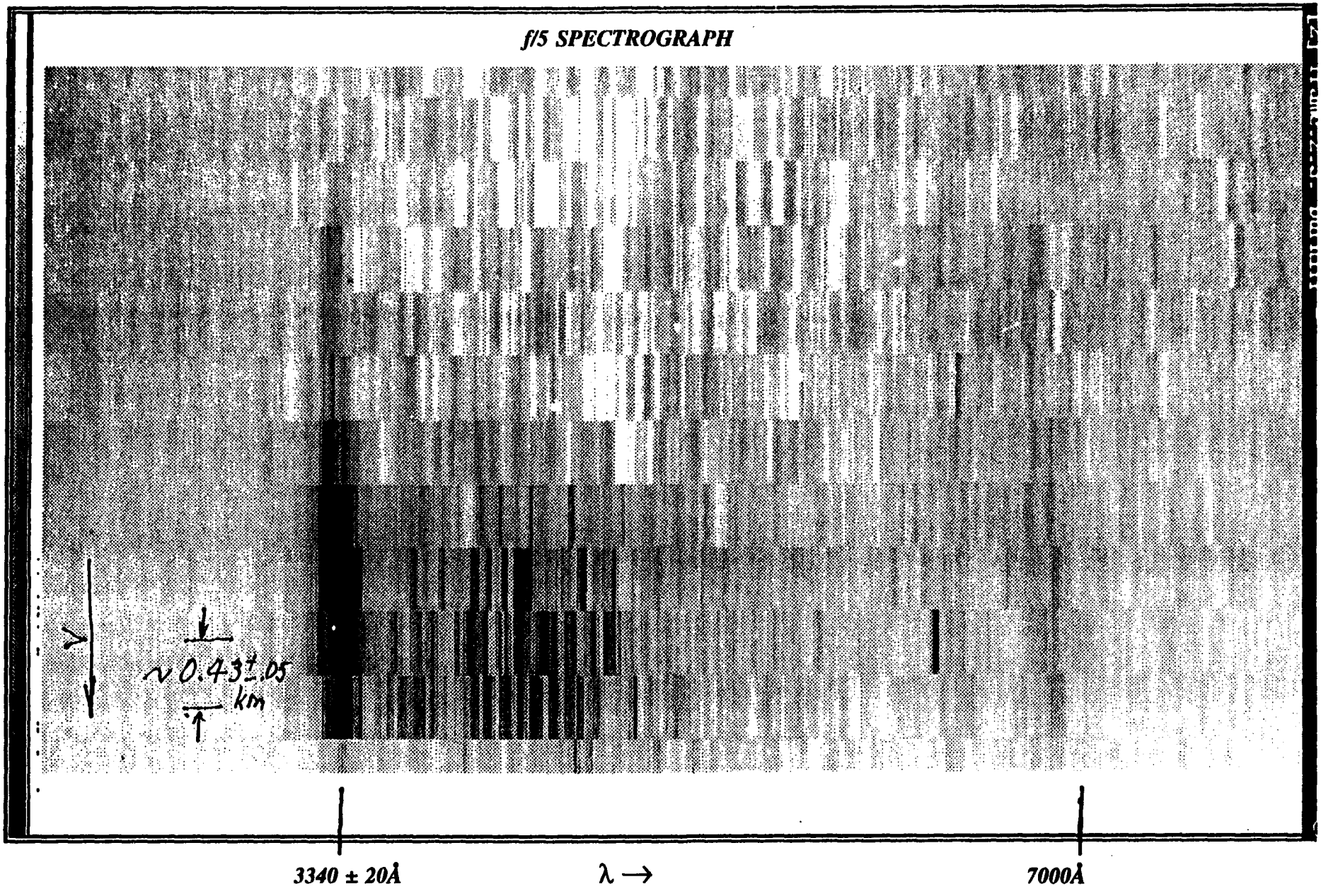

pixel = 0.022, sum over 16 = 0.35 mm at detector
0.35 mm ÷ f/1.2 x f5 = 1.47 mm in focal plane
1.47 ÷ F(1016 mm) x Range (300 km) = 0.43 km

Figure 11

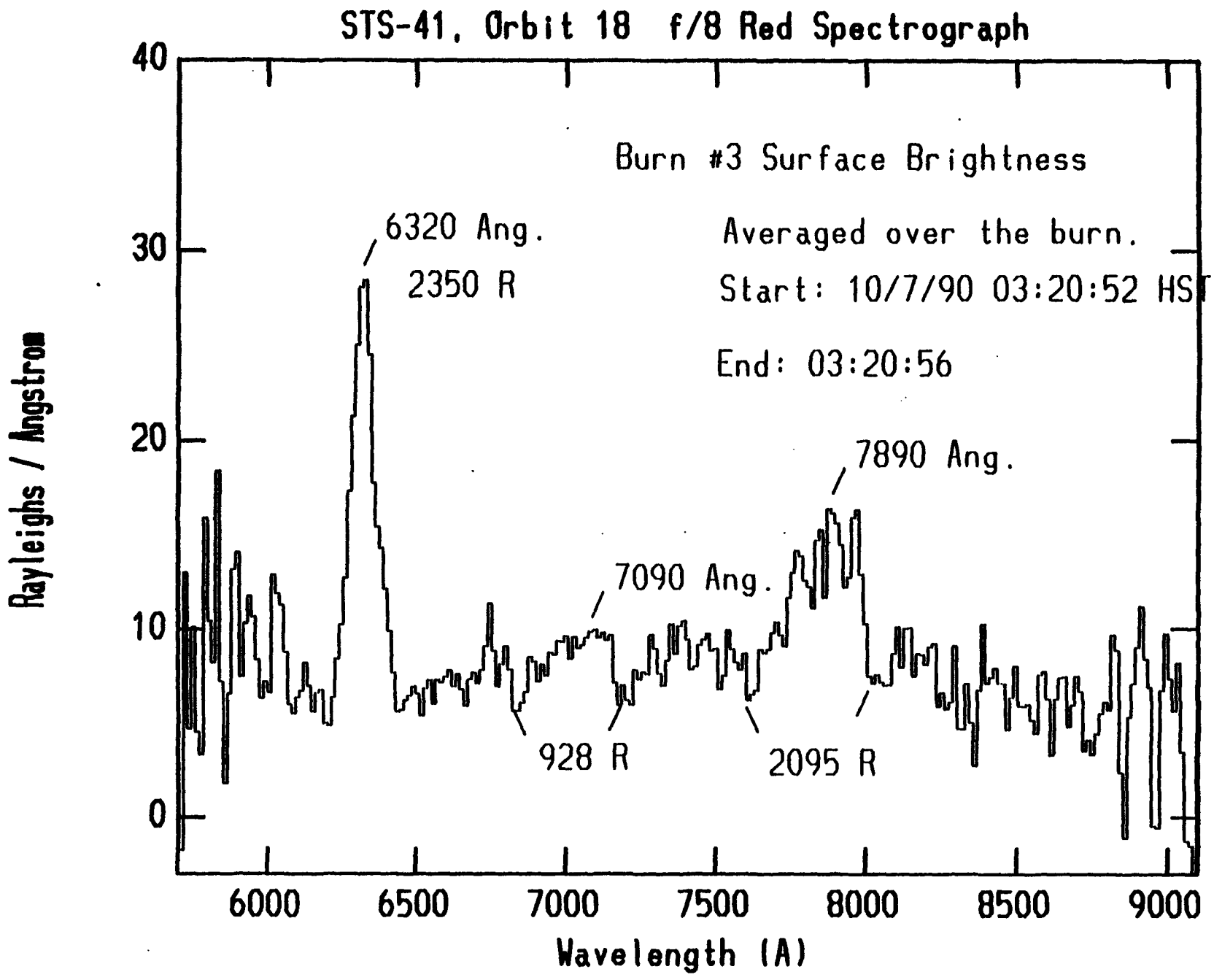
STS-41, Orbit 18 f/8 Red Spectrograph
Burn #3 Surface Brightness
Averaged over the burn.
Start: 10/7/90 03:20:52 HST
End: 03:20:56
6320 Ang.
2350 R
7890 Ang.
7090 Ang.
928 R
2095 R
Rayleighs / Angstrom
Wavelength (A)
0
10
20
30
40
6000
6500
7000
7500
8000
8500
9000

Figure 12

These data were processed to extract both spatial and time signatures. Most of this data appears in the published literature now.

2.5 Conclusions

1) The strong emissions should be examined at higher resolution to identify their species. [They were subsequently verified to be NH and O (6300, 6364 Å) emissions.]

3. Shuttle Mission STS-38 (November 16, 1990)

New high resolution spectrographs were designed and fabricated for the STS-38 opportunity but most of the system remained the same as for STS-41.

3.1 New Spectrographs

The new design used plane gratings on a turret for more utility in changing resolution to adapt the experiment for different conditions. We maintained the high throughput by using an all-reflective f/1.4 lens to feed the grating. The configuration is shown in Figure 13. This spectrograph was adapted to the two telescopes by adjusting the foreoptics from f/5 to f/8, otherwise the system was unchanged.

Since only one wavelength region could be observed with the 1.6-meter mount instrument, it was set for the 3000 to 4500-Å region since the feature at 3300 Å was considered highest priority.

The BDT was equipped with two spectrographs again to cover the wavelength ranges 3100 to 4500 Å and 6200 to 7200 Å at about 10-Å resolution.

3.2 Operations

This was a poor weather situation. We barely had enough clear time prior to the flight to align the instruments. It was overcast the night of the pass until a few minutes before the overflight and became overcast again during the pass.

3.3 Results

The spectrum in Figure 14 was obtained with the f/5 telescope system on the 1.6-meter mount. The strong emission at about 3360 Å was quickly identified as an NH band system which has the unique

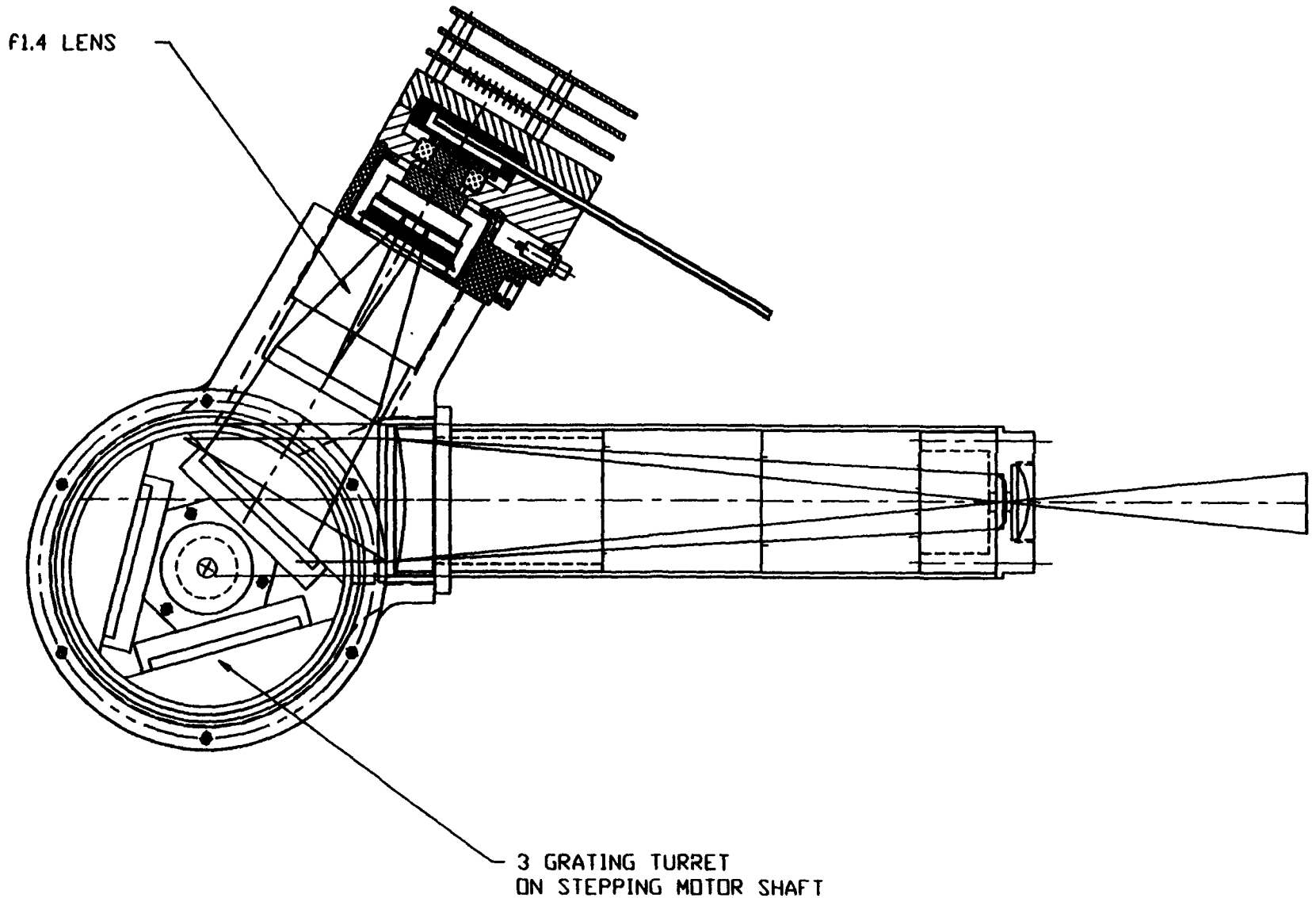

Figure 13

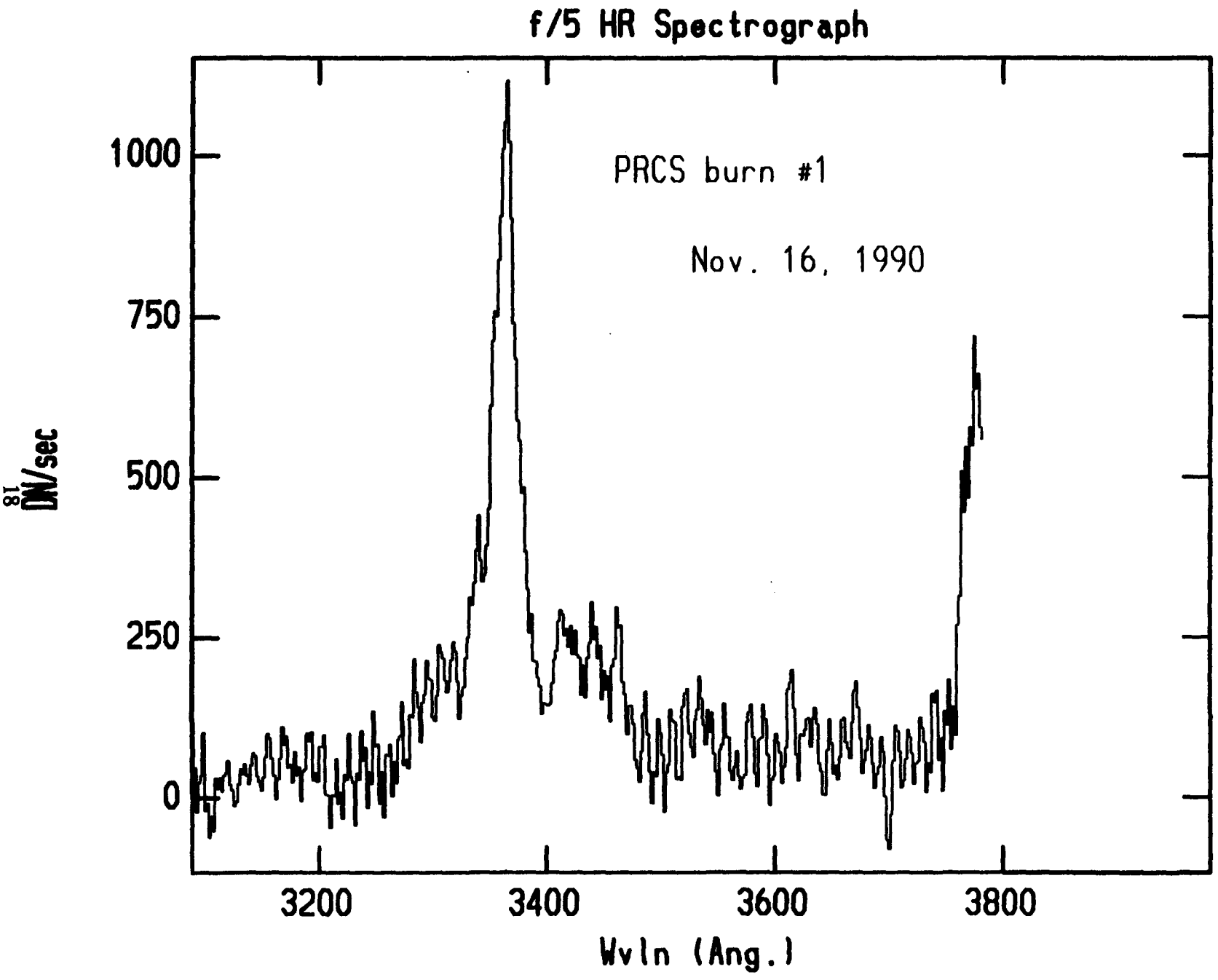
f/5 HR Spectrograph
PRCS burn #1
Nov. 16, 1990
1000
750
500
250
0
3200
3400
3600
3800
Wvln (Ang.)
10^18 DN/sec

Figure 14

characteristic of all the bands being heavily blended in the 3360-Å region. Synthetic spectra were used for the confirming test.

The spectra were noisy due to pickup from the local TV station which transmits from the same hilltop on Haleakala.

Weak emissions at 6300 Å and 6364 Å were detected by the BDT f/8 system in the long wavelength channel. Unfortunately we could not separate the Shuttle-related emission from the background atmospheric 6300-Å emission. We did not realize at the time the importance of sky data to this particular observation. The clouds cleared for just a few minutes. The spectrum is shown in Figure 15.

The observation was confused somewhat by a companion experiment of another group. A mirror was used to split the 6-inch beam and feed an IR experiment. The IR interferometer used an internal HeNe laser for scan control. Some of the light was scattered out into the entrance optics and was detected in our experiment at 6328 Å, between the OI lines (6300, 6364 Å).

3.4 Conclusions

1) We successfully identified the short wavelength emission in the plume to be NH.

2) We expected to detect OH emission at 3060 Å; however, the spectrograph was not very sensitive at that wavelength, because a corrector lens in the f/1.4 spectrograph was made of BK7, which cuts off near 3000 Å. Although the advertised limit of the lens was 2900 Å, that was not true.

3) We did observe the 6300, 6364-Å emissions of OI and no other emissions in the wavelength range covered by the red spectrograph on the BDT. However, we were not able to say unambiguously that the emission was plume related.

4) At the next opportunity we must improve our sensitivity near 3000 Å in search of the OH emission.

5) The development of the plume in various emissions should be studied with monochromatic imaging.

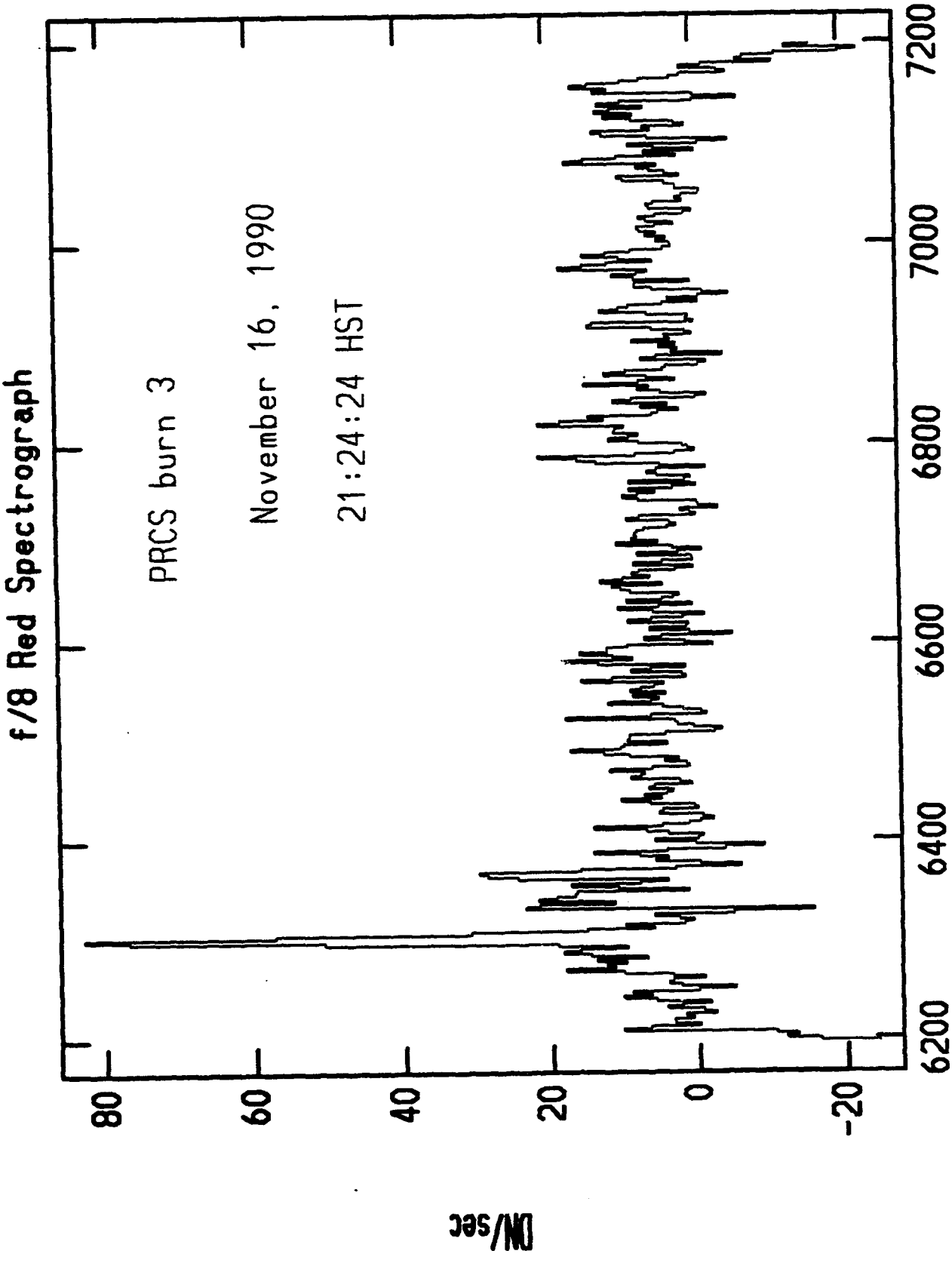
f/8 Red Spectrograph
PRCS burn 3
November 16, 1990
21:24:24 HST
DN/sec
80
60
40
20
0
-20
6200
6400
6600
6800
7000
7200
Wvln (Ang.)

Figure 15

4. STRYPI-XI Mission (February 18, 1991)

The STRYPI mission involved a number of observational facilities, including aircraft, spacecraft, and ground-based instrumentation. For our part, the trajectory could only be observed by the 1.6-meter mount instrumentation.

We had determined that the boresight of the f/5 telescope experiment on the 1.6-meter mount tended to change with respect to the 1.6-meter tracker angle because the attaching bracket was not strong enough. A new bracket was built prior to the STRYPI-XI experiment. We mounted two auxiliary telescopes on the new bracket, an 8-inch diameter and a 10-inch diameter, both f/5. The bracketing and telescope interface drawing are reproduced in Figure 16.

We used the f/1.2 spectrograph as described in Section 2. We also used a 6-channel monochromatic imager for the first time with the 8-inch telescope. The schedule was rushed and we had some problems getting filters but some imaging was acquired. The spectrograph did a good job again and the data were analyzed. The imagers did not produce significant results.

An unpublished report on the STRYPI mission by Knecht et al. is attached as Appendix A. This report describes the instrumentation and the results.

5. Shuttle Mission STS-43 (July 29, 1991)

Some major changes were made in the experiment to solve some of the instrumental problems and continue the development of the science.

5.1 Cassegrain Focus of the BDT

We had determined that the coudé optical path had too many reflections to support UV transmission. We decided to make a fairly major change in the system by moving our equipment to the Cassegrain focus. This required some special fixturing to support the instruments which also had to be fairly lightweight.

The BDT primary and secondary mirrors were recoated to enhance the reflectivity to 3000 Å.

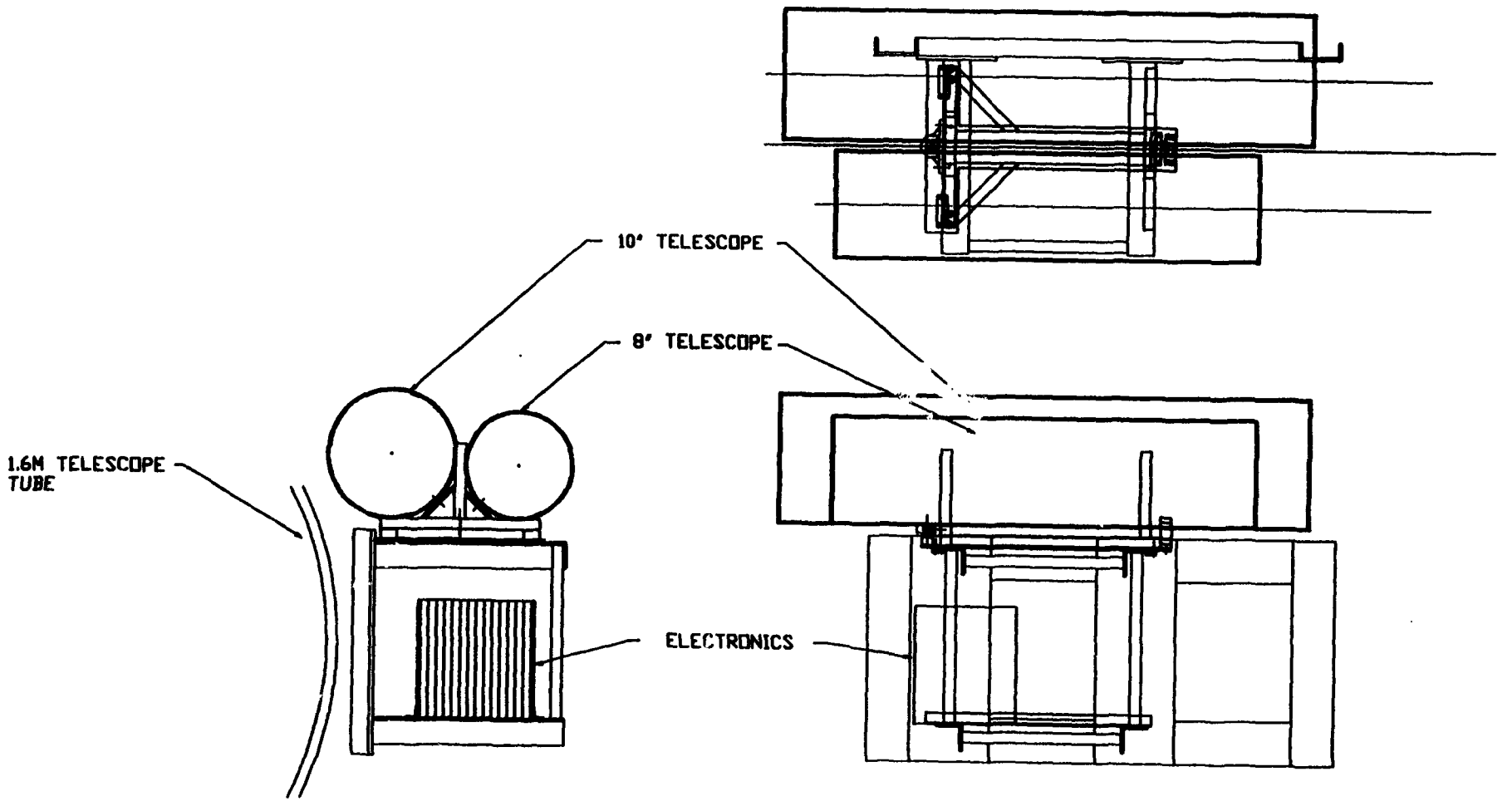

Figure 16

A new spectrograph was designed also to enhance the throughput at 3000 Å; a fast lens with UV transmitting capability was not found for the f/1.4 design. The new spectrograph was designed around the JY holographic concave grating. Although the f-ratio was only 3, there was no doubt about the sensitivity at 3000 Å.

The new spectrograph is outlined in Figure 17. Although not as fast as the turret spectrograph (f/1.4), it has only one reflection and satisfies our UV requirement. Also, there is a series of gratings which may be used with this instrument for different wavelengths and resolutions.

The Cassegrain mounting on the BDT is shown in cross-section in Figure 18 along with the bolt pattern on the mirror cell. A closer view, Figure 19, shows the optical bench and light paths. Two spectrographs and one 6-channel imager are supported. The spectrographs are fed by a reflective strip on two transparent quartz windows at the focal point of the BDT. The images have two lines where the spectrograph reflective strips remove the light from the beam. The reflective strip is re-imaged on the spectrograph slit with f-ratio conversion lenses in the optical path. The optics of the Cassegrain telescope is shown in Figure 20. The field of view as seen by the instruments is shown in Figure 21.

5.2 1.6-Meter Mount Experiment

The experiment on the 1.6-meter mount was expanded to provide two spectrographs and a 6-channel monochromatic imager. Each spectrograph had its own f/5 8-inch diameter telescope, and the imager had an f/5 6-inch diameter telescope. The arrangement on the bracket is shown in Figure 22. The electronics box is inside the bracket.

The electronics underwent a major reconfiguration to maintain high-speed communication with the remote computers and support three CCD's on the mount.

5.3 Results

Excellent results were obtained from the instrumentation on the 1.6-meter mount. We were able to read all three instruments and store the data at a repetition rate of ~0.53 sec. The raw data are shown in Figures 23, 24a and 24b. Figure 23 is a combined six-wavelength contour image showing the ram

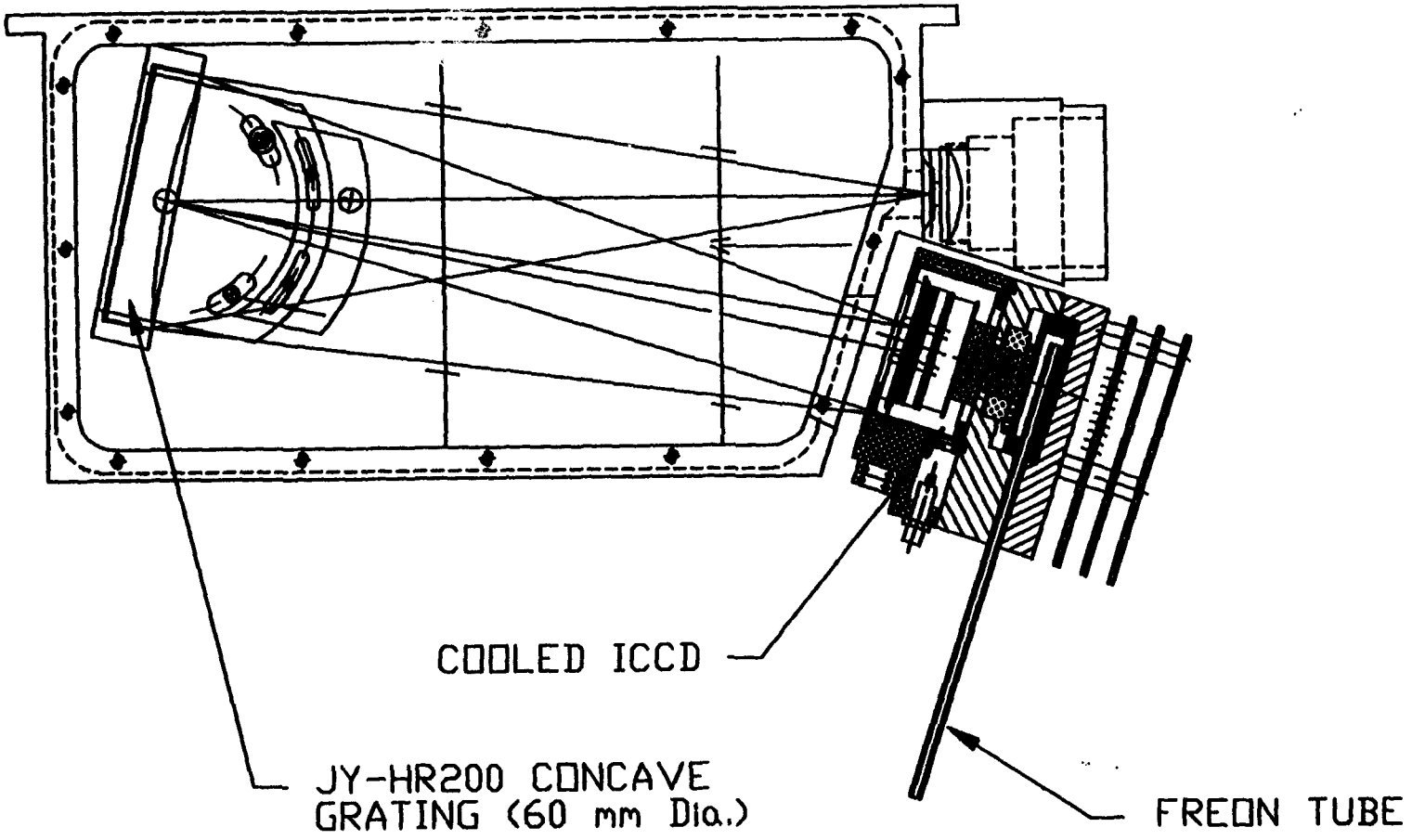

Figure 17

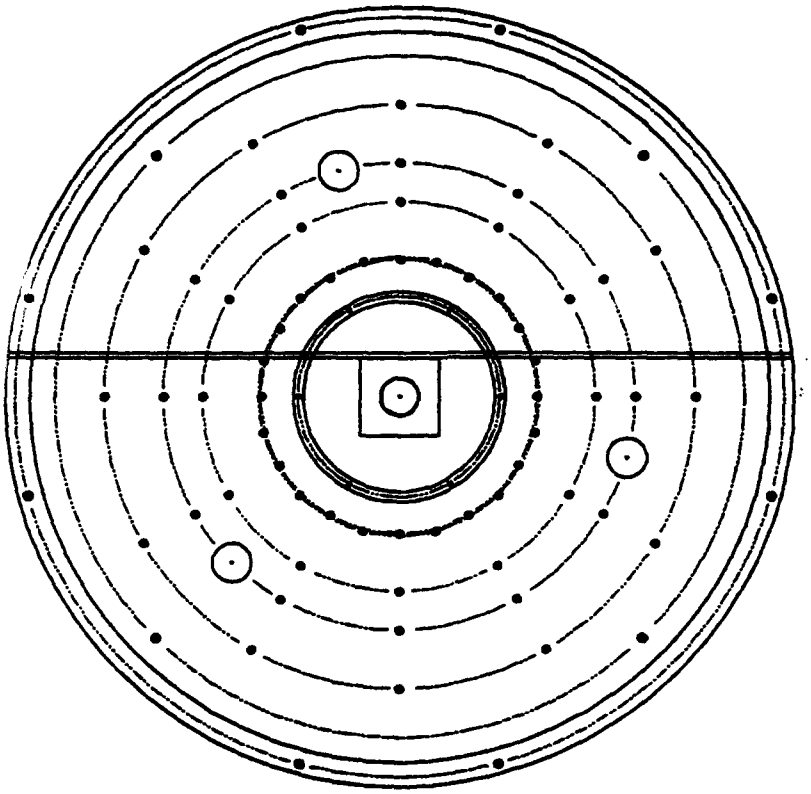

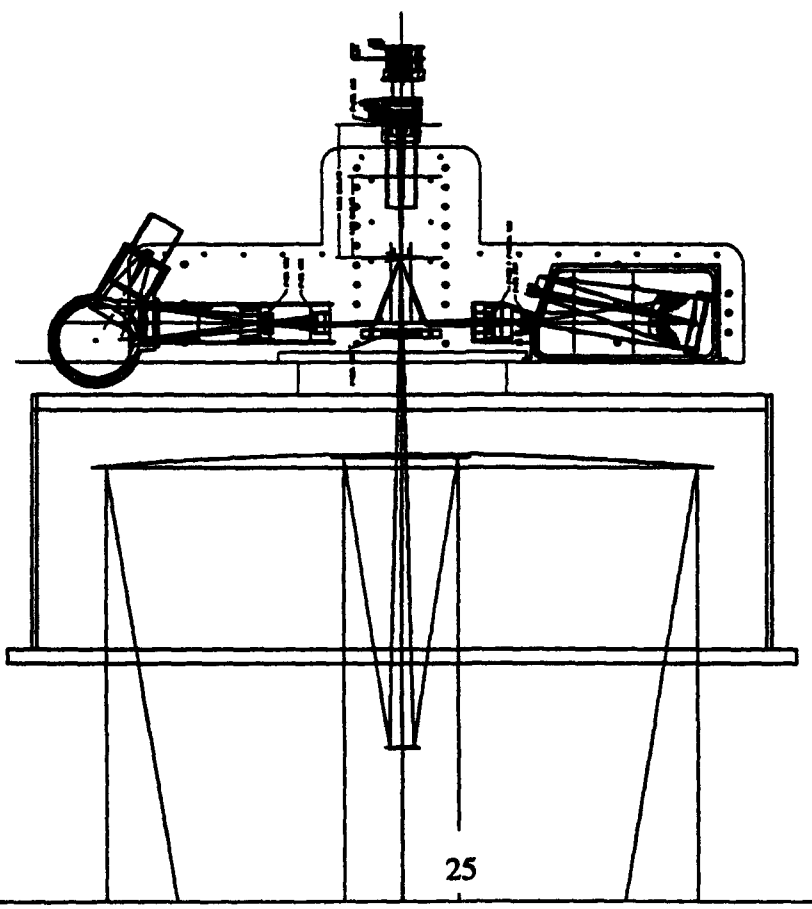

Figure 18

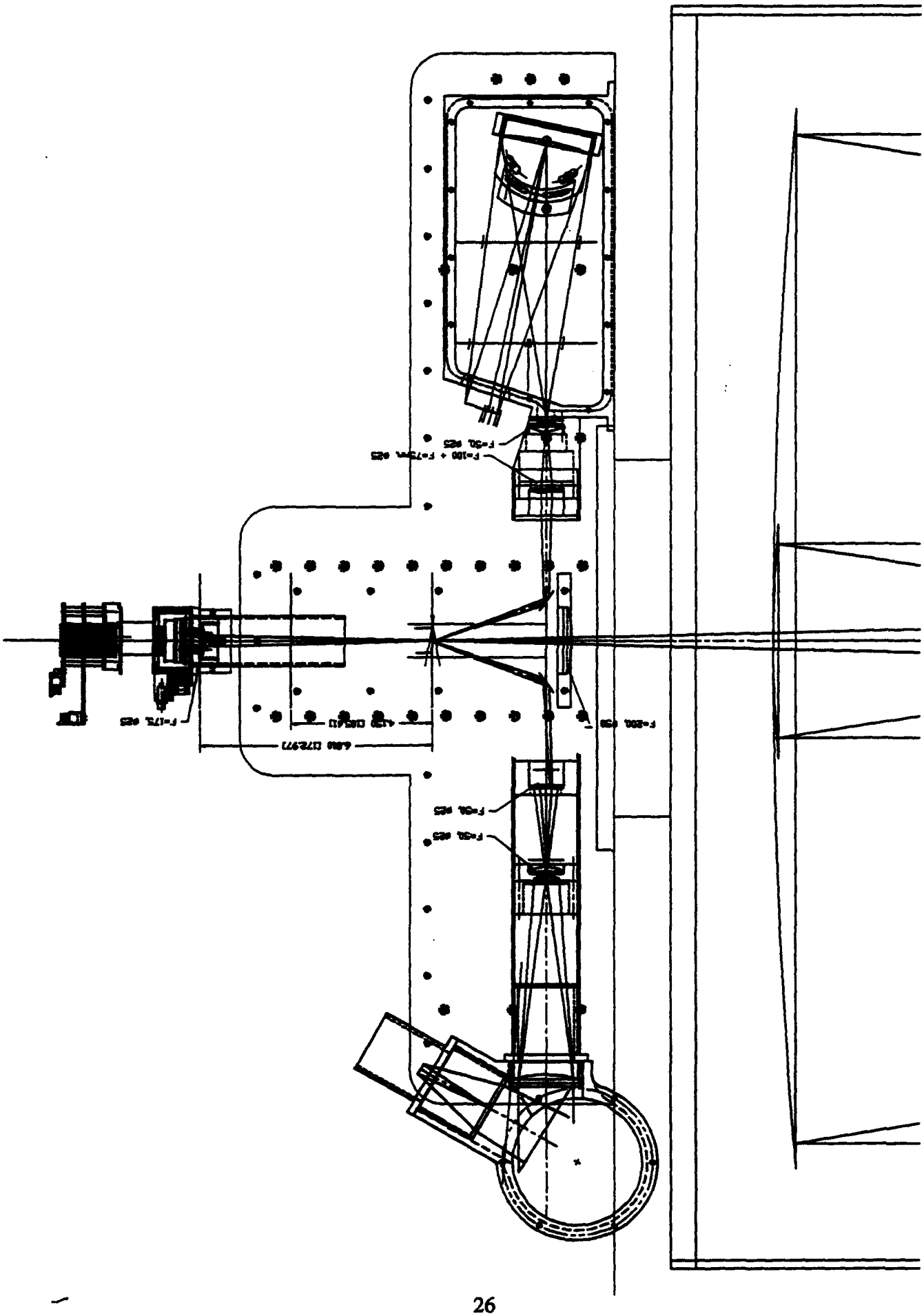

Figure 19

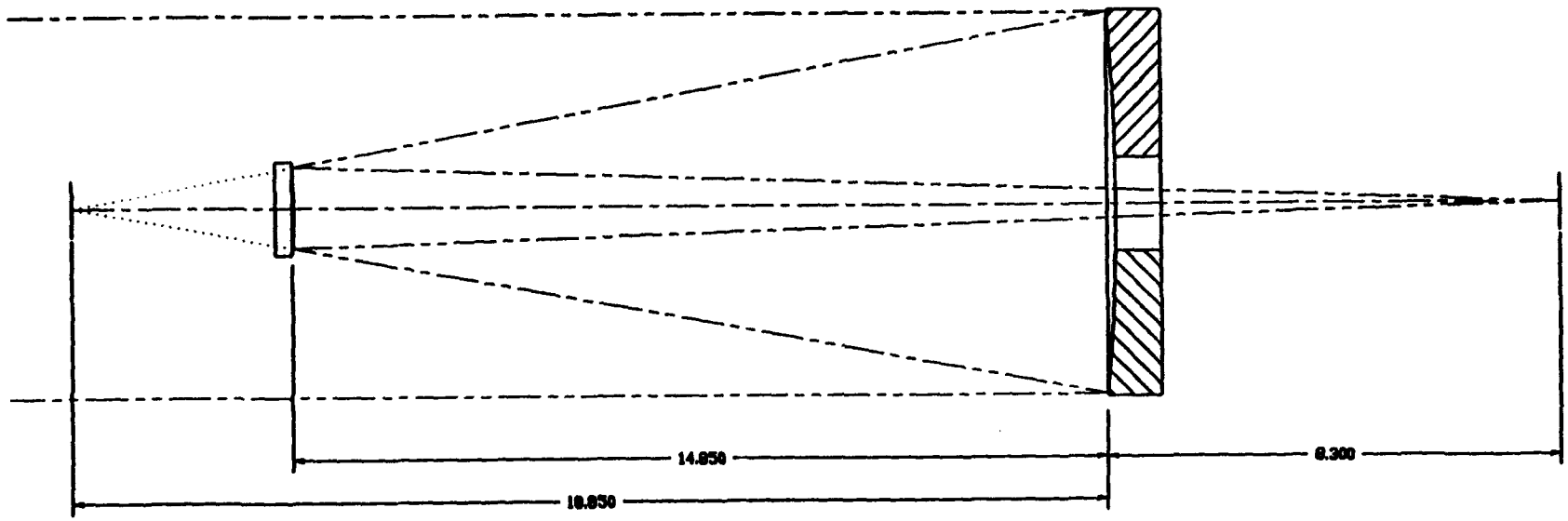

SECONDARY MIRROR

Diameter:	1.700
Clear Aperture:	1.60
Radius:	-9.7
Edge Thickness:	0.31
Figure:	Hyperboloid 60-40 Finish
Bevels:	0.04 Radius
Fine Grind Back:	320 Grit or Finer
Material:	PYREX

PRIMARY MIRROR

Diameter:	7.0
Clear Aperture:	6.8 Minimum
Radius:	37.9 FL=18.9 F/2.78 EFL=120.0 F/17
Edge Thickness:	1.0
Figure:	Paraboloid 60-40 Finish
Bevels:	0.06 Radius
Fine Grind Back:	320 Grit or Finer
Material:	PYREX
Hole Diameter:	1.7
Wedge:	0.015 TIR

LUNAR & PLANETARY LABORATORY

TITLE: CASSEGRAIN TELESCOPE

DO NOT SCALE DRAWING

Figure 20

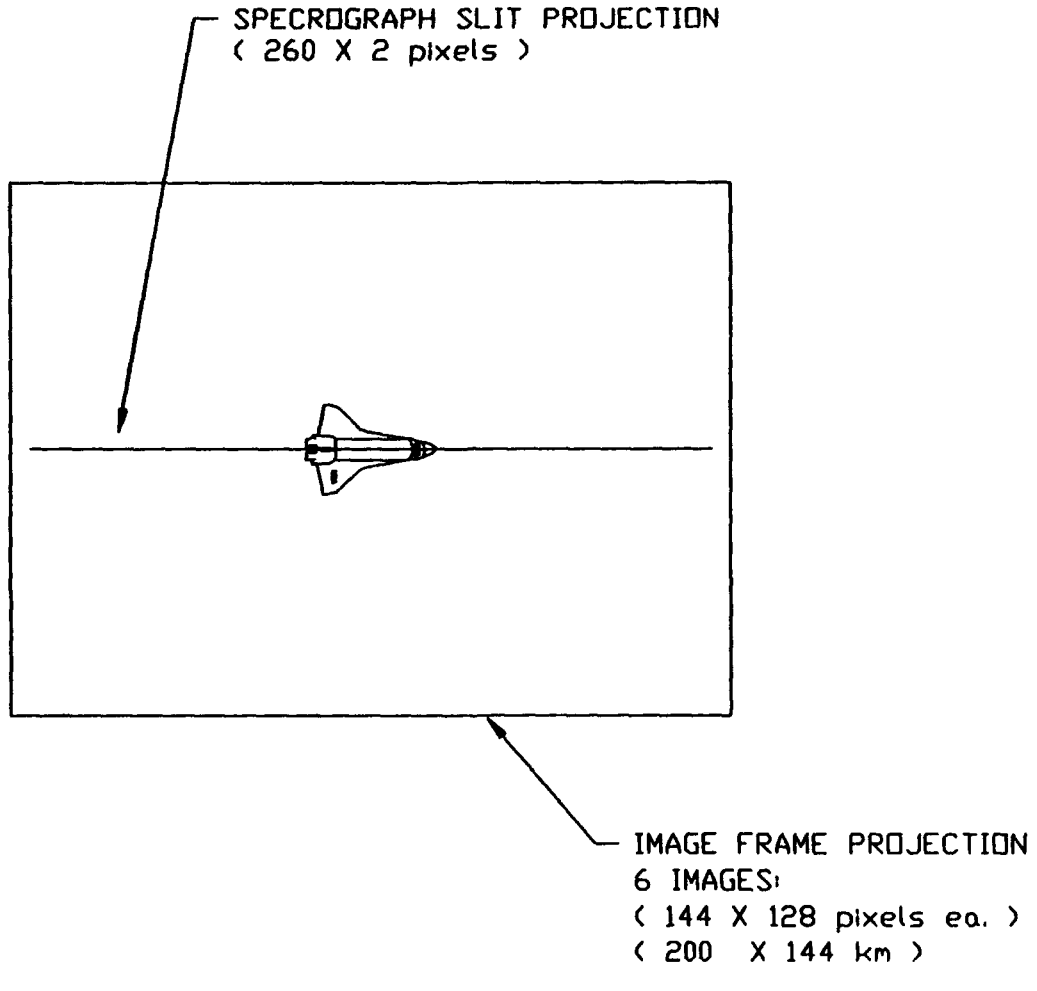

FIELDS of VIEW SIZE at 300 km

Figure 21

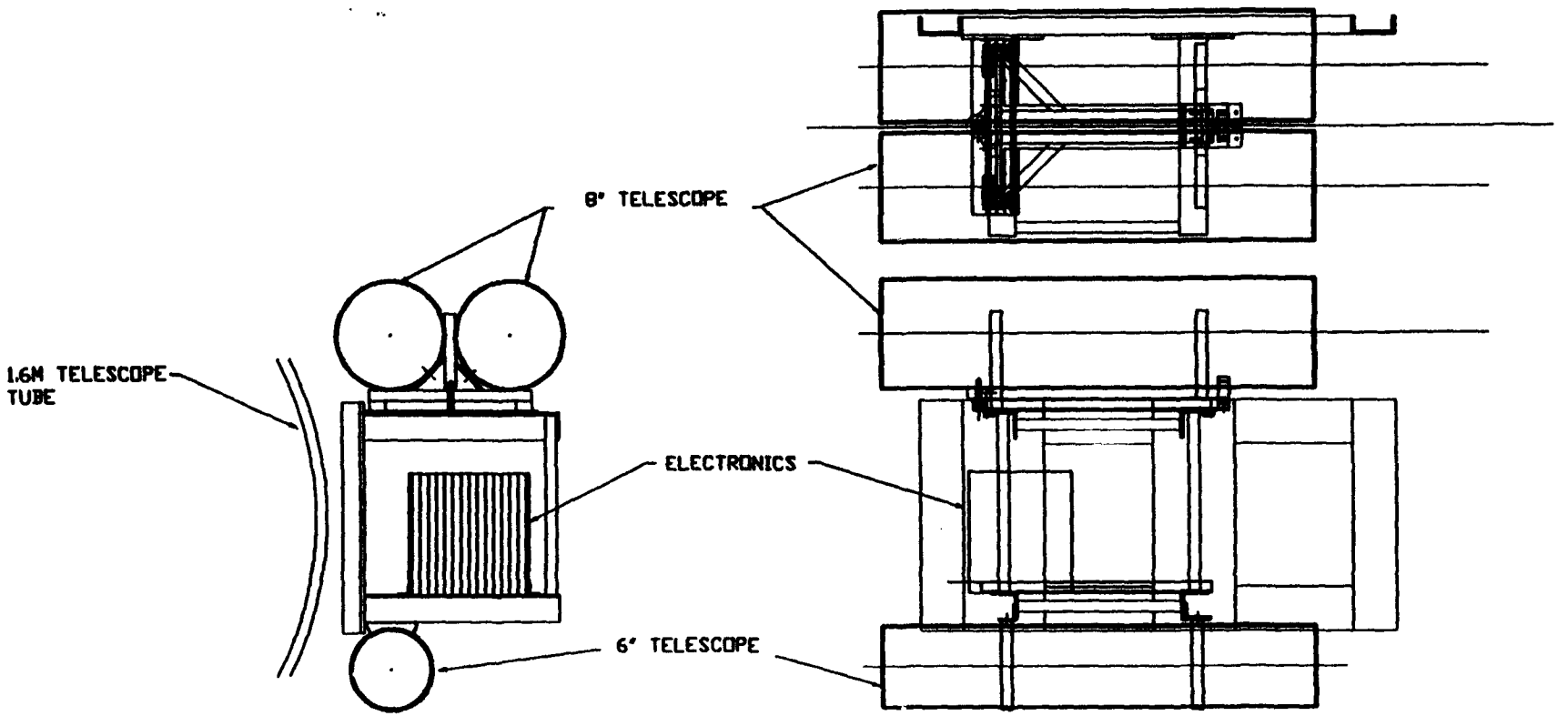

Figure 22

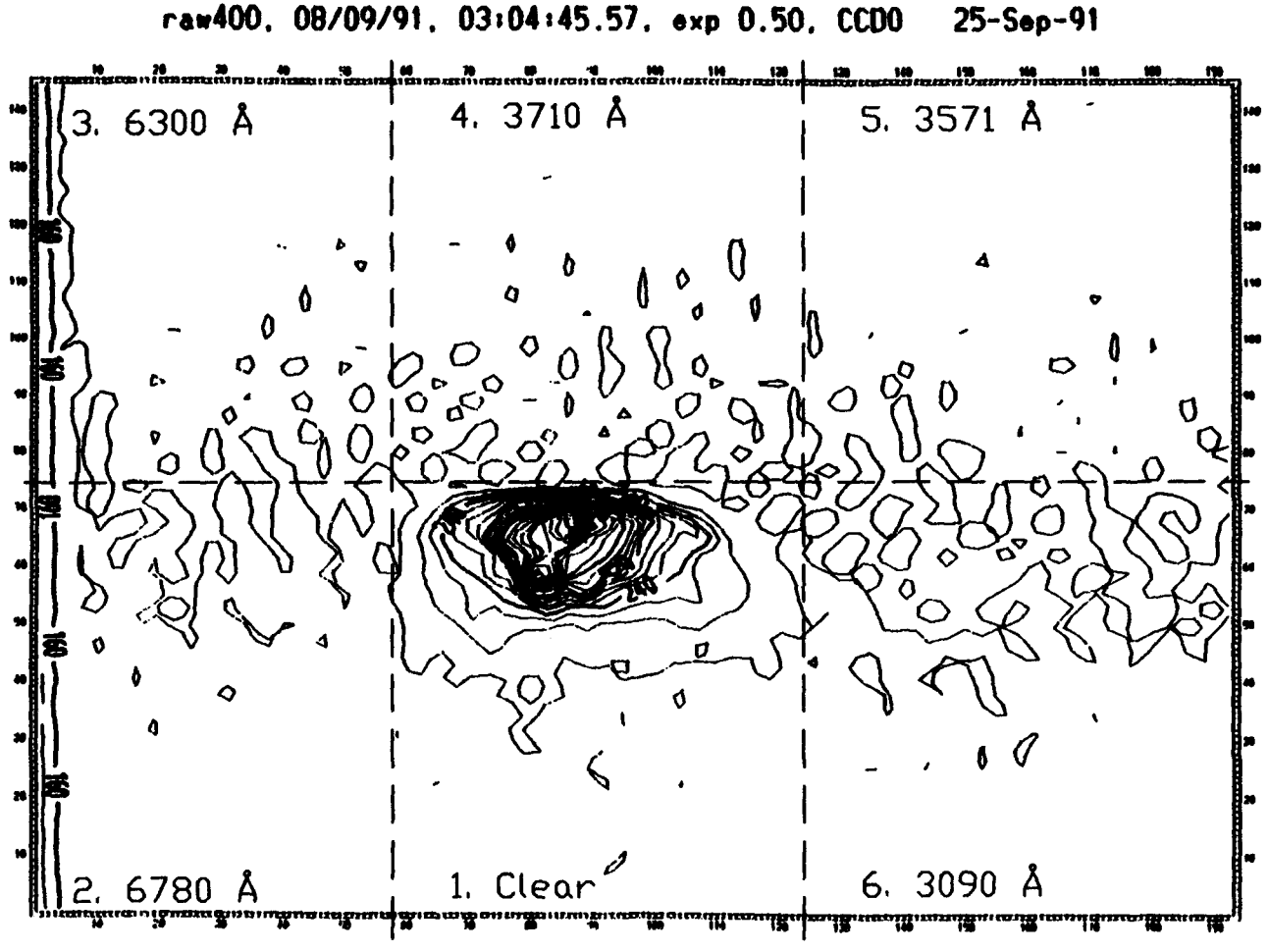
raw400, 08/09/91, 03:04:45.57, exp 0.50, CCD0 25-Sep-91
3. 6300 Å
4. 3710 Å
5. 3571 Å
2. 6780 Å
1. Clear
6. 3090 Å
contoured from 120. to 560., interval = 20.
NOAO/IRAF V2.9.1EXPORT joep@abraxas Wed 12:35:31 25-Sep-91

Figure 23

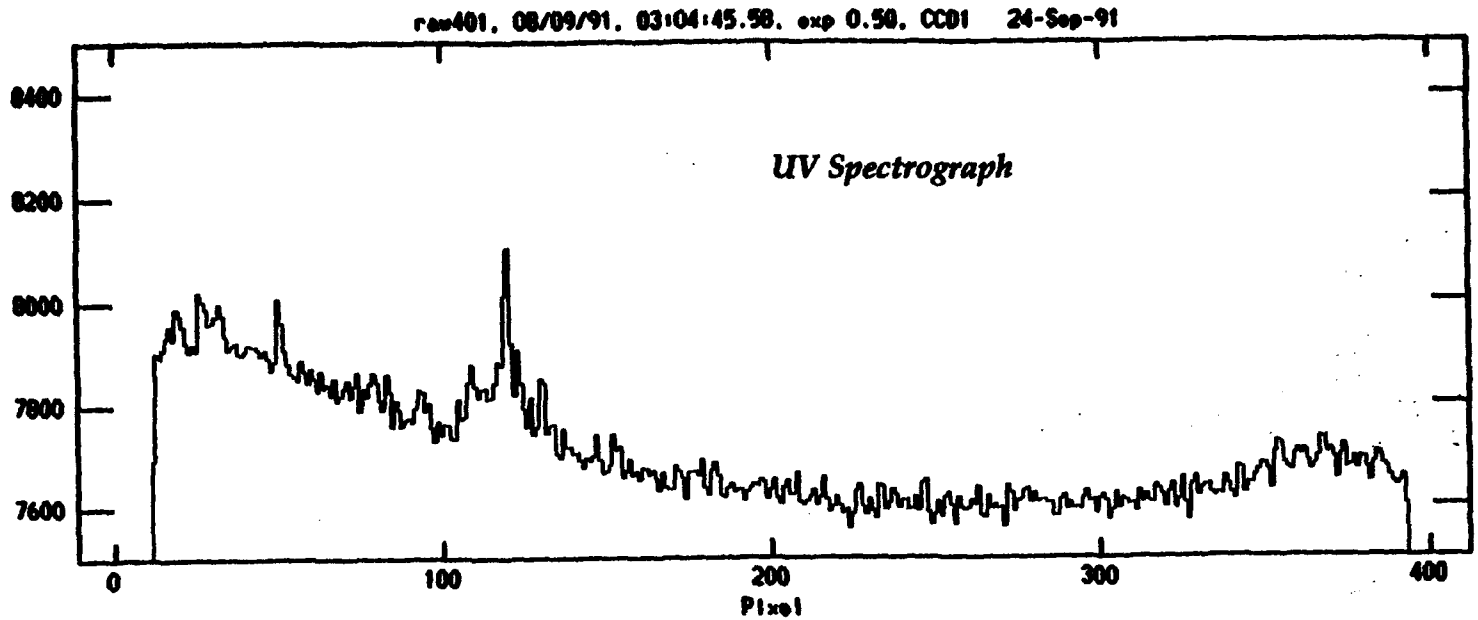

Figure 24a

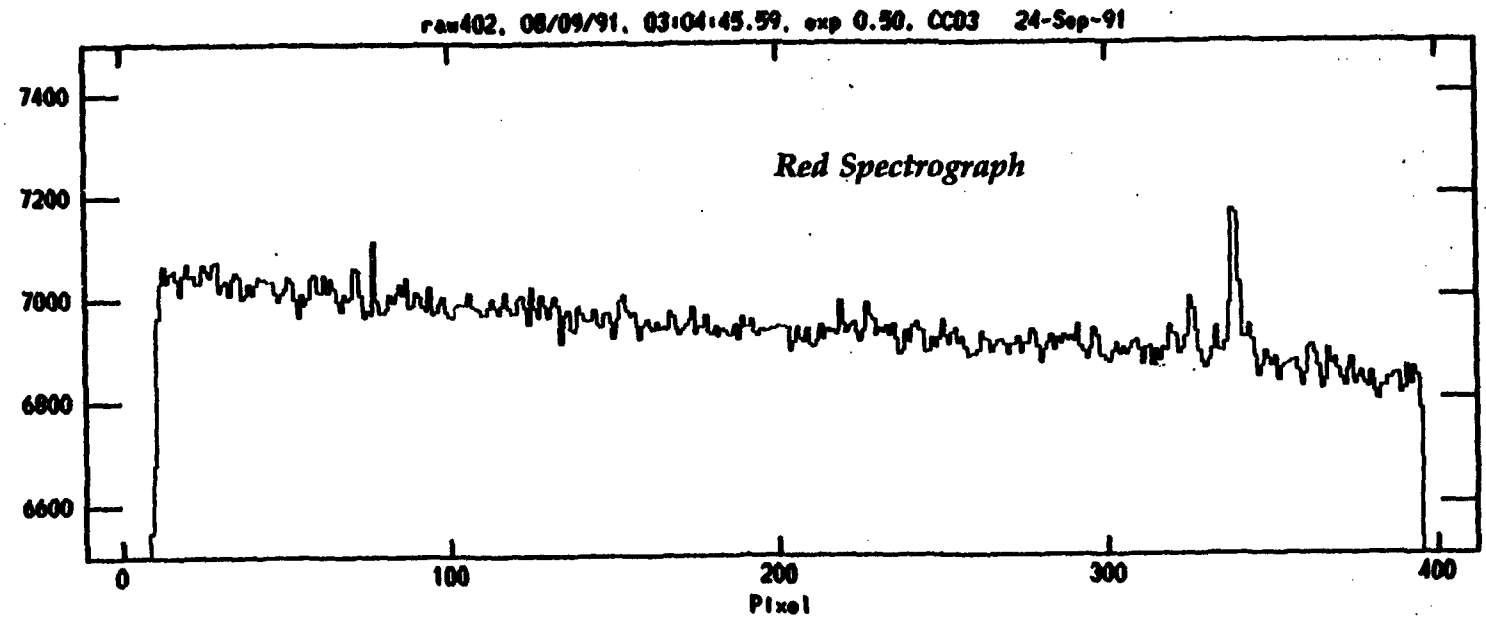

Figure 24b

thruster firing taken at the same time as the two spectra in Figure 24. Figure 24a shows the UV spectrograph, with the feature at ~100 pixels being the NH emission near 3370 Å. In Figure 24b, near pixel 350, the two OI lines at 6300, 6364 Å are shown clearly.

The processed data, Figures 25 and 26, in the upper panel show the spectrograms from which the integrated spectra in the lower panels were prepared. Each pixel in the image is a combination of twelve pixels on the CCD, summed in the spatial direction (i.e., along the slit). There was no doubt that the OI lines were responsible for the long-wavelength feature. The NH emission had been verified earlier. OH was not detected.

The spatial distribution of the emissions can be seen clearly in the spectrograms. The NH peaks 1.5 km in front of the orbiter, while the long-lived OI emission spreads into the wake. Some continuum emission in front of the Shuttle is seen in the band 6300 - 8000 Å, consistent with the spatial region defined by the NH emission about 1.5 km in front of the orbiter. It is noteworthy that the OH band at 3060 Å is not detectable in the UV spectrum.

The 6-channel imagers were not quite ready for a good experiment. The UV bandpass filters were supplied without red blocking filters which complicated the assembly. Some of the channels allowed light to leak around the filter requiring more careful assembly and probably a small loss of aperture. This loss will not hurt the performance very much since the image is intensified. We were developing better techniques for manufacture and assembly of the imager.

Images were recorded but did not contribute to the science product.

5.4 Conclusions

1) The OI (6300, 6364 Å) emission has been positively verified as a strong emission arising from the interaction of the Shuttle thruster plumes with the local oxygen environment through which the Shuttle is passing.

2) The expected emission from OH was not detected. Since we had optimized the sensitivity at that wavelength, we are satisfied the emission rate is below our threshold of detection.

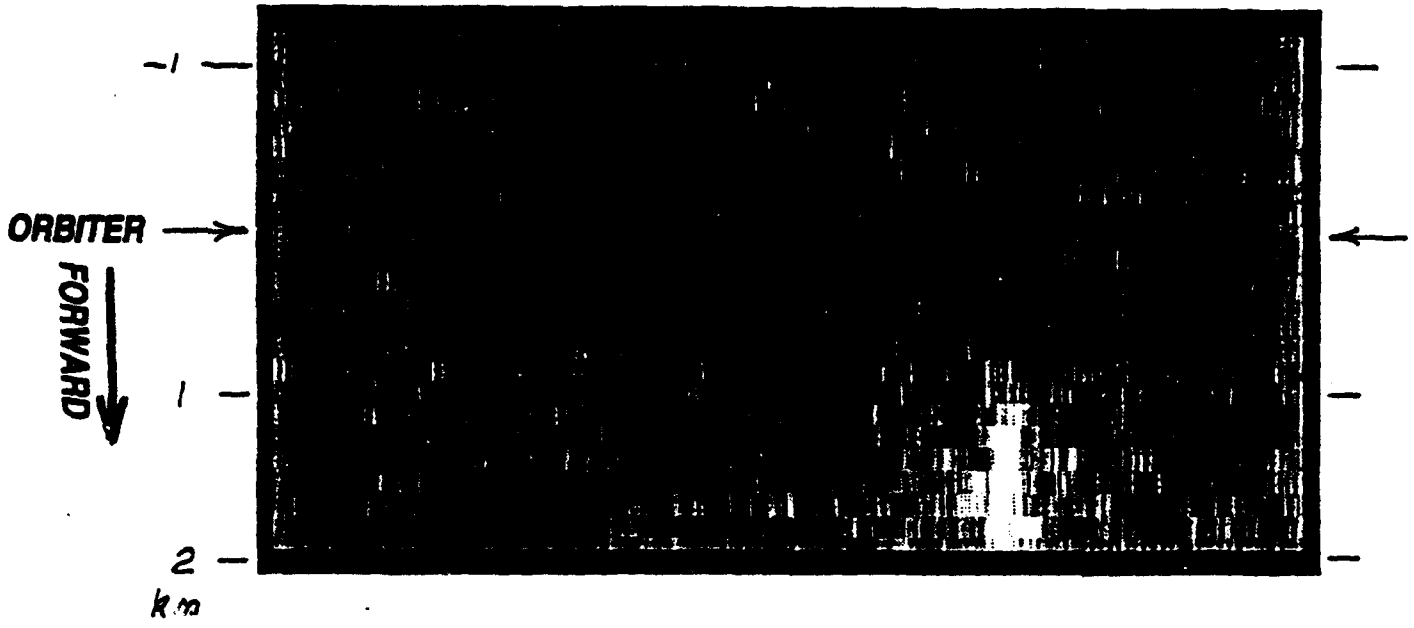

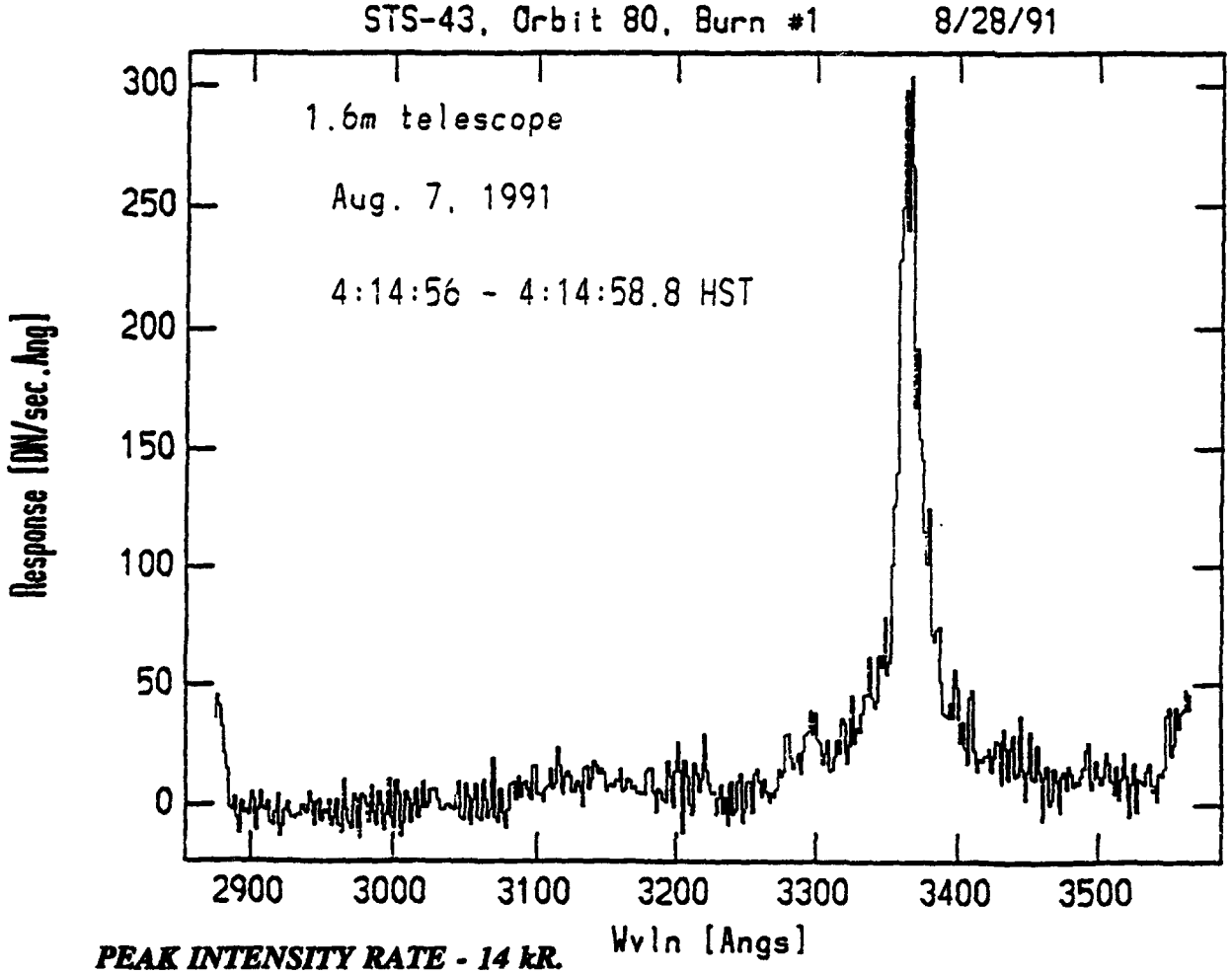

PEAK INTENSITY RATE - 14 kR.

Figure 25

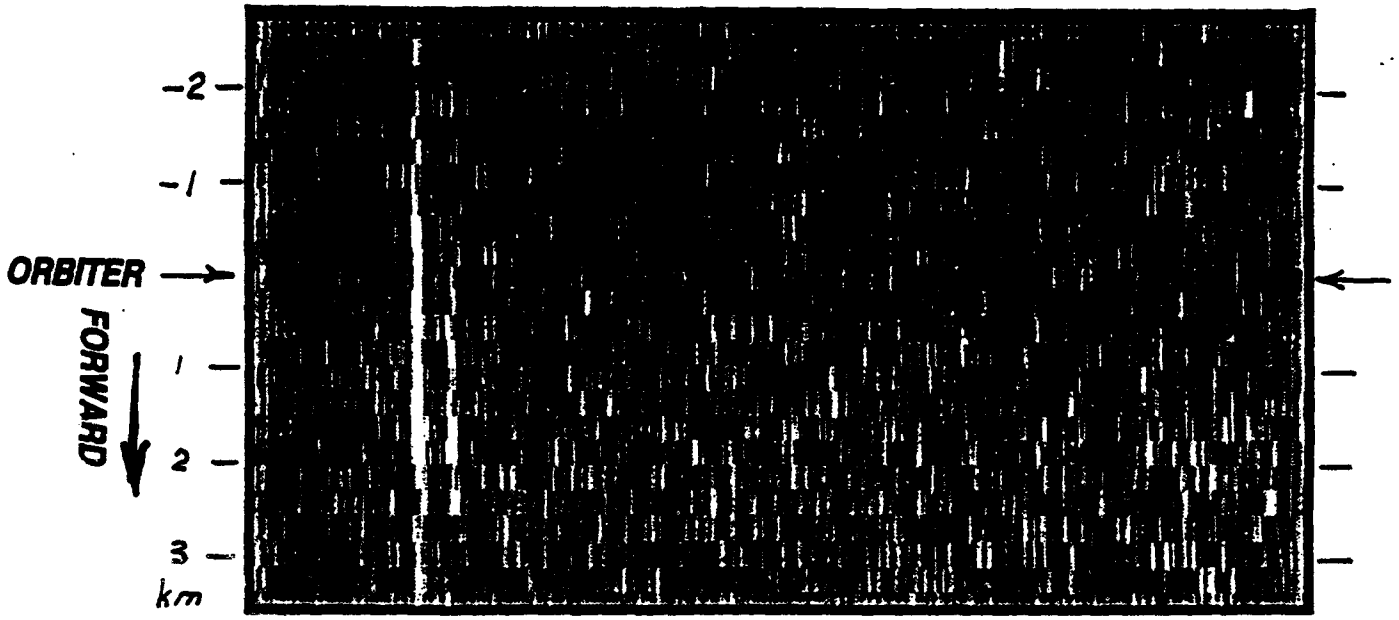
-2
-1
ORBITER
FORWARD
1
2
3
km

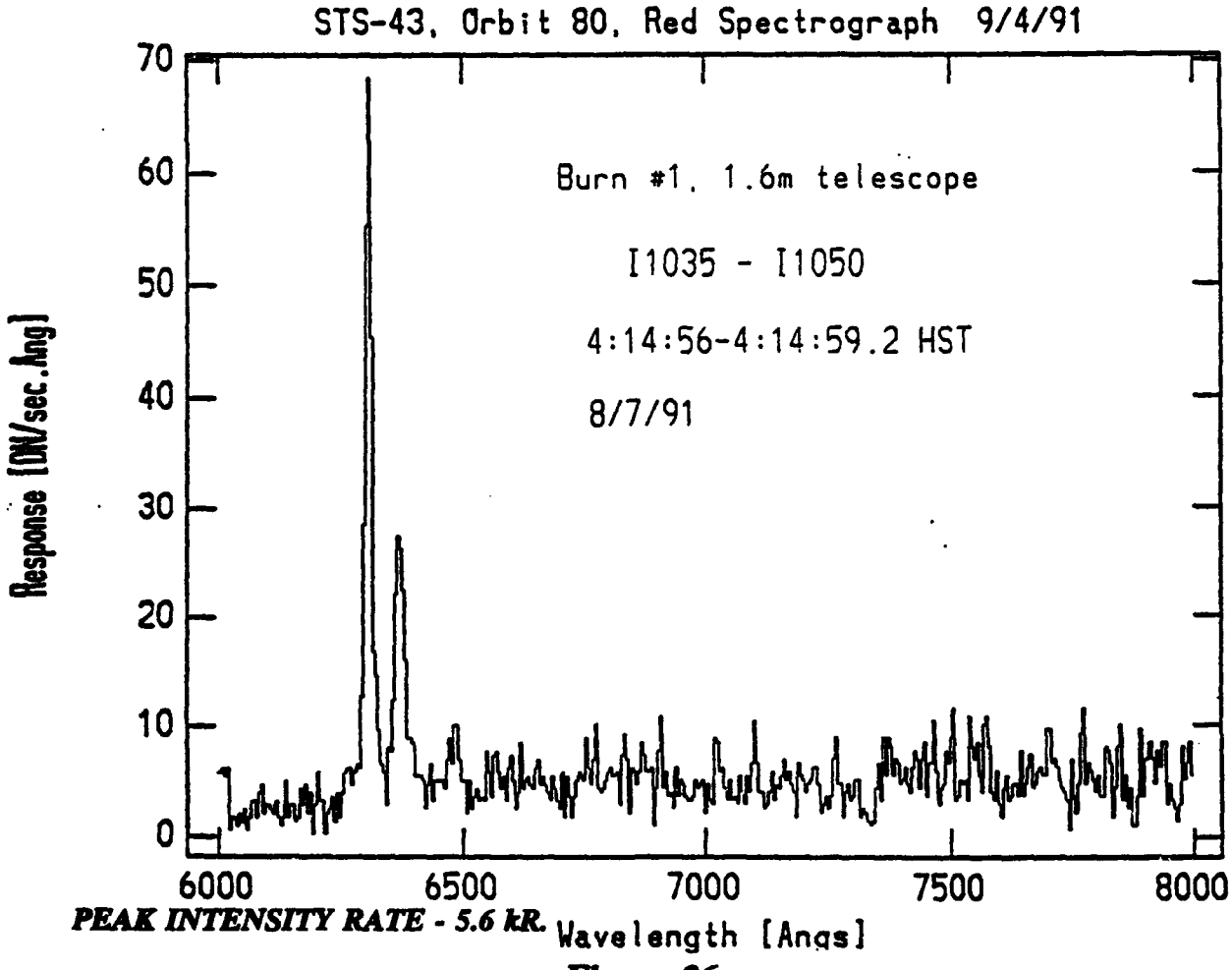
STS-43, Orbit 80, Red Spectrograph 9/4/91
Burn #1, 1.6m telescope
I1035 - I1050
4:14:56-4:14:59.2 HST
8/7/91
Response [DN/sec.Ang]
70
60
50
40
30
20
10
0
6000
6500
7000
7500
8000
PEAK INTENSITY RATE - 5.6 kR.
Wavelength [Angs]

Figure 26

3) The 6-channel imagers produced some good images but were compromised by light scattered around the filter. Better internal blocking is required. Better filters were required.

4) Since the primary emissions have been identified, the next step is to study the continuum more closely and determine its relationship to the interaction. This means returning to lower resolution spectrographs.

6. Shuttle Mission STS-44 (November 24, 1991)

The experiment during this opportunity used an almost identical setup as for STS-45 (Section 5). However, some improvements were made in software and the imagers. Better filters were purchased. The coverage afforded by the combination of filters and spectrographs is illustrated in Figure 27. The guiding spectrum shown is that obtained from STS-41 early in the program. The UV (#1) and red (#2) spectrograph ranges are shown as heavy black bars. The six bandpass filters used in the 6-channel imager are also plotted on this old spectrum. Figure 28 shows the organization of the six fields of view on the CCD, and the filters for each channel are identified. The experiment was identical for the BDT and the 1.6-meter mount instruments. Excellent data were obtained from the 1.6-meter mount experiment. We have spent most of our time preparing those data for analysis. Data were recorded from the BDT, but a close inspection has not yet occurred.

6.1 Results

Good spectral data were recorded on two Shuttle passes, orbits 6 and 37. The data will not be presented here because of their similarity to previous spectra. However, for the second opportunity, orbit 37, the spectrograph slit was oriented 90° to the trajectory to see if we could measure the spatial extent of the emission. Good data were recorded.

The imaging was quite successful during the mission. Figure 29 shows a series of contiguous exposures beginning shortly before the thruster firing. The clear channel, center right, shows the development of the plume. Varying levels of signal were detected in the other channels. Note that the framing rate was 0.5 sec. Figure 30 can be made into a transparent overlay for Figure 29 which then

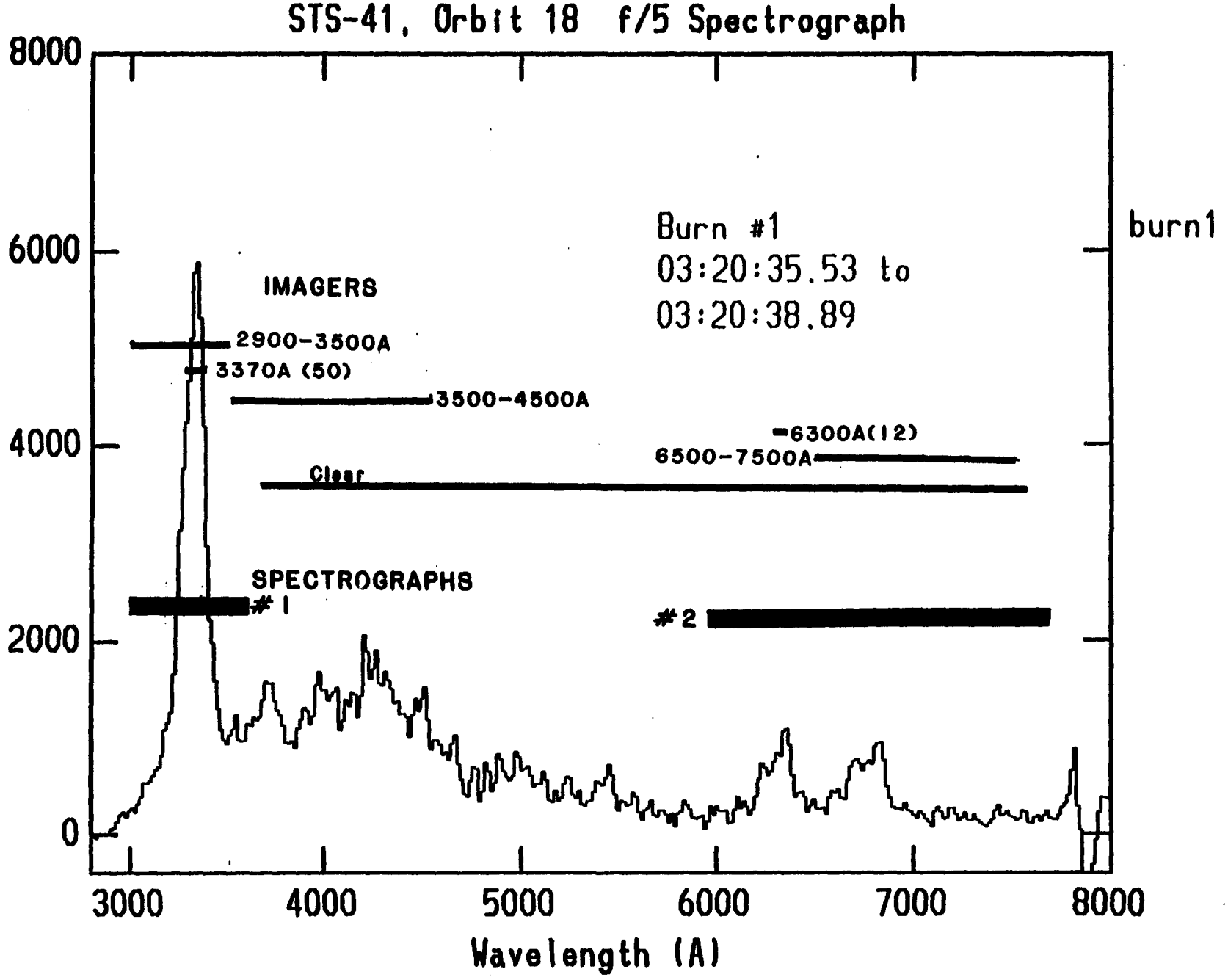
STS-41, Orbit 18 f/5 Spectrograph
8000
6000
4000
2000
0
DN
Burn #1
03:20:35.53 to
03:20:38.89
burn1
IMAGERS
2900-3500A
3370A (50)
3500-4500A
6300A(12)
6500-7500A
Clear
SPECTROGRAPHS
#1
#2
3000
4000
5000
6000
7000
8000
Wavelength (A)

Figure 27

STS-44 Imagers

1.6m Telescope System

Orbit 6, 11/24/91

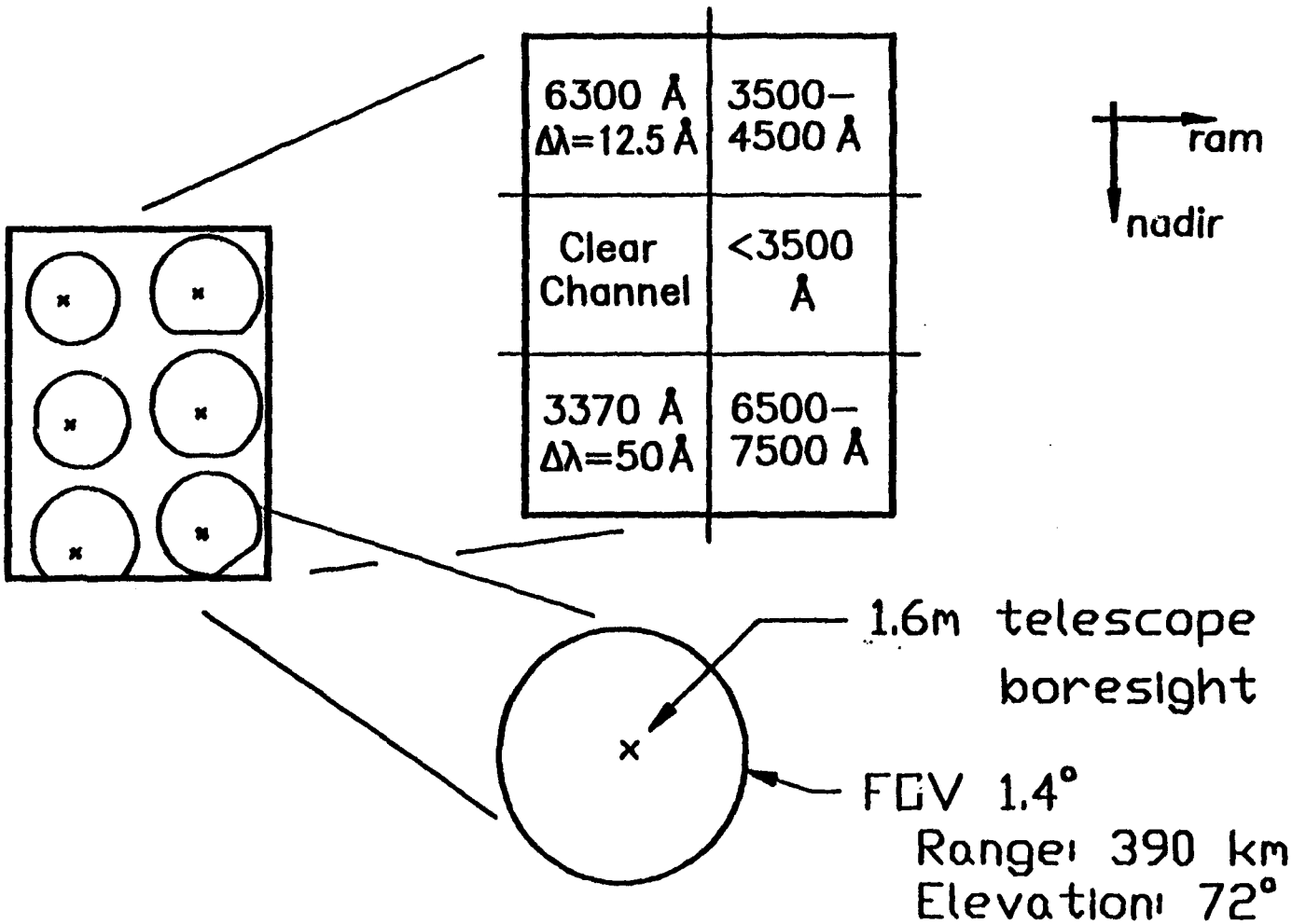

Figure 28

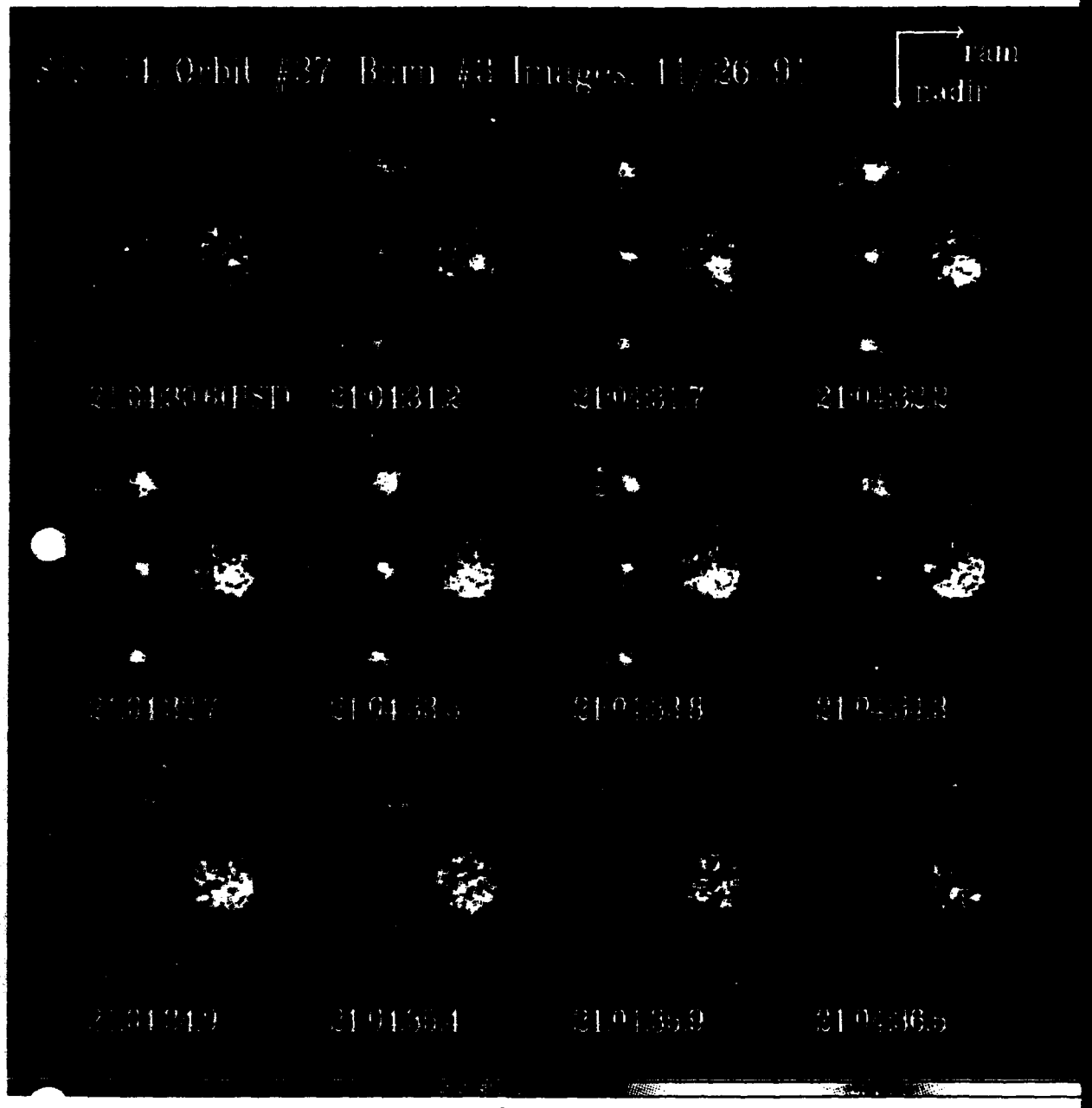

Figure 29

STS-44 Orbit 6, 11/24/91
1.6m Telescope System

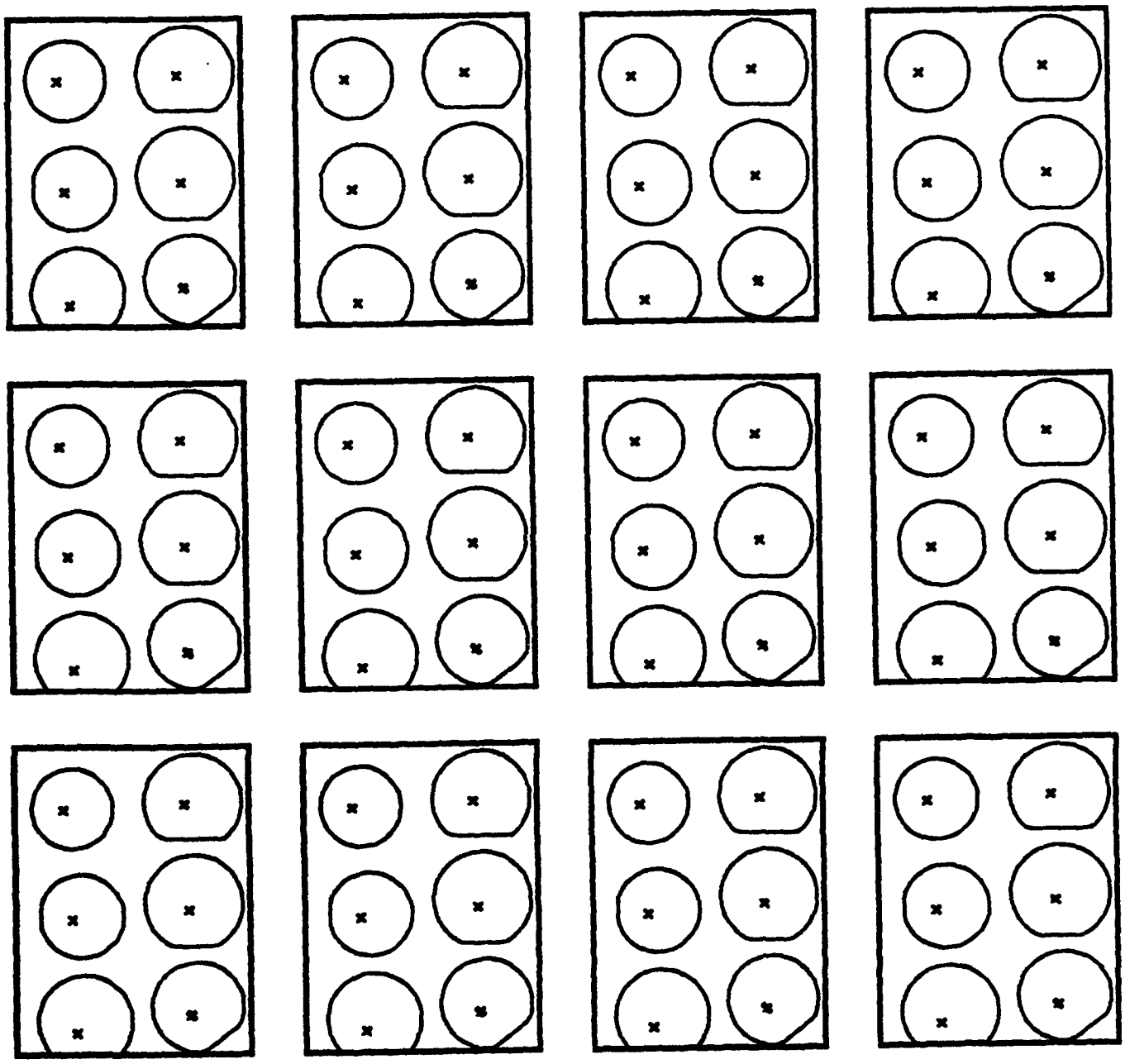

Figure 30

shows the extent of each imager; the "x" marks the common boresight. The images were processed in various ways. As an example, two contour plots from the 300 -350 nm channel, Figures 31 and 32, show the difference in the emission envelope between the beginning and end of the thruster burn. Comparative studies, as illustrated in Figures 33 and 34, are possible with these image data. The key to the image analysis is the comparison with the modeling done with the SOCRATES code. A selected data set has been forwarded to E. Murad for further analysis. The bulk of the data is available with analysis software.

We were disappointed to discover that the center of the narrow band filter on the 6300-Å channel had shifted off center enough to exclude that emission from detection.

6.2 Conclusions

1) The development of the thruster plume was recorded at 0.5 sec intervals during two passes of the orbiter over AMOS.

2) Excellent images and spectra were recorded and preliminary data analysis is complete.

3) The experimental equipment worked well.

4) For future opportunities we will use still lower resolution to record the continuum and separate it from the stronger emissions.

5) We observed only that part of the 6300, 6364-Å emission from OI atoms which had taken up the velocity of the Shuttle. We expect much more of the forbidden OI emission to be excited but not tied to the orbital system. On future opportunities we will use a broader angle camera from the ground to look for the 6300-Å emission trailing the orbiter.

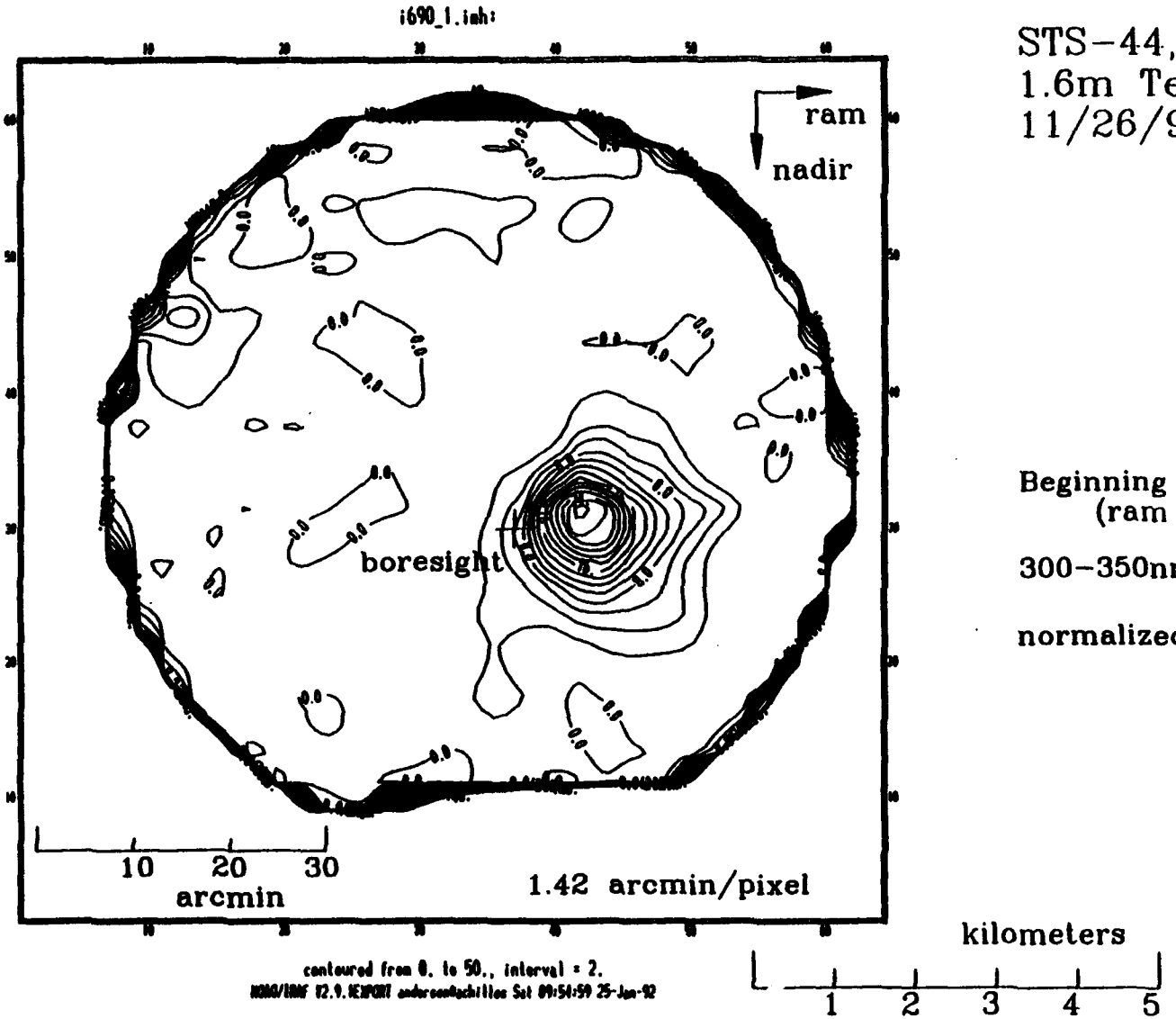

STS-44, Orbit #37
1.6m Telescope System
11/26/91

Beginning of Burn #1
(ram burn)

300-350nm channel

normalized to night sky

Figure 31

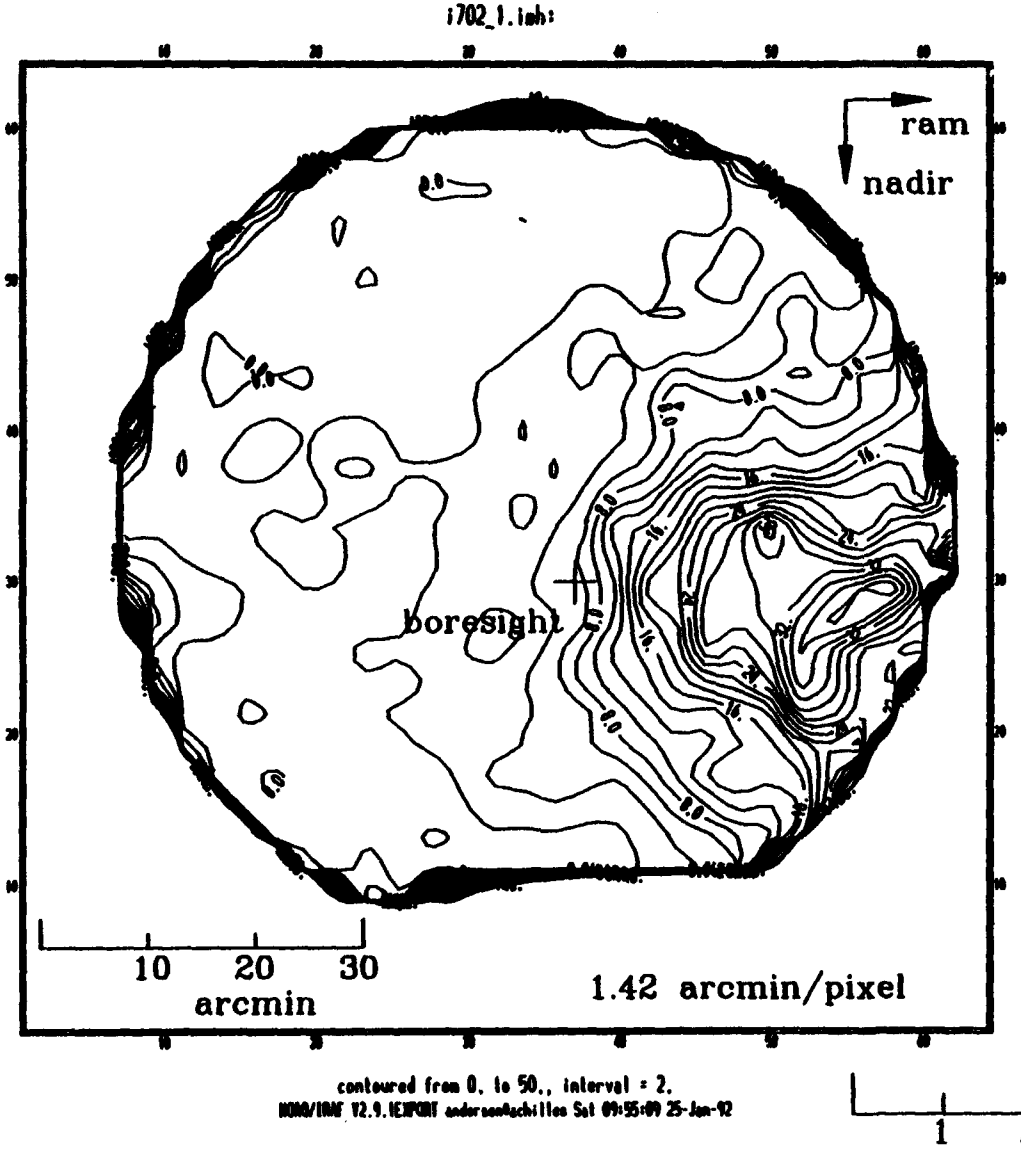

STS-44, Orbit #37
1.6m Telescope System
11/26/91

End of Burn #1
(ram burn)

300-350nm channel

normalized to night sky

kilometers

1 2 3 4 5

Figure 32

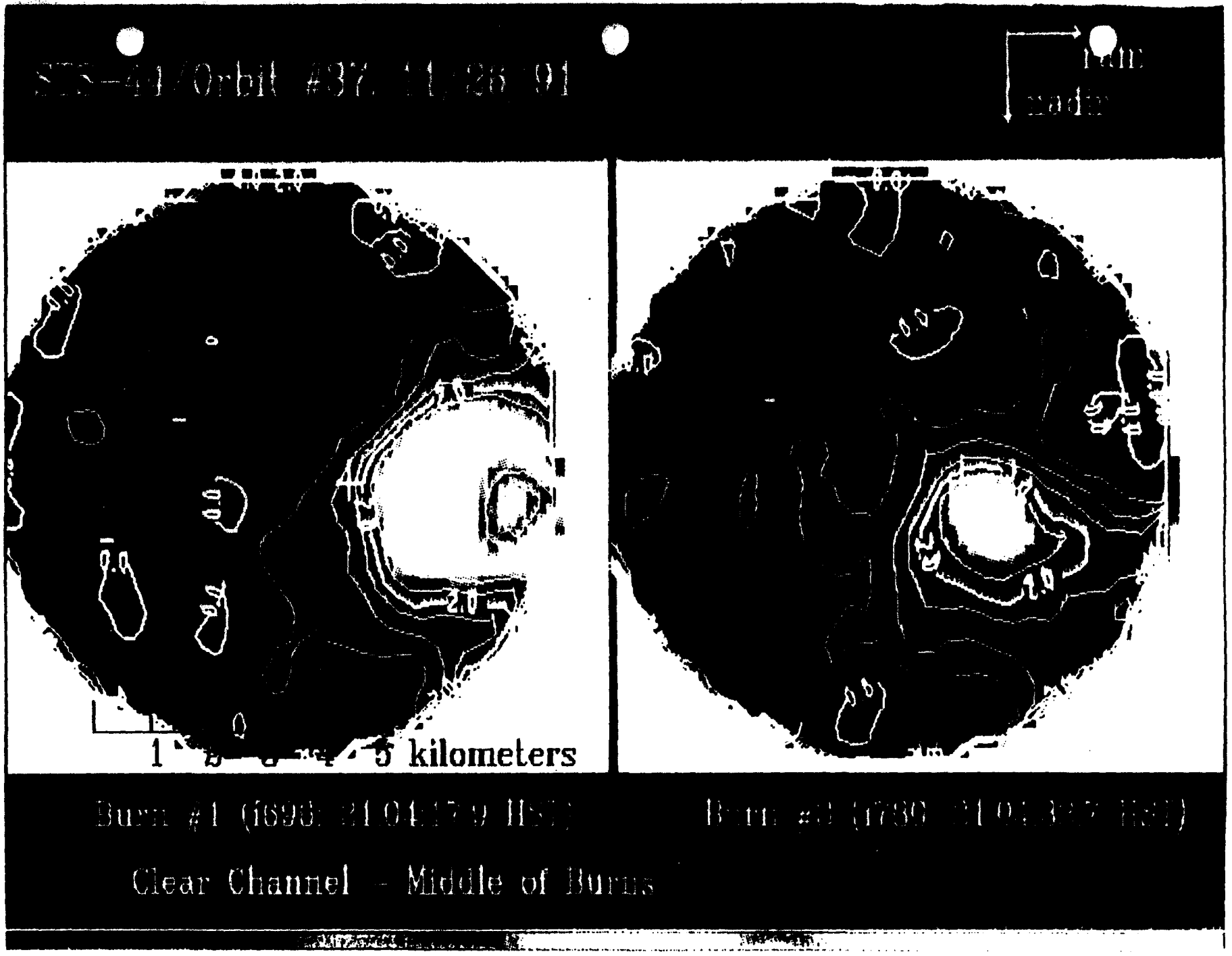

Figure 33

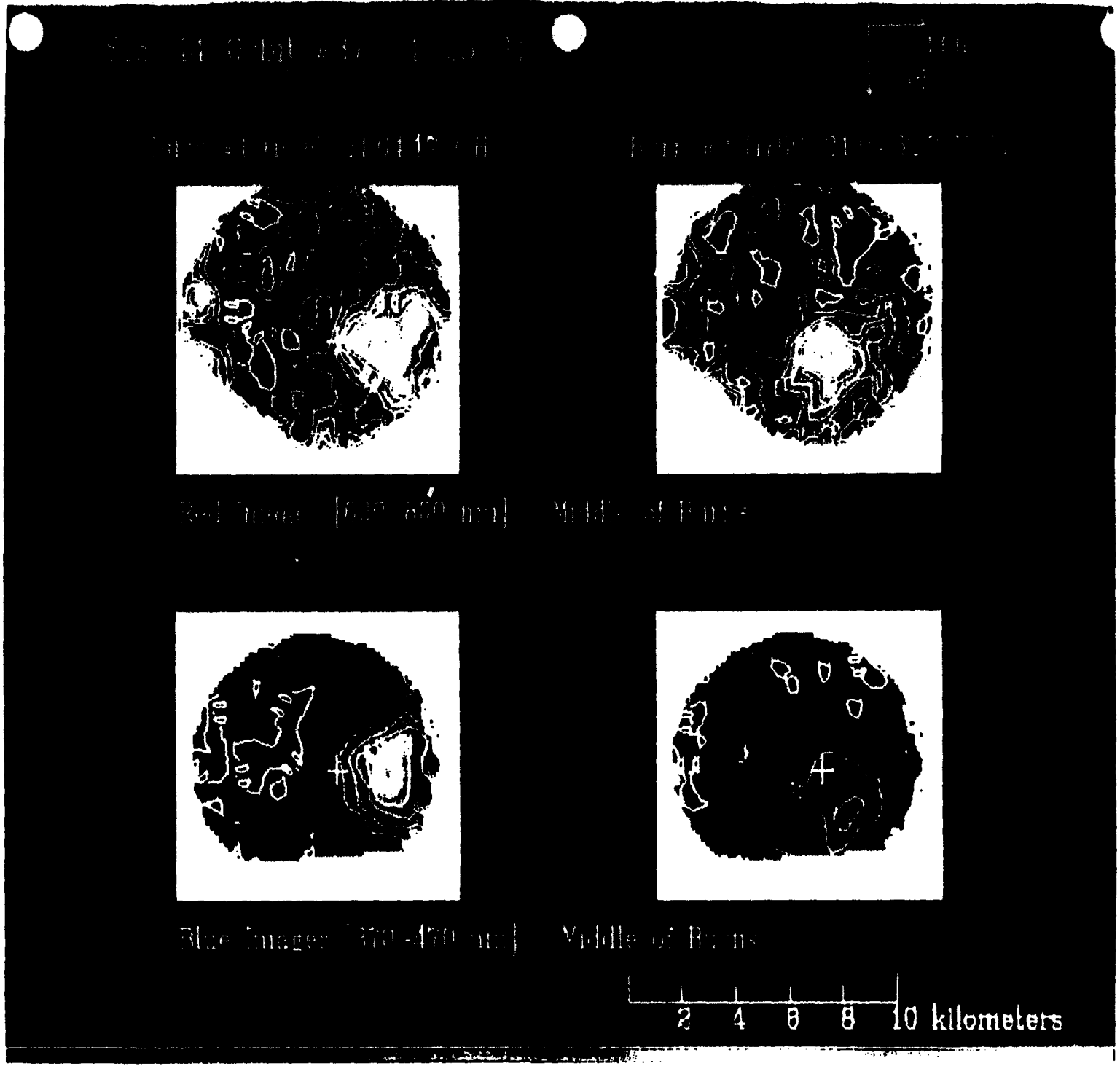

Figure 34

APPENDIX A

"Observations from AMOS of the Second and

Third Stages of the STRYPI-XI Rocket"

by

D. J. Knecht, A. L. Broadfoot, P. Sherard, I. L. Kofsky, D. L. A. Rall,
E. Murad, C. P. Pike, A. T. Stair, Jr., and L. Twist

OBSERVATIONS FROM AMOS OF THE SECOND AND THIRD STAGES OF THE STRYPI-XI ROCKET

D. J. Knecht,[1] A. L. Broadfoot,[2] P. Sherard,[2] I. L. Kofsky,[3] D. L. A. Rall,[3]
E. Murad,[1] C. P. Pike,[1] A. T. Stair, Jr.,[4] and L. Twist[5]

ABSTRACT

We report in this paper the results and preliminary analysis of measurements conducted at the AMOS facility of the recent SDIO Bow Shock experiment, which was initially designed to study the signature of the bow shock of rockets. Our primary objective was the study of the interaction of the exhaust of the engine burns with the atmosphere, after cooling had taken place. In fact, most of the data turned out to be related to the hot exhaust. We derive an approximate temperature of 1800-2200 K for the solid alumina particles at the exit of the rocket engine.

INTRODUCTION

The Spacecraft Interactions Branch of Phillips Laboratory (PL/WSSI) at Hanscom AFB, Massachusetts, undertook to make several observations of the STRYPI-XI rocket flight from the Air Force Maui Optical Station (AMOS) on the island of Maui. Our observations consisted of two instruments brought from the mainland and three supplied by AMOS. The AMOS facility was responsible for the difficult task of tracking. The results that will be presented in this paper are very preliminary in nature, are subject to change and reinterpretation.

EXPERIMENT

The cartoon of Figure 1 illustrates the location of AMOS (on Maui) relative to the launch site (on the island of Kauai) and the flight path of the rocket. During its second- and third-stage burns, the rocket is between 250 and 400 km from AMOS. These distances, along with the low altitude of the trajectory, result in elevation angles lower than AMOS normally can track, but special efforts by AMOS personnel resulted in full coverage from second-stage ignition through third-stage burnout.

1. Phillips Laboratory, PL/WSSI, Hanscom AFB, MA, 01731.
2. Lunar and Planetary Laboratory, University of Arizona, Tucson, AZ, 85721.
3. PhotoMetrics, Inc., Woburn, MA, 01801
4. A. T. Stair Associates, Bedford, MA, 01730
5. Rockwell Power Systems, Puunene, Maui, HI

The instruments chosen included two that were developed for PL/WSSI at the University of Arizona: (1) an ICCD spectrograph and (2) a set of banded imagers. They also included three that are part of the AMOS complement: (3) a platinum-silicide IR camera, (4) the 1.2- and 1.6-mount acquisition telescope systems, and (5) the AMTA long-wave IR sensor. Several other AMOS sensors were also operated.

1. Spectrograph

The complete spectrograph instrument includes its own telescopic foreoptics and a spectrograph head. The spectrograph, shown schematically in Figures 2 and 3 will be described only briefly here. The telescope is an 8-inch f/5 parabolic reflector used in a Newtonian telescope configuration. The first image, formed just outside the telescope tube, is reimaged onto the spectrograph slit by a lens inside the spectrograph head, changing the f-ratio to f/1.1 to match that of the spectrograph. The spectrograph itself consists of the entrance slit, a concave holographic grating, and an intensified CCD detector in the focal plane. The concave grating images the slit on the focal plane, preserving spatial information in the direction of slit width and spectrally dispersing the image in the direction of slit width. A monochromatic image of the slit covers an area of 3 by 192 pixels on the ICCD. In the direction of dispersion there are 384 pixels, which cover the spectral range of 300 to 800 nm, so the nominal spectral resolution is about 4 nm. The intensifier used for this mission had an S-20 photocathode, and it was operated with a gain sufficient that single photons were counted.

The detector electronics is controlled by 8088 and 80286 computers that permit great flexibility in reading out and processing the detector output. At a sufficiently slow exposure rate, it would be possible to read out and store each of the 73,728 pixels in the spectrograph image. For this mission, an acceptable exposure rate was achieved by reading every pixel in the spectral direction but summing groups of 16 pixels in the direction of slit length. The effect is to break the slit into twelve segments (192 divided by 16) of spatial information. The exposure interval was about two seconds. (The electronics was shared by the ICCD of the banded imagers.) The maximum data rate was limited by the real-time storage of data to an optical disk.

To provide the required pointing, the spectrograph was mounted on the side of the AMOS 1.6-meter telescope. During much of the flight, this mount was controlled by the Phillips Laboratory Advanced Modular Tracker, which provided excellent tracking. Last-minute changes made by AMOS in the settings chosen to achieve best coverage of the trajectory precluded our making an intended offset in pointing the instrument; the offset would have centered the field of view slightly behind the rocket and farther back in the plume. Therefore, the center of the slit was located on the 1.6-meter boresight. It was also intended to orient the slit perpendicular to the velocity vector in order to cut across and sample the plume as shown schematically in Figure 4. This was of marginal value on this mission partly because the phenomena were of small scale and at a large distance from AMOS. If we project a single slit segment (3 by 16 pixels) to the distance of STRYPI-XI (300 km at third-stage ignition), we find the field of view covers about 100 by 500 meters, while the maximum dimension of the detectable plume and bowshock in the IRCCD images is only about 190 meters, so much of the region of interest falls within the

smallest resolvable element.

2. *Banded Imagers*

This instrument is shown schematically in Figure 5. It has its own telescope, which is the same as that of the spectrograph except that its primary mirror is ten (rather than eight) inches in diameter and has a UV-reflective coating. After passing through its focus, the telescope beam is recollimated by an f/5 lens. In the collimated region, its circular cross section is divided into six pie-shaped wedges, each of which contains a filter followed by a smaller-diameter f/2 reimaging lens. Six small images are formed in a circular arrangement in the common focal plane. A rigid assembly of six fiberoptic couplers conducts the images to the photocathode of an intensified CCD detector, which is identical to that of the spectrograph. The six images form a two-by-three arrangement that covers one half (384 by 288 pixels) of the full 384-by-576-pixel CCD array; each image covers an area of 128 by 144 pixels.

It was discovered (too late to reorder) that the UV filters obtained for these imagers had very serious leaks at longer (red) wavelengths. In an effort to recover from this misfortune, two of the channels that would have carried other filters were given over to measurement of the red leak in the hope that this would not be too large and could be subtracted as a background correction from the UV data. The remaining four channels carried narrow-band filters centered at wavelengths (in nm) of 309.0 (2.0 width), 337.1 (5.0 width), 630.0 (1.25 width), and 732.0 (1.25 width). In addition, each of the two UV channels had a red-blocking filter. Each of the two red-leak monitoring channels carried the same two filters as the corresponding UV channel plus a UV-blocking filter.

The CCD readout is performed by the same electronics system that services the spectrograph and is similar except that pixels in a group of two by two (rather than one by sixteen) are summed and stored.

3. *PtSi IR Camera*

This instrument, known at AMOS as the IRCCD, is an infrared camera built some years ago by Dr. Freeman Shepherd and his group.[1,2] It is mounted with other IR instrumentation on the side Blanchard surface of the 1.6-meter telescope; the beam is brought out to this location by inserting a flat tertiary mirror to intercept the beam from the secondary mirror. The camera consists of a platinum silicide array detector of 64 by 128 pixels and the electronics and cooling needed to operate the array. The overall shape of the array is square, since each pixel is twice as long as it is wide. A final refractive lens near the detector, which images the beam onto the detector, can be selected to change the beam to either f/10 or f/3, providing an angular field of view of either three or one arc minute square. For this mission only the three-minute field of view was used.

The detector is a monolithic PtSi Schottky-barrier device (detectors and CCD on the same silicon substrate). It is operated at a temperature of 65 K, with a readout rate of 30 exposures

per second. The pixel values are digitized by electronics on the telescope near the detector, and the 12-bit digital values are transmitted to the control room, where they are recorded digitally. They are also converted (with eight-bit accuracy) to a standard video signal that is displayed and recorded in video format.

One of several filters in a filter wheel can be selected from the control room. Figure 6 shows the estimated instrument response during the STRYPI-XI mission. It results from three factors: (1) The detector has its maximum sensitivity (curve b) near three microns and has fallen by nearly an order of magnitude at five microns. (2) The filter used for this mission is a long-pass filter that blocks wavelengths shorter than 2.5 microns. (3) The estimated transmission of the atmosphere varies greatly, with opaque regions around 2.7 and 4.3 microns. The result of folding all three curves together is the overall relative response shown in Figure 6. However, better characterization of the IRCCD is needed.

4. Acquisition Telescopes

The Acquisition Telescope Systems on the MOTIF 1.2-meter mount (MATS) and AMOS 1.6-meter mount (AATS) have three selectable fields of view: 0.1, 0.5, and 3.0 degrees. Because of the requirements of trackers, only the 3-degree field of view was used on this mission. The two narrower fields of view use a 22-inch primary mirror, while the 3-degree field uses an 8-inch primary. Both MATS and AATS use ISIT cameras with S-20 photo-cathode at the focal plane, but they are of different vintage and design, and our experience is that the MATS is more sensitive and produces better images. The data from these cameras are recorded on standard videotapes.

Both of these systems performed well during this mission. Each was serving not only to produce image data for scientific purposes but also to provide the signal on which the tracking depended. Our usual procedure is to have the sensitivity threshold set very close to dark-sky background; in this case our request was that it be kept as low as possible, consistent with the tracking requirement that background be low. In at least one instance these conflicting goals caused a temporary loss of track; however, the images, especially from the MATS, are excellent and show good detail.

5. AMTA Sensor

The AMTA is a 5-by-5 array of cadmium-doped germanium (photo-conductive) detectors. The array is operated at a temperature of 12 K and is sensitive over the spectral range of 3 to 22 microns. It is located on the 1.2-meter B-29 telescope. A filter wheel carries seven bandpass filters for spectral analysis. This instrument can be used as a tracker, placing the tracked image at the common corner location of four of the 25 detectors and using their outputs to derive error signals. At the same time, the secondary mirror can be tilted slightly to shift the image from this tracking position to another position at the center of another detector in the array. This shifting is done at a frequency (square-wave) of 50-Hz, so the image can be used for tracking at the four-detector corner and also for radiometric measurement at the single-detector location.

6. Other Sensors

Four other AMOS instruments, the Low-Light-Level TV (LLLTV), the B29 boresight camera, the Contrast Mode Photometer, and the ASR boresight camera were also operated and recorded.

PRELIMINARY RESULTS

1. Spectrograph

This instrument was designed to provide a first basic survey of phenomena for which no previous spectral information is known; it emphasizes high sensitivity (f-ratio of 1.1 and a photon-counting focal plane) and broad spectral range (300-800 nm), while sacrificing optical quality and spectral resolution. It was the first spectrograph used to find the spectral regions of shuttle-plume emissions and was chosen for this mission for the same reasons. All of the sensitivity was not needed here; the STRYPI-XI plumes were bright enough to saturate the central region of the detector at some times. The saturation was not enough to preclude obtaining satisfactory spectra.

The sacrifice in optical quality is not serious if the emissions being studied do not include components that differ greatly in magnitude, as is the case for shuttle plumes.[3,4] In the case of STRYPI-XI, the brightness of the hot plume core prevented seeing any much weaker emissions that may have been present. Both optical aberrations and scattered light contribute to a broadening of the image that is great enough to preclude gaining much valid spatial information along the slit length.

Raw data from the spectrograph during the period of second-stage ignition are shown in Figures 7, 8, 9, and 10. At the top is shown the focal-plane image. At the bottom are shown twelve traces, which are the spectra for each of the twelve slit segments. In Figure 7 the burn has not yet begun. The burn begins at some time during the two-second exposure of Figure 8, burns during all of Figure 9, and is even brighter through Figure 10. A similar sequence for second-stage burnout is shown in Figures 11, 12, 13, and 14. In this case, the intensity, which has greatly diminished (Figure 11) starts to increase (Figure 12) to produce a very bright burst (Figure 13) before disappearing completely (Figure 14). The units of DN (data number) in these figures is the digital output of the A/D converter that measures the pixel charge. The calibration response curve must be folded into these values to obtain the spectrum in units of Rayleighs per nanometer. The transmission of the atmosphere must also be accounted for, especially at the shorter wavelengths.

The spectra obtained throughout third-stage burn until tracking was lost have a similar appearance. Figure 12 shows the spectrum observed during a two-second exposure starting about ten seconds after third-stage ignition. These have been converted to units of brightness per unit wavelength. They have also been smoothed by integrating over four pixels in the dispersion direction. This is appropriate to the spectral resolution of the instrument; retaining each pixel

in that direction is oversampling. One feature seen in these spectra is a change in slope at around 430 nm.

A common feature of all spectra is the absence of any line or band structure of the sort one might expect from chemical interactions, and which we have observed in space shuttle plumes. If such emissions were present during the STRYPI flight, they were too weak to be detected in the presence of the very bright continuum spectrum shown in these figures.

2. Imagers

This type of banded imager is useful when the object being viewed has certain characteristic emissions that match the filters chosen; it is less appropriate (and must possess much better rejection) when the emissions are overwhelmingly dominated by a continuum. The imagers operated properly and recorded images throughout the flight, but they were most often saturated in the center, with the image blooming well beyond the true spatial extent of the plume. Because long wavelengths dominated in the emissions, the attempt to solve the red-leak problem by monitoring failed, and the UV channels were swamped by longer wavelengths. Moreover, a readjustment of bias level just prior to launch inadvertently caused there to be a sensitivity threshold well above zero, so even if the bright plume were absent, much dimmer objects could not have been detected. Finally, the angular size of the phenomena was much smaller than the imager field of view, so the spatial resolution was poor.

Most of the images conform to the foregoing description, consisting of a single bright blur spilling over into adjacent regions. A slightly more interesting example of these data is given in Figure 19, which shows the image at 732.0-nm wavelength with the exposure starting just after second stage burnout; it shows both the bright rocket plume along with the dimmer "smoke ring" left behind at second-stage ignition.

3. PtSi Camera

The camera performed as expected throughout the mission and produced continuous imaging as long as the object was tracked well enough to keep it within the three-minute field of view. In addition to the tracking by the mount itself (controlled by the Advanced Modular Tracker, as noted above), additional precision was obtained by use of a Hamamatsu tracker that actively controlled the flat tertiary mirror using error signals from the video output of the IRCCD.

The IRCCD observed the entire second-stage burn before tracking was lost. Tracking was recovered about three seconds after third-stage ignition and observations continued until the image was lost at or near third-stage burnout. A bowshock phenomenon was clearly observed for about 11 seconds. Between the nominal Star27 burnout and the IRCCD loss of track the bright plume did not disappear abruptly but dimmed gradually. First efforts have been directed to (1) a preliminary examination of the videotape images and (2) the development of software to process the 12-bit digital images. Figure 15 shows a processed image, when the bowshock was very pronounced.

4. Acquisition Telescopes

Like other instruments, these cameras were saturated in the regions of the hot plume core, and the images bloom to cover a much larger area. However, at larger distances from the rocket plume, the wide fields of these cameras have permitted observing the trail behind the rocket. The principal features are these: (1) At second-stage ignition, there is a large puff of material (the so-called smoke-ring) that is left behind as a glowing cloud that remains almost stationary. (2) During both engine burns, the plume leaves behind a brightly glowing trail. (3) During the coast period between second- and third-stage burns, the expended engine continues to leave a weaker glowing trail behind it. All of these features continue to glow until they leave the field of view. Figure 25 shows the "smoke ring" left behind at second-stage ignition.

5. AMTA Sensor

Although the data from this sensor have not been examined at this time, we expect to analyze them in the near future.

6. Other Sensors

The LLLTV, which has a very high magnification (4.4-minute field of view), observed second-stage ignition. Its image includes what appears to be a part of the preceding stage falling away. It also seems to show the plume cloud moving forward to surround the engine producing it. So far none of these data has received more than a cursory examination.

DISCUSSION

It seems likely that the spectra observed during the Antares and Star27 burns represent the radiation from glowing hot aluminum-oxide particles. In Figure 16 the spectra taken at about 14 seconds after third-stage ignition have been converted to units of energy and compared to black-body radiation at three temperatures. At the longer wavelengths, the data are fit fairly well by the black-body curves for 1800 or 2000 K, but for wavelengths shorter than about 450 nm the data are consistently higher than the black-body prediction. We expect that the discrepancy at shorter wavelengths will be resolved if we account for (1) the actual emissivities of the alumina particles and (2) the actual atmospheric transmission.

The detectable length of the plume and bowshock in Figure 15 is about 190 meters. At that point the rocket velocity should have been close to 5 km/s, traversing 200 meters in 40 milliseconds. If the observed radiation is grey-body emission from hot alumina particles, this 40 milliseconds must represent the time needed for the particles to cool enough to be undetected. Since the alumina must solidify before cooling further, the temperature will remain on a plateau at the melting point (2070 K) until all of the heat of solidification is radiated away and will then drop sharply. Tables 1 and 2 show preliminary calculations to estimate the radiation rates and solidification times for several particle sizes. The data appear to be roughly consistent with these estimates if the particle size is on the order of one micron.

The magnification of the IRCCD (three-minute FOV) was extremely well matched to the size of the observed bowshock, so it is possible to measure its spatial shape and dimensions quite accurately. The IRCCD line of sight to the bowshock was almost perpendicular to the velocity vector; this means that column lengths through the plume and shock are very simple, and relative volume radiances can be easily and accurately obtained from the images.

All of these three glowing features in the acquisition telescope pictures can be seen to be essentially at rest in the atmosphere by observing that spatial features within the glowing material do not move relative to stars within the field of view. Since the material left behind remains within the field of view for several seconds, while the blackbody radiation from the hot alumina must decay very much faster, another cause for the long-lasting radiation must be found.

One possibility is that chemical reactions occur in the interaction of the plume clouds and the ambient atmosphere. We presume that the principal rocket-fuel components are aluminum and ammonium perchlorate. Table 3 lists the main combustion products and typical values for their abundance and heats of formation. Also listed at the end are values for ambient atomic oxygen and chlorine. One can expect that eventually the only end products will be Al_2O_3 and chlorine. In the various reactions that occur to reach this condition, there appears to be a large amount of energy available to be dissipated in optical emissions. During this mission the spectrograph tracked the rocket closely, so we have no spectra of the glowing clouds, and the characterization of interactions of these gases with the ambient atmosphere must wait for another experiment. Potential sources of emission in the visible region of the spectrum, where the acquisition telescope detectors are sensitive, are AlCl, AlO, as well as high chlorides and oxides. For example, the reaction

$$O + AlCl \rightarrow AlO + Cl \qquad (1)$$

is exoergeic by 0.10 eV, since $D^\circ_o(AlO) = 5.25$ eV and $D^\circ_o(AlCl) = 5.15$ eV.[5] During the burn of the second stage, the vehicle was travelling at 0.25 km/s. This velocity is not enough to provide excitation of the products in reaction (1). In view of this, the surface recombination process suggested by Dimpfl[6] seems reasonable.

TABLE 1

Thermal Radiation Lifetime of Al_2O_3 Particles

Particle radius, r = 0.1 - 10.0 μm
Emissivity, ε = 0.04 (for particles of r = 1 μm[7])
Heat capacity, C_p = 0.7752 J/g-K
Density, ρ = 3.965 g cm^{-3}
Boiling temperature, T_{vap} = 2980 K
Melting temperature, T_{fus} = 2070 K
Heat of fusion, ΔH_{fusion} = 1071 J/g

Heat loss rate = Radiative loss rate

Heat loss rate = $(4/3)\pi r^3 \rho C_p (dT/dt)$

Radiative loss rate = $4\pi r^2 \varepsilon \sigma T^4$

$\therefore (dT/dt) = (3\varepsilon\sigma T^4)/(r\rho C_p) = (2.2 \times 10^{-13}\ cm\ K^3\ s^{-1})(T^4/r)$

T	dT/dt		
	r = 0.1 μm	r = 1.0 μm	r = 10.0 μm
2900 K	1600×10^3 K s^{-1}	160×10^3 K s^{-1}	16×10^3 K s^{-1}
2500 K	900×10^3 K s^{-1}	86×10^3 K s^{-1}	8.6×10^3 K s^{-1}
2100 K	400×10^3 K s^{-1}	43×10^3 K s^{-1}	4.3×10^3 K s^{-1}

An alumina droplet, whose r = 10 μm, and at T = 2900 K, cools to 200 K in 13 ms.

TABLE 2

Solidifying Time of Liquid Al_2O_3 Particles at the Fusion Temperature

Heat of solidification = Radiative heat loss

Heat of solidification = $(4/3)\pi r^3 \rho \Delta H_f$

Radiative heat loss = $4\pi r^2 \varepsilon \sigma T^4 t$

$t = (r\rho \Delta H_f)/(3\varepsilon\sigma T^4)$

Solidification time, $t_s = (6.2 \times 10^{15}) r/T^4$

$= (340\ cm^{-1}\ s)r$ at the fusion temperature (2070 K)

r	t_s
0.1 μm	3.4 ms
1.0 μm	34 ms
10.0 μm	340 ms

TABLE 3

Heats of Formation of Combustion Products of

Al-NH_4ClO_4 Solid Rocket

Species	Thermodynamic Abundance†	ΔH_f (kcal/mol)‡
AlCl(g)	0.052	-11
$AlCl_3$(g)	0.091	-139
Al_2O(g)	0.003	-31
AlO(g)	0.010	+22
Al_2O_3(s)	0.31	-397
Cl(g)	0.016	+29
HCl(g)	0.30	-22.06
OH(g)	0.010	+9.3
O(g)	Ambient	+60

† Shorr and Zaehringer.[9]
‡ Chase et al.[5]

LIST OF FIGURES

REFERENCES

1. Shepherd, F. D., and A. C. Yang, Silicon Schottky Retinas for Infrared Imaging, *1973 International Electron Devices Meeting*, Technical Digest, 310-313, 1973.

2. Shepherd, F. D., Silicide Infrared Staring Sensors, *Proc. SPIE, 930*, 1-12, 1988.

3. Murad, E., D. J. Knecht, R. A. Viereck, C. P. Pike, I. L. Kofsky, C. A. Trowbridge, D. L. A. Rall, G. Ashley, L. Twist, J. B. Elgin, A. Setayesh, A. T. Stair, Jr., and J. E. Blaha, Visible Light Emission Excited by Interaction of Space Shuttle Exhaust with the Atmosphere, *Geophys. Res. Lett., 17*, 2205-2208, 1990.

4. Broadfoot, A. L., E. Anderson, P. Sherard, J. W. Chamberlain, D. J. Knecht, R. A. Viereck, C. P. Pike, E. Murad, J. B. Elgin, L. S. Bernstein, I. L. Kofsky, D. L. A. Rall, J. Culbertson, Spectroscopic Observation of the Interaction Between the Atmosphere and Space Shuttle Exhaust in the Visible Region of the Spectrum, *In Preparation.*

5. Chase, Jr., M. W., C. A. Davies, J. R. Downey, Jr., D. J. Frurip, R. A. McDonald, and A. N. Syverud, JANAF Thermochemical Tables (Third Edition), Suppl. 1, *J. Phys. Chem. Ref. Data, 14*, 1985.

6. Dimpfl, W. F., Private Communication.

7. Jeffrey, W. A., Private Communication

8. Shorr, M., and A. J. Zaehringer, *Solid Rocket Technology*, p. 327, Wiley, New York, 1967.

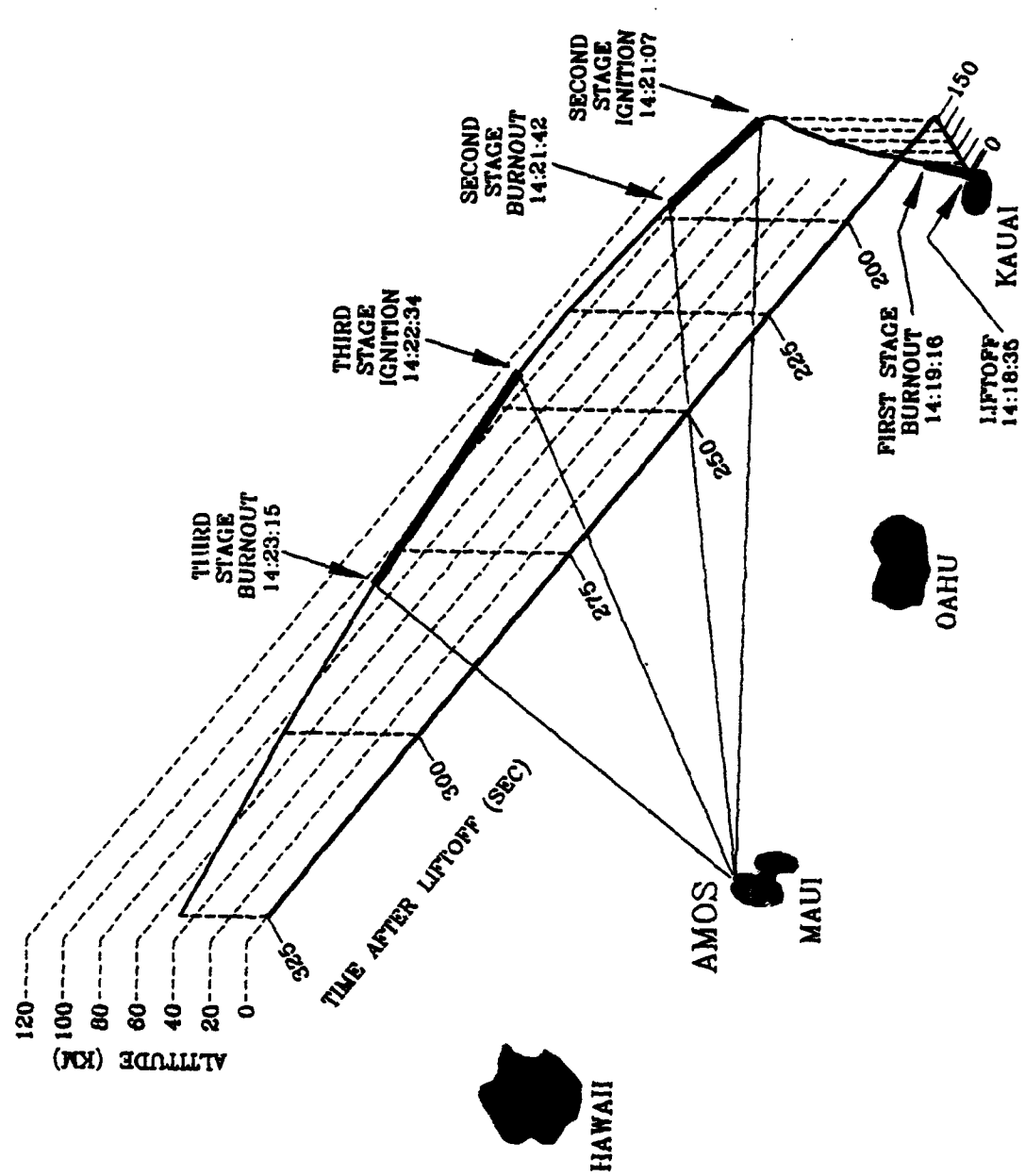
SECOND STAGE IGNITION 14:21:07
SECOND STAGE BURNOUT 14:21:42
THIRD STAGE IGNITION 14:22:34
THIRD STAGE BURNOUT 14:23:15
FIRST STAGE BURNOUT 14:19:16
LIFTOFF 14:18:36
KAUAI
OAHU
MAUI
AMOS
HAWAII
TIME AFTER LIFTOFF (SEC)
ALTITUDE (KM)
120
100
80
60
40
20
0
150
0
200
225
250
275
300
325

Figure 1

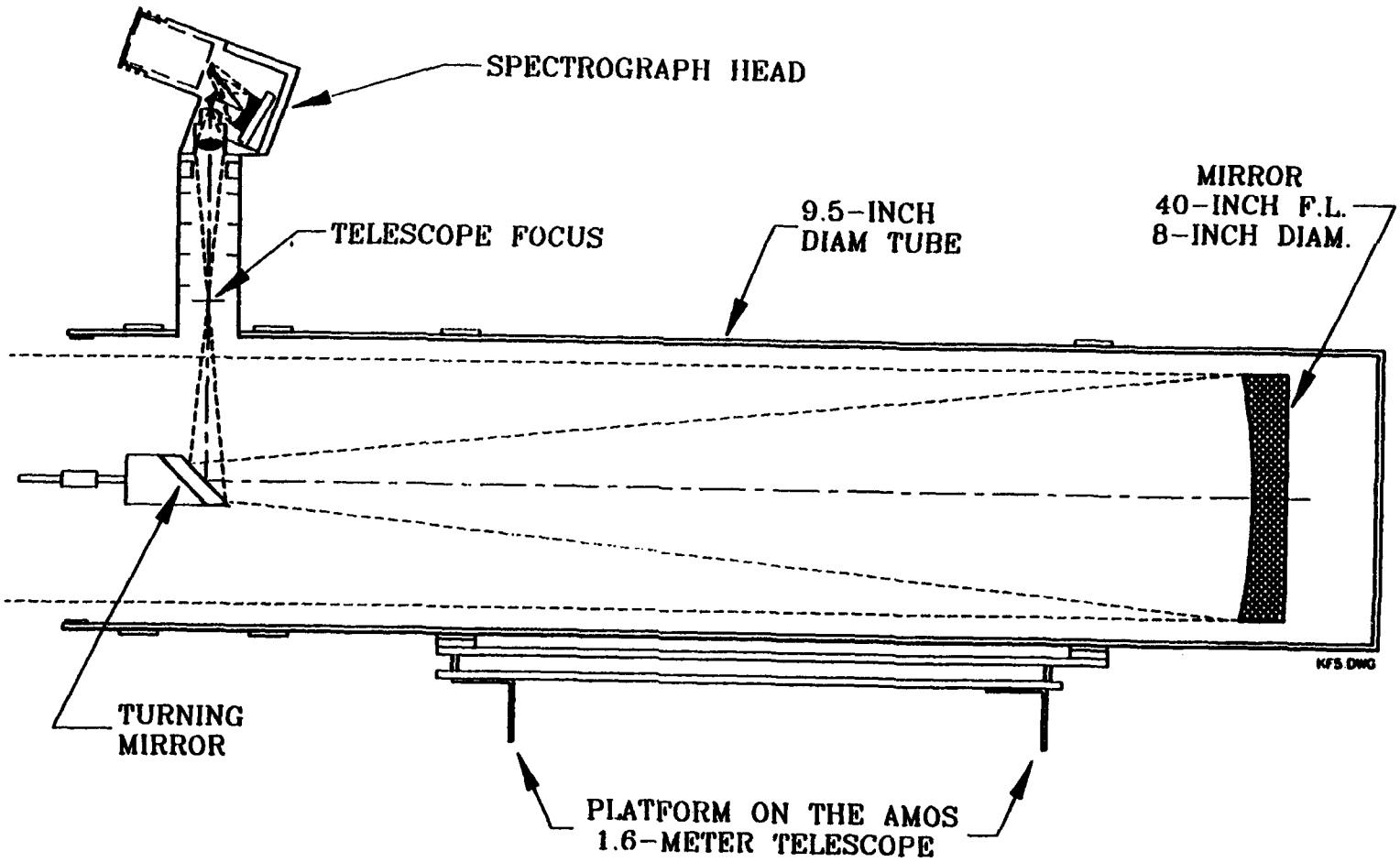
SPECTROGRAPH HEAD
TELESCOPE FOCUS
9.5-INCH
DIAM TUBE
MIRROR
40-INCH F.L.
8-INCH DIAM.
TURNING
MIRROR
PLATFORM ON THE AMOS
1.6-METER TELESCOPE
KFS.DWG

Figure 2

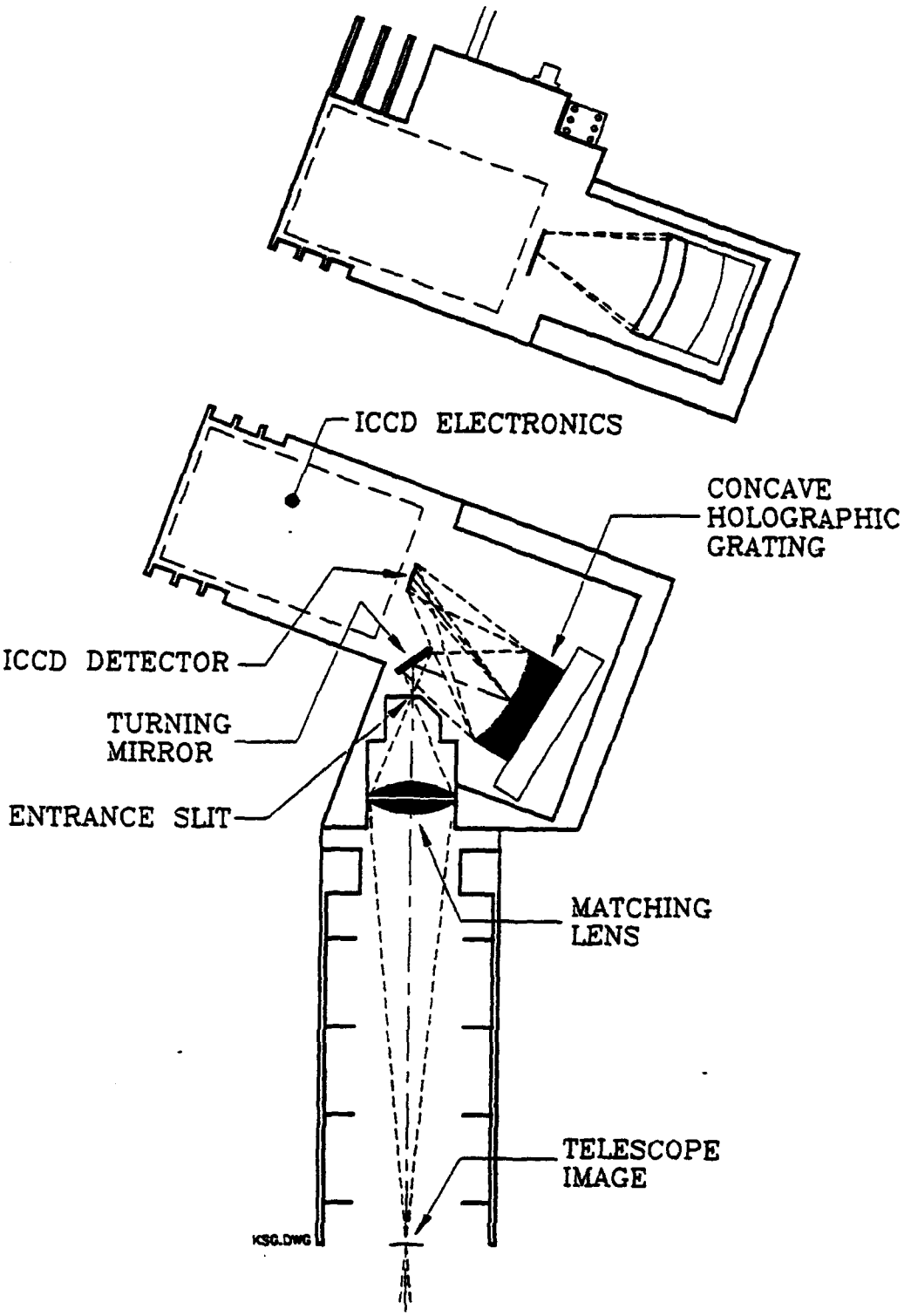
ICCD ELECTRONICS
CONCAVE
HOLOGRAPHIC
GRATING
ICCD DETECTOR
TURNING
MIRROR
ENTRANCE SLIT
MATCHING
LENS
TELESCOPE
IMAGE
KSG.DWG

Figure 3

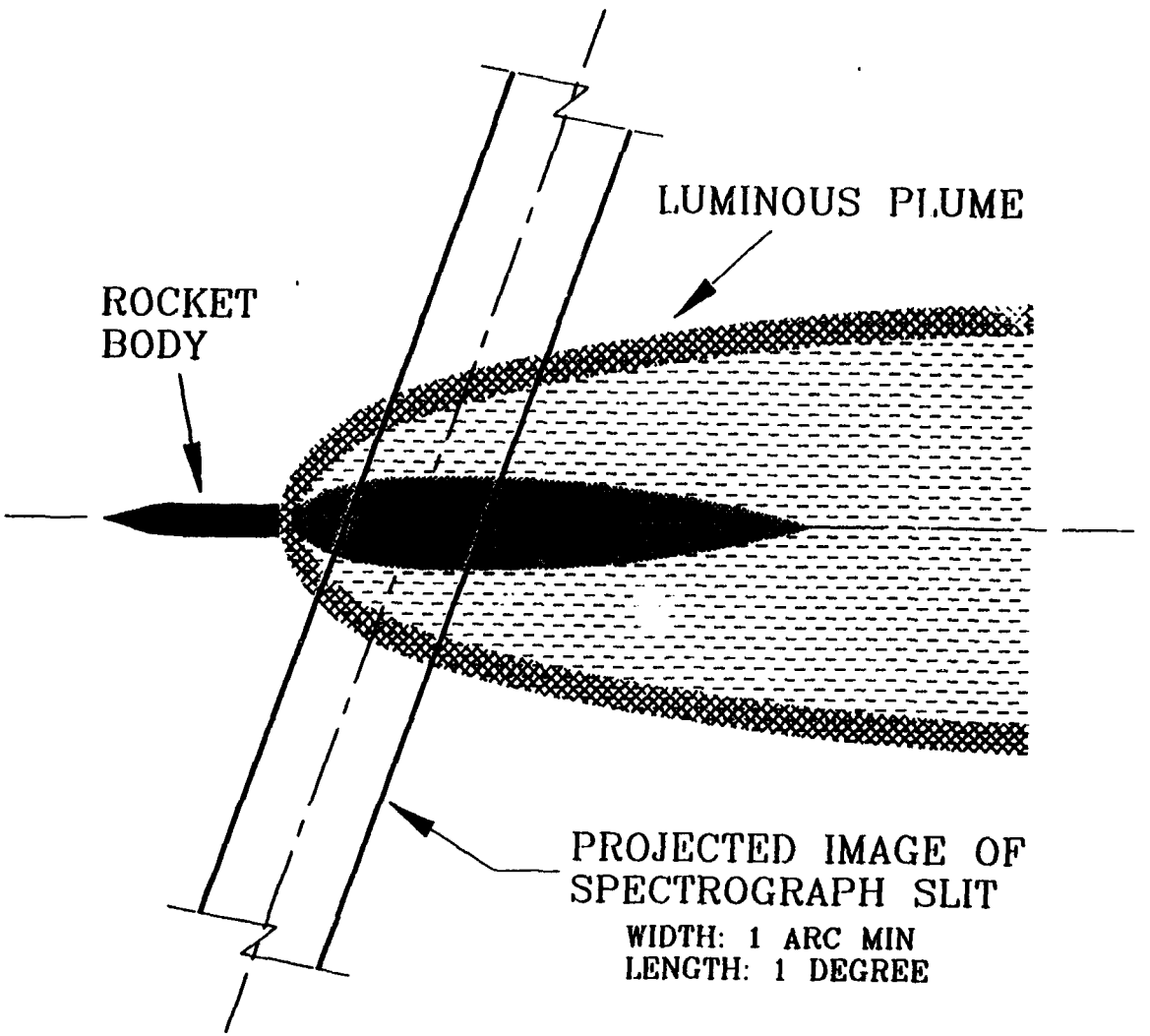
LUMINOUS PLUME
ROCKET
BODY
PROJECTED IMAGE OF
SPECTROGRAPH SLIT
WIDTH: 1 ARC MIN
LENGTH: 1 DEGREE

Figure 4

BANDED IMAGERS (SCHEMATIC DRAWING)

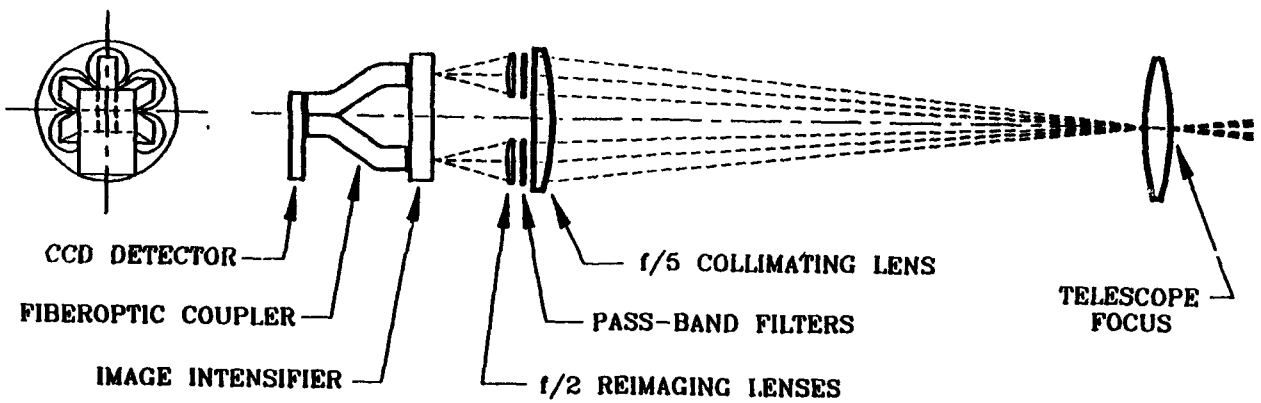

Figure 5

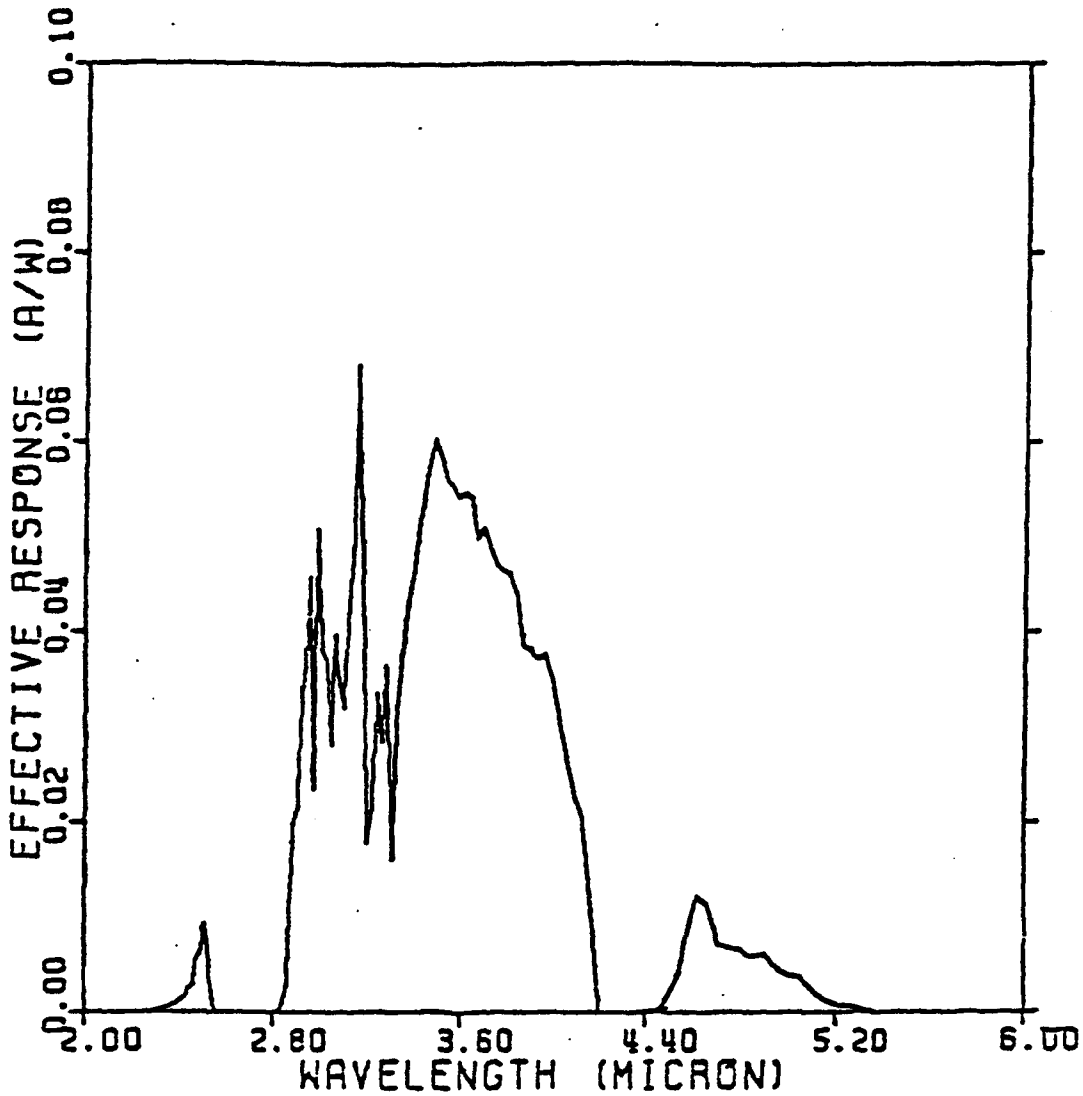

Effective wavelength response $S(\lambda)\ T_a(\lambda)$
of the sensor plus atmosphere

Figure 6

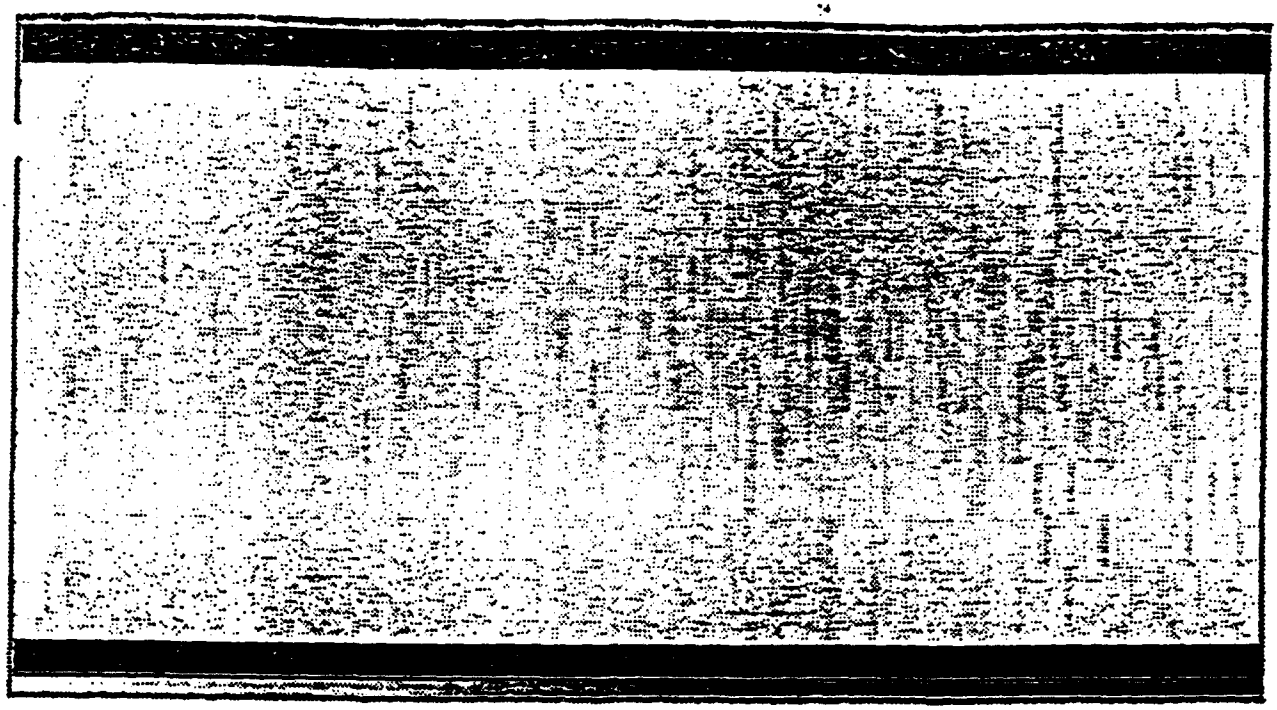

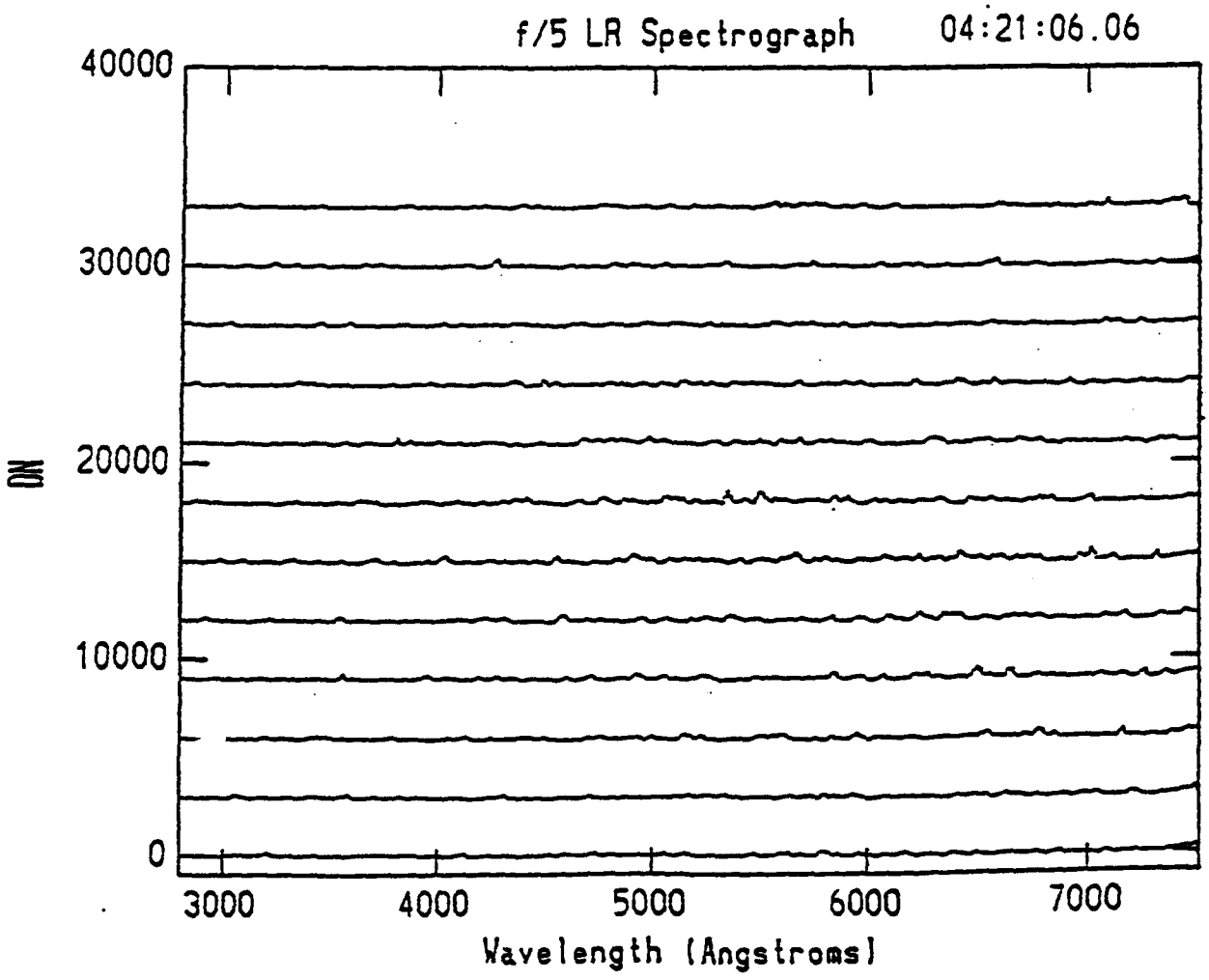
f/5 LR Spectrograph
04:21:06.06
40000
30000
20000
10000
0
DN
3000
4000
5000
6000
7000
Wavelength (Angstroms)

Figure 7

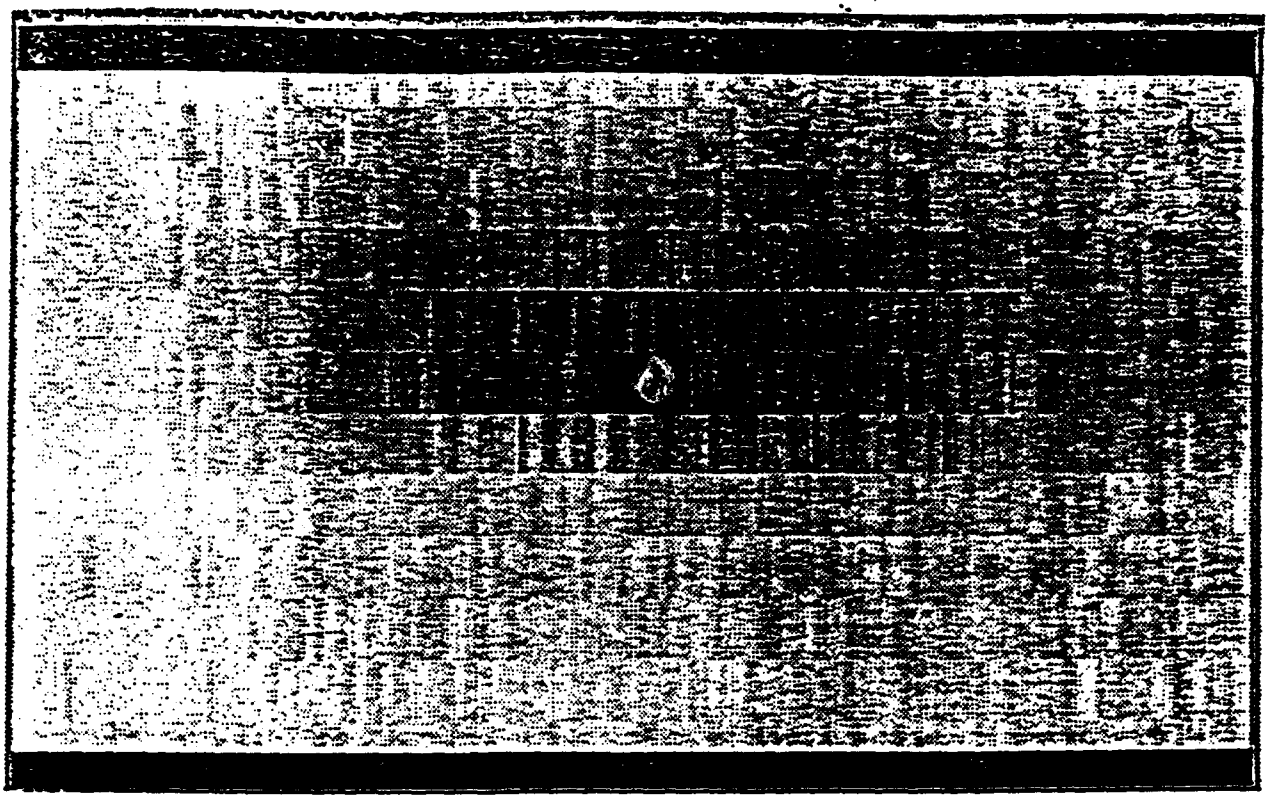

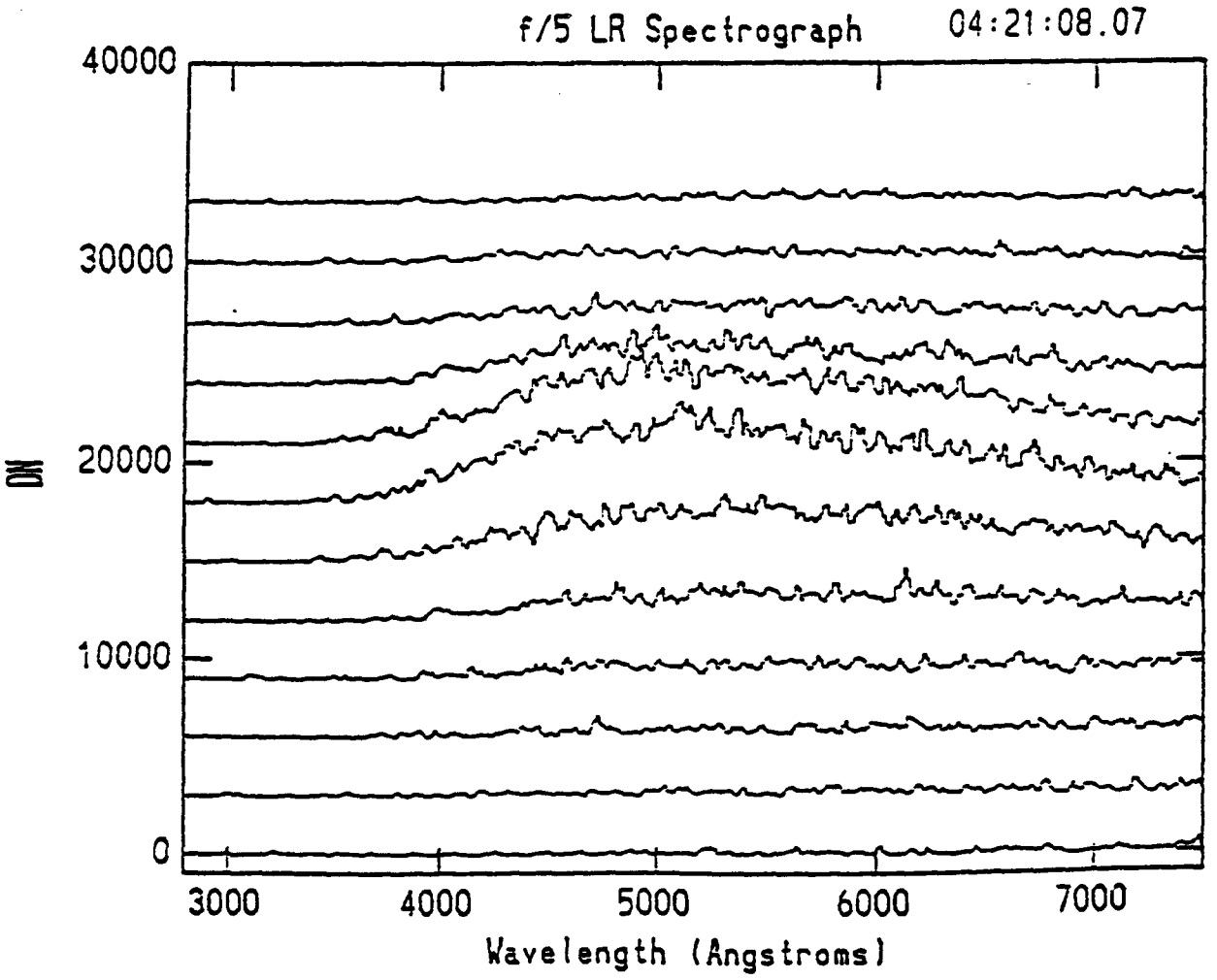
f/5 LR Spectrograph
04:21:08.07
40000
30000
20000
10000
0
DN
3000
4000
5000
6000
7000
Wavelength (Angstroms)

Figure 8

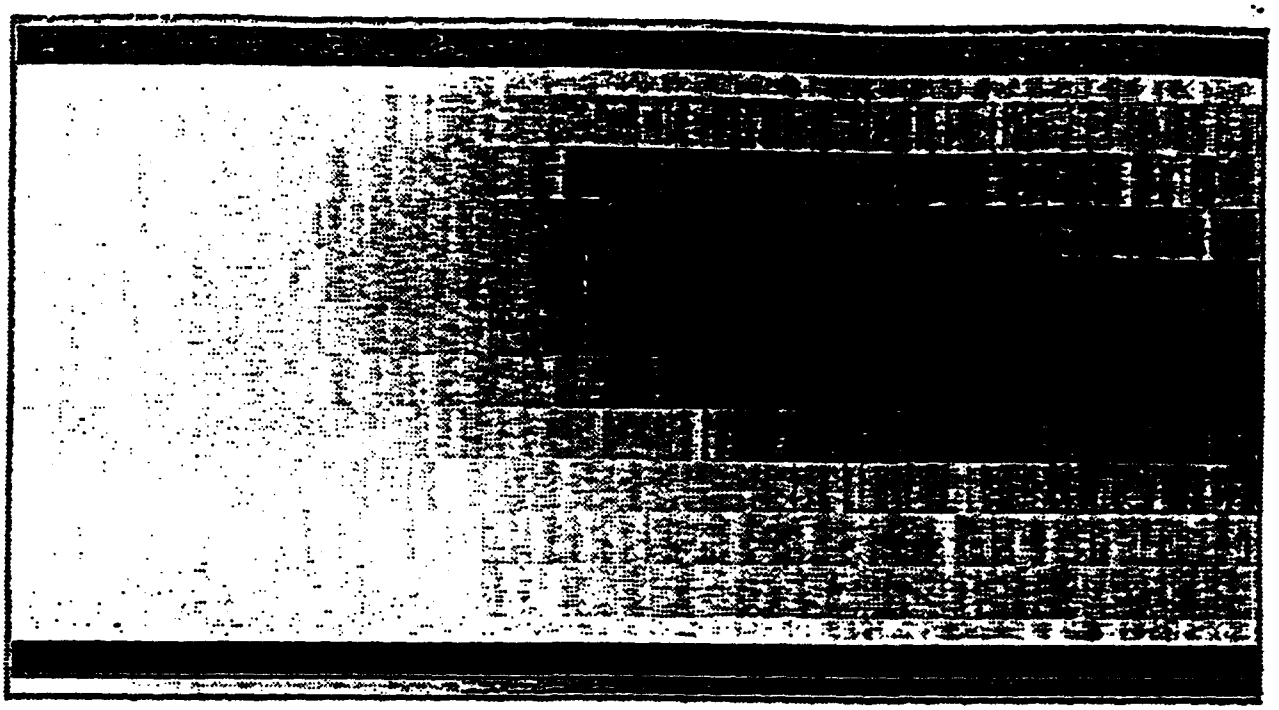

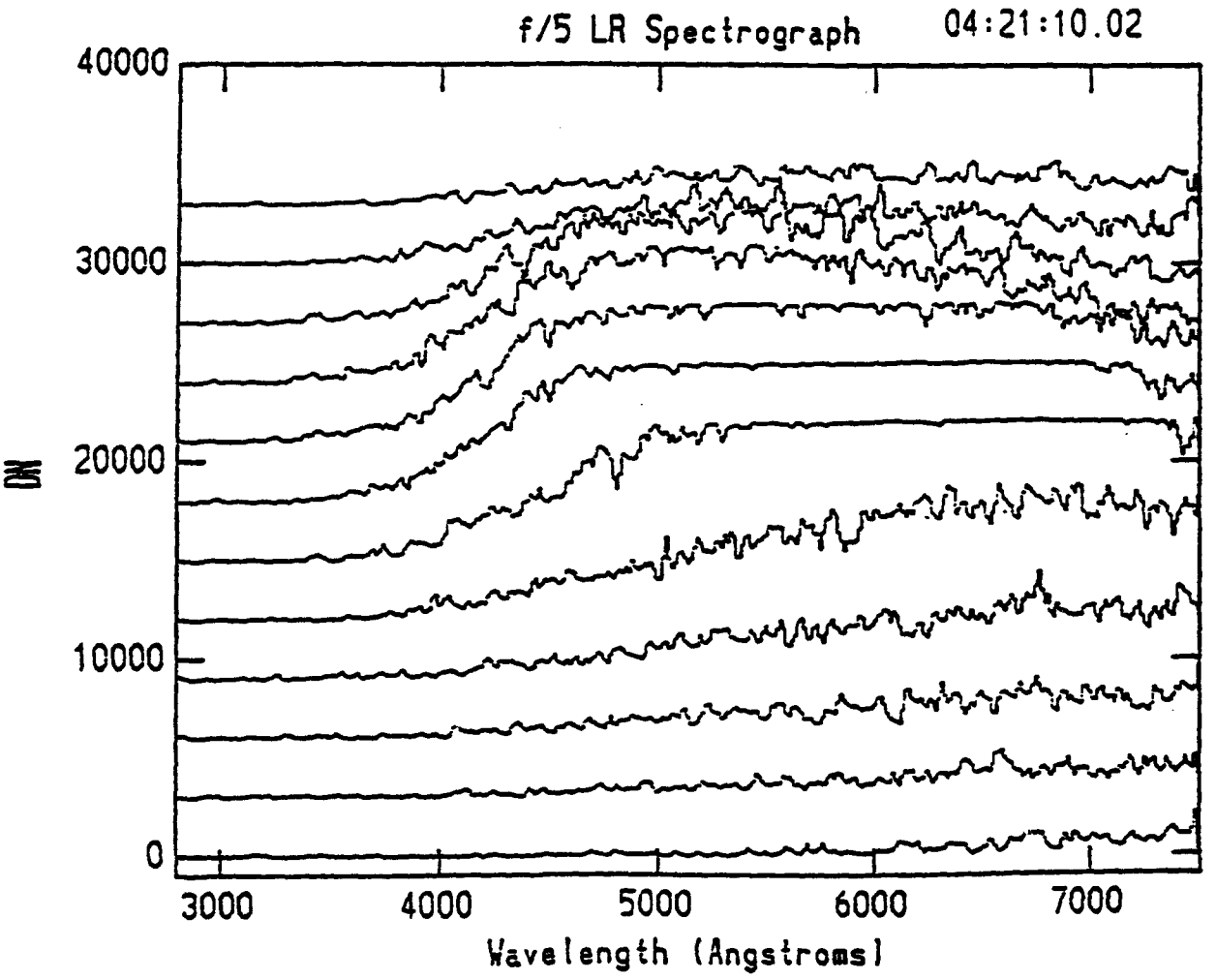
f/5 LR Spectrograph
04:21:10.02
40000
30000
20000
10000
0
DN
3000
4000
5000
6000
7000
Wavelength (Angstroms)

Figure 9

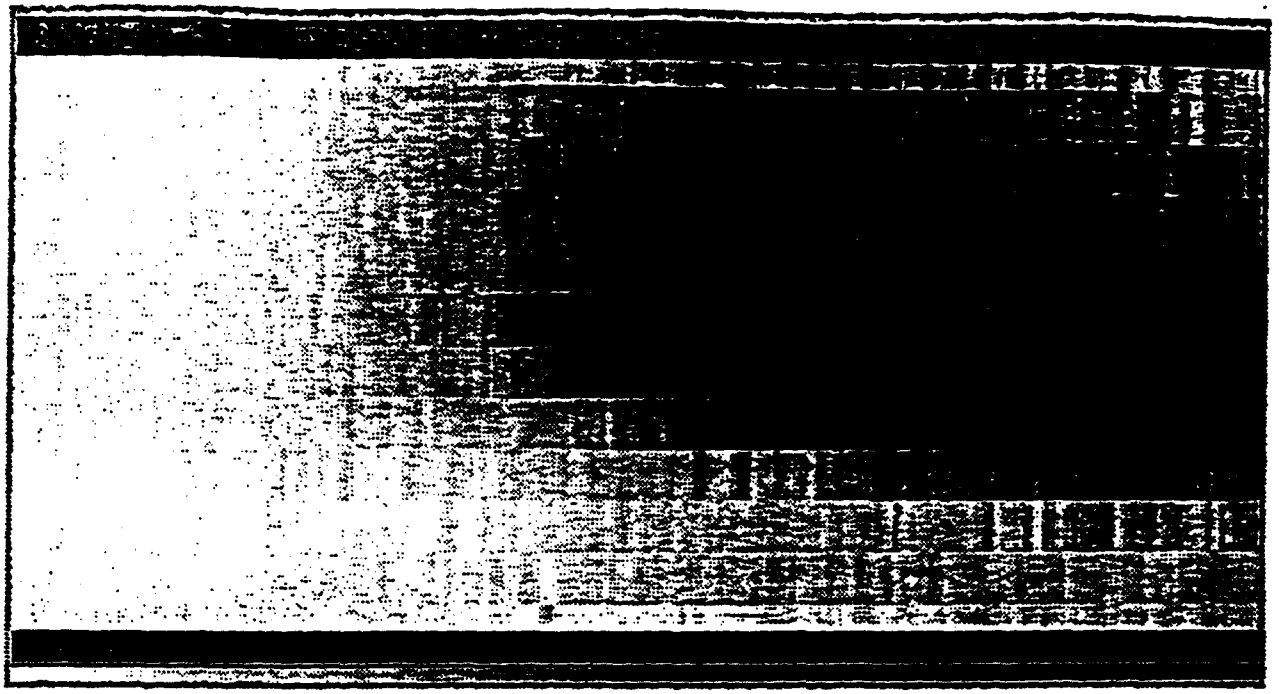

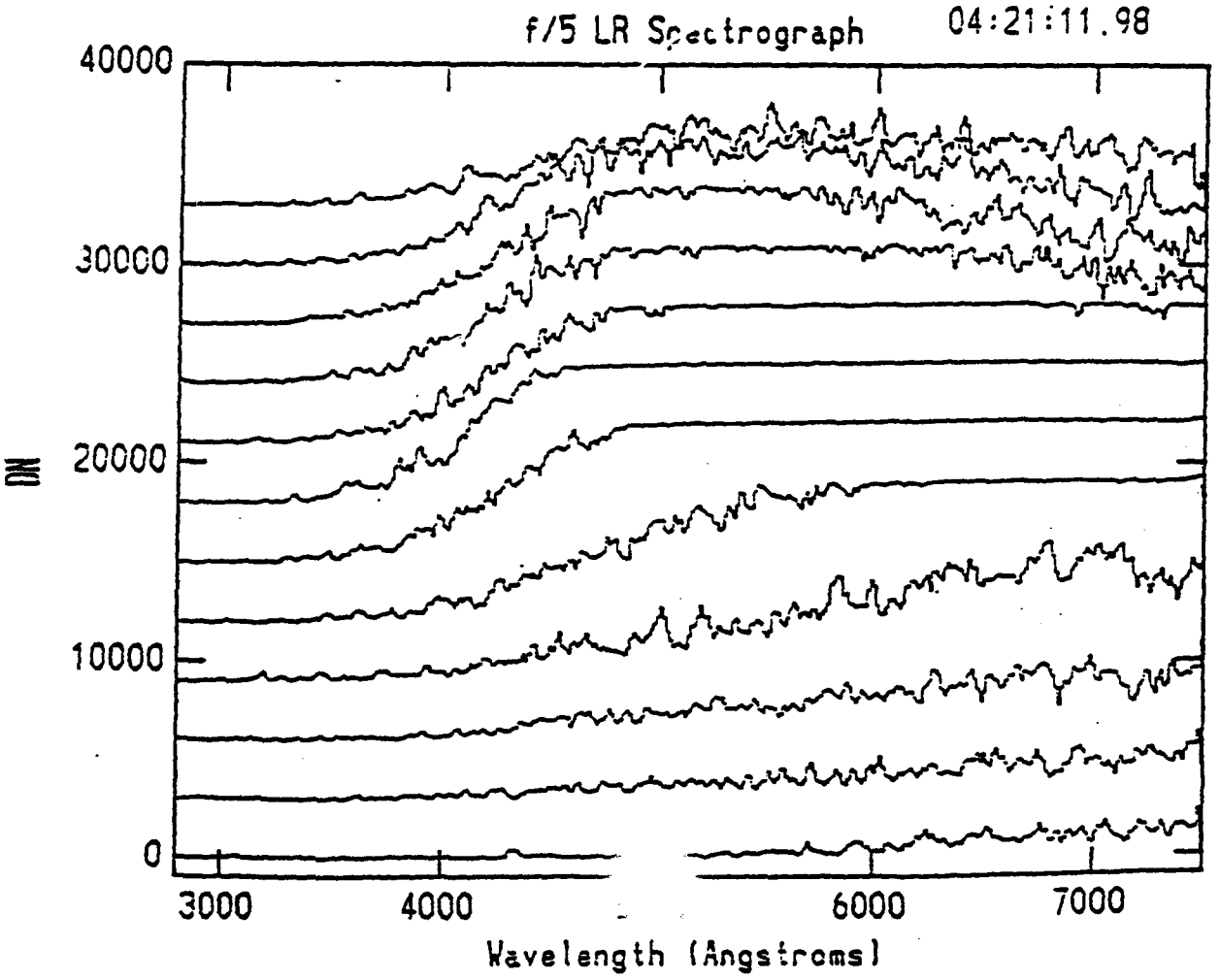
f/5 LR Spectrograph
04:21:11.98
40000
30000
20000
10000
0
DN
3000
4000
6000
7000
Wavelength (Angstroms)

Figure 10

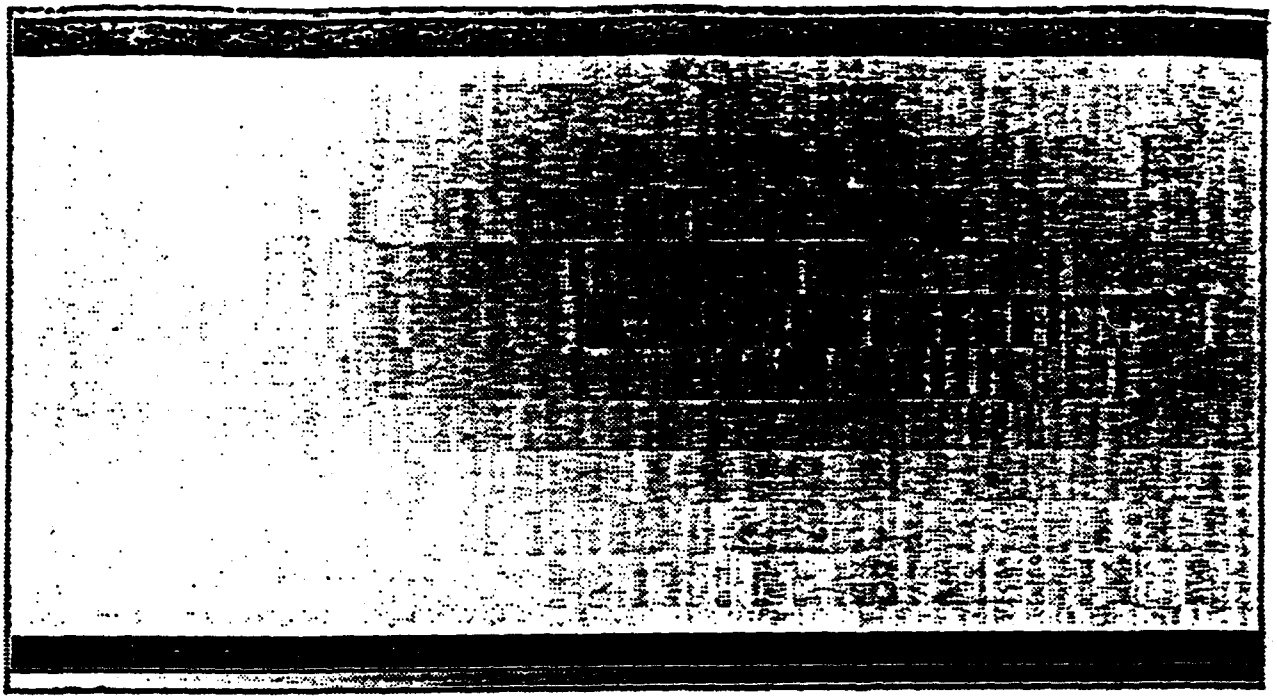

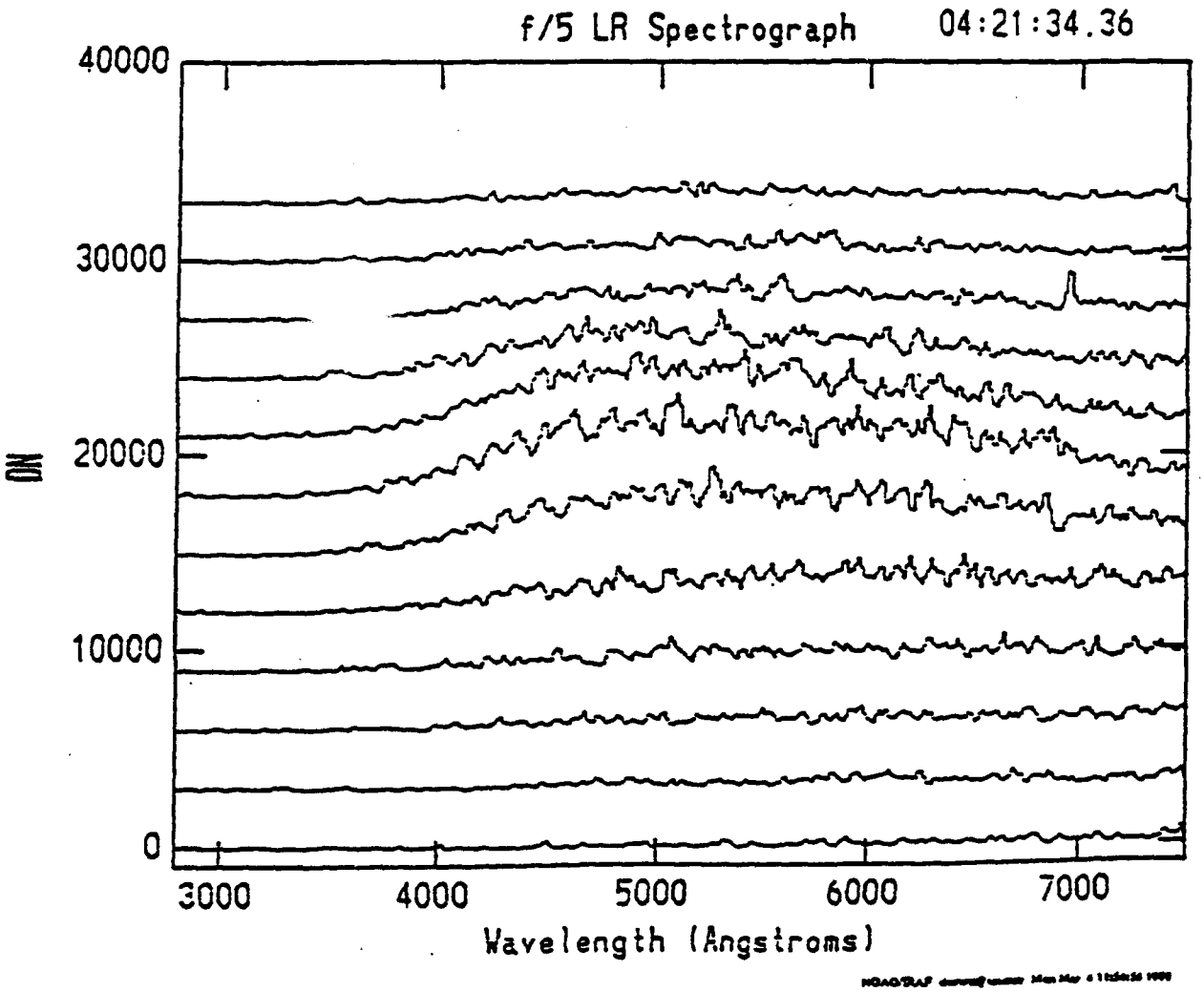
f/5 LR Spectrograph
04:21:34.36
40000
30000
20000
10000
0
DN
3000
4000
5000
6000
7000
Wavelength (Angstroms)

Figure 11

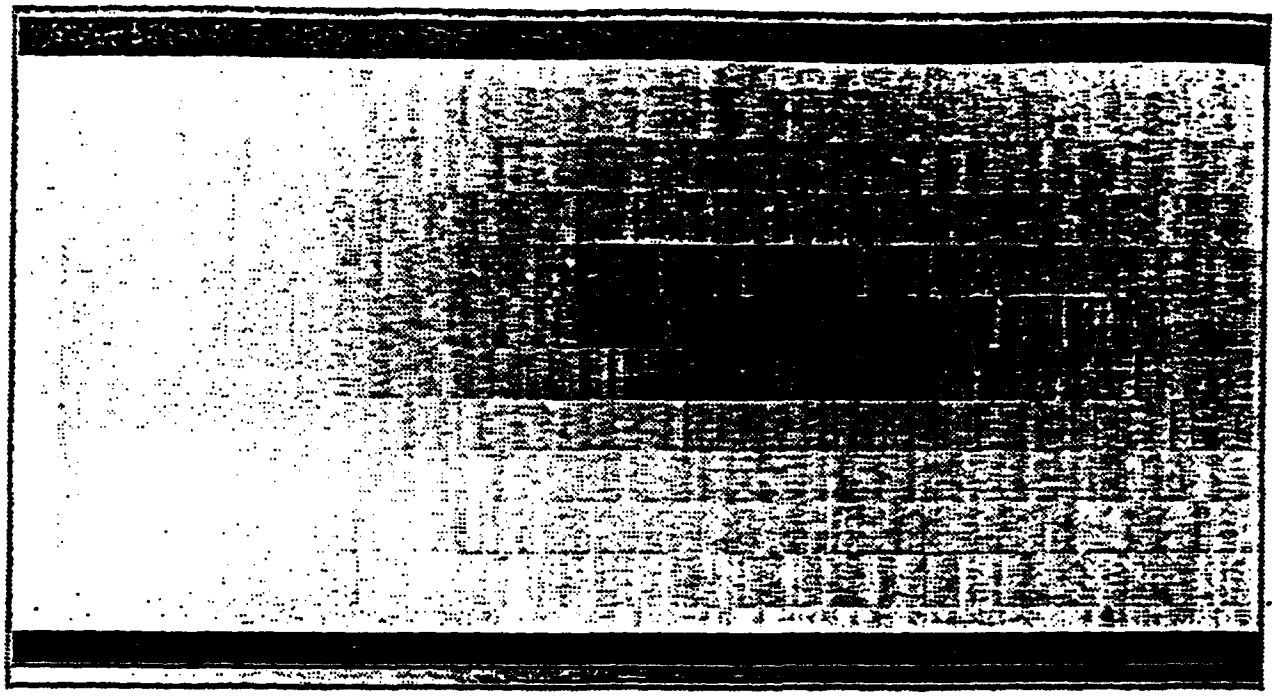

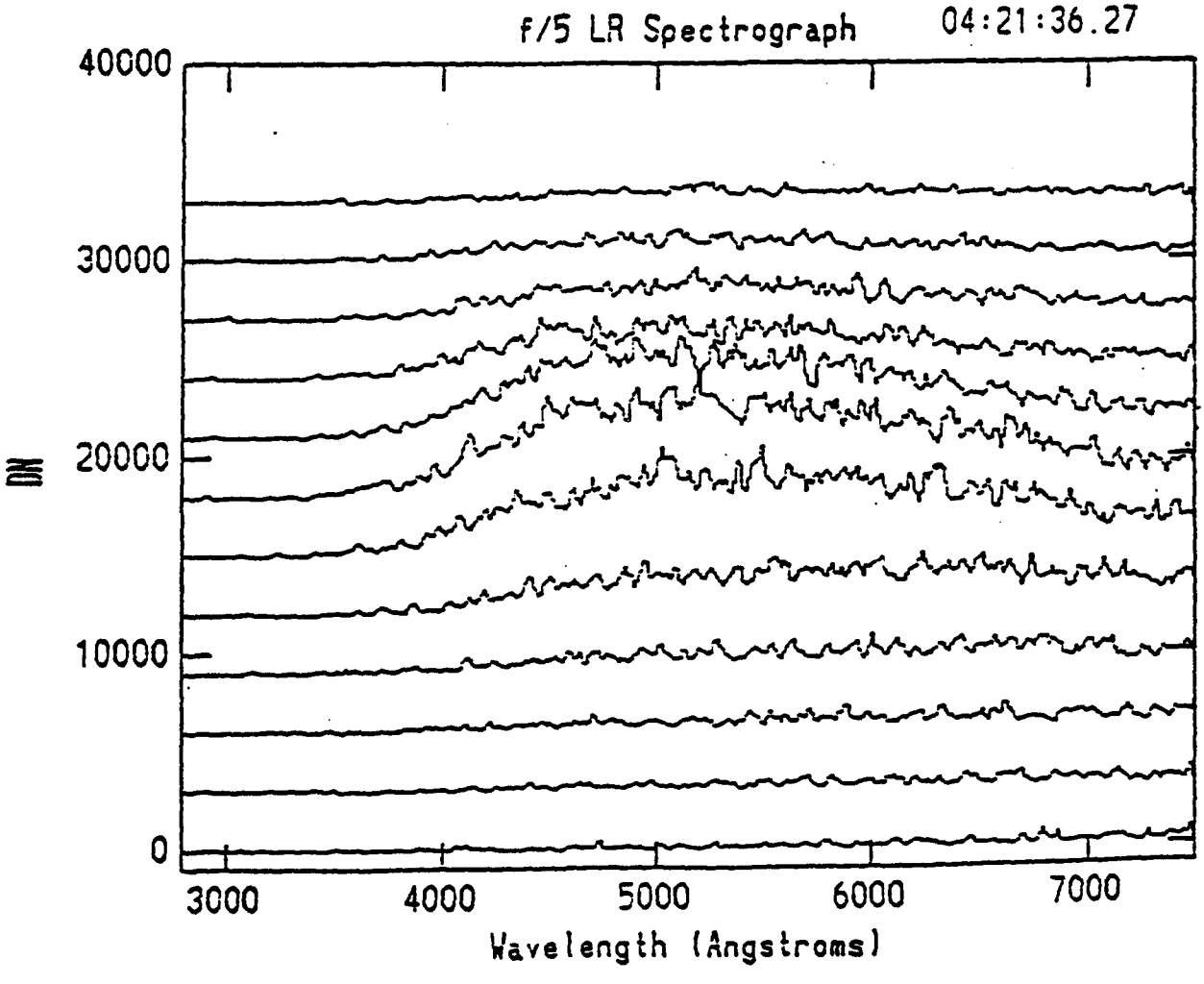
f/5 LR Spectrograph
04:21:36.27
40000
30000
20000
10000
0
DN
3000
4000
5000
6000
7000
Wavelength (Angstroms)

Figure 12

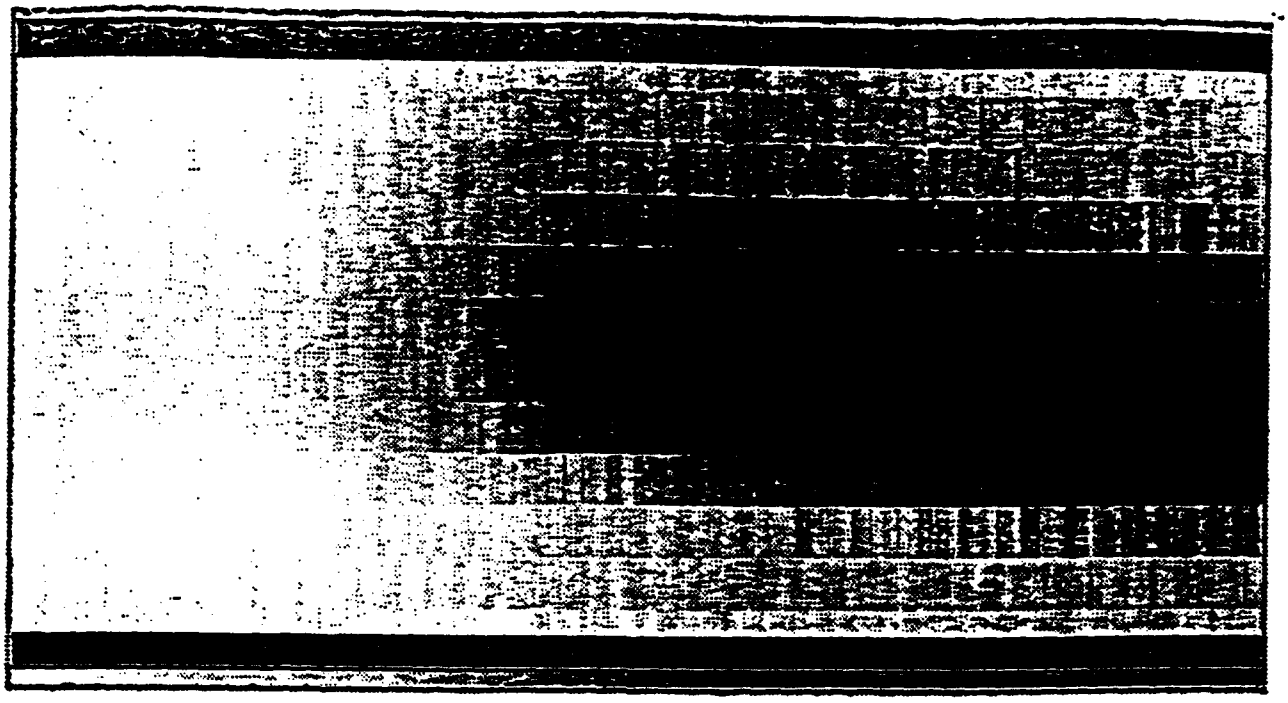

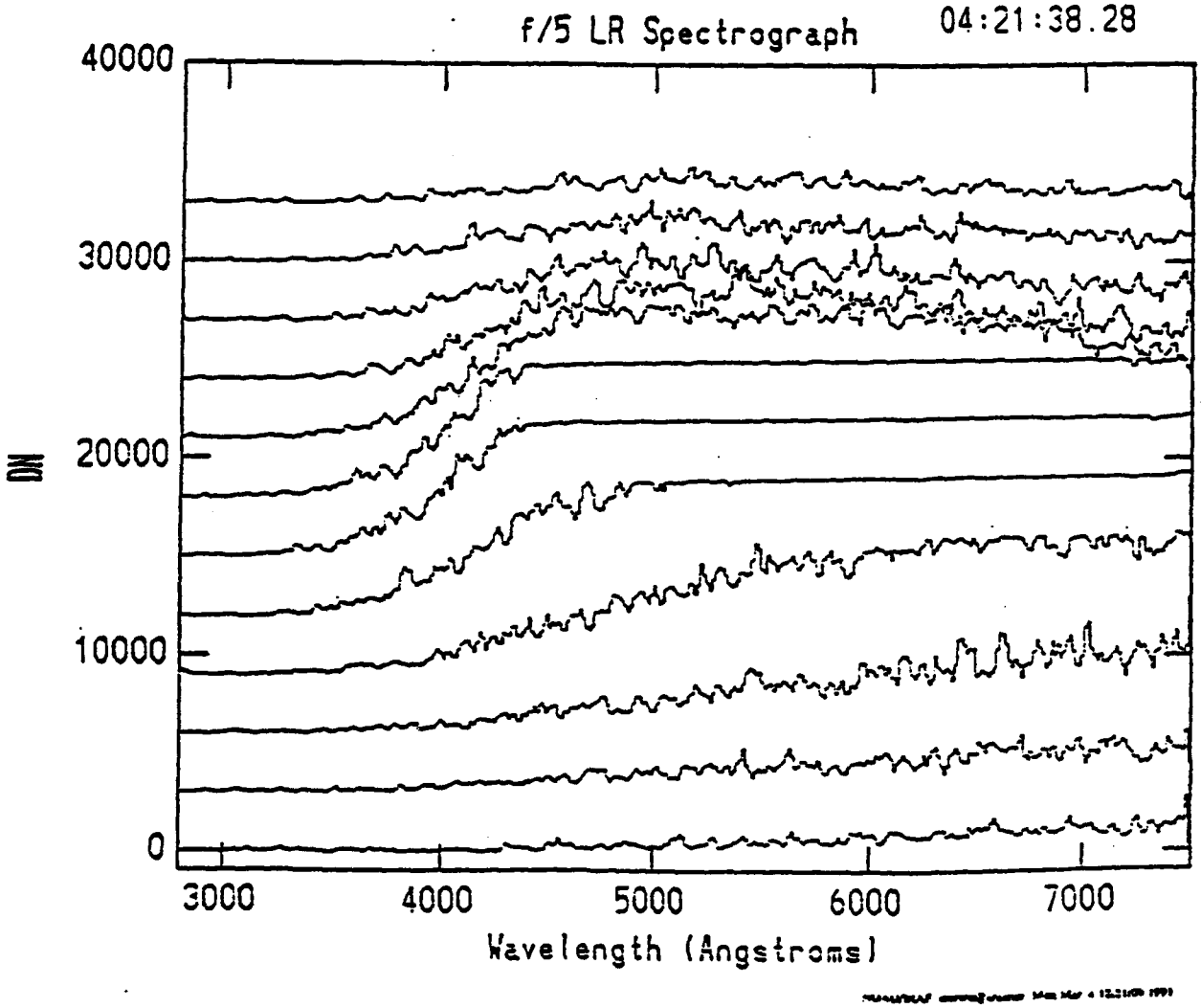
f/5 LR Spectrograph
04:21:38.28
40000
30000
20000
10000
0
DN
3000
4000
5000
6000
7000
Wavelength (Angstroms)

Figure 13

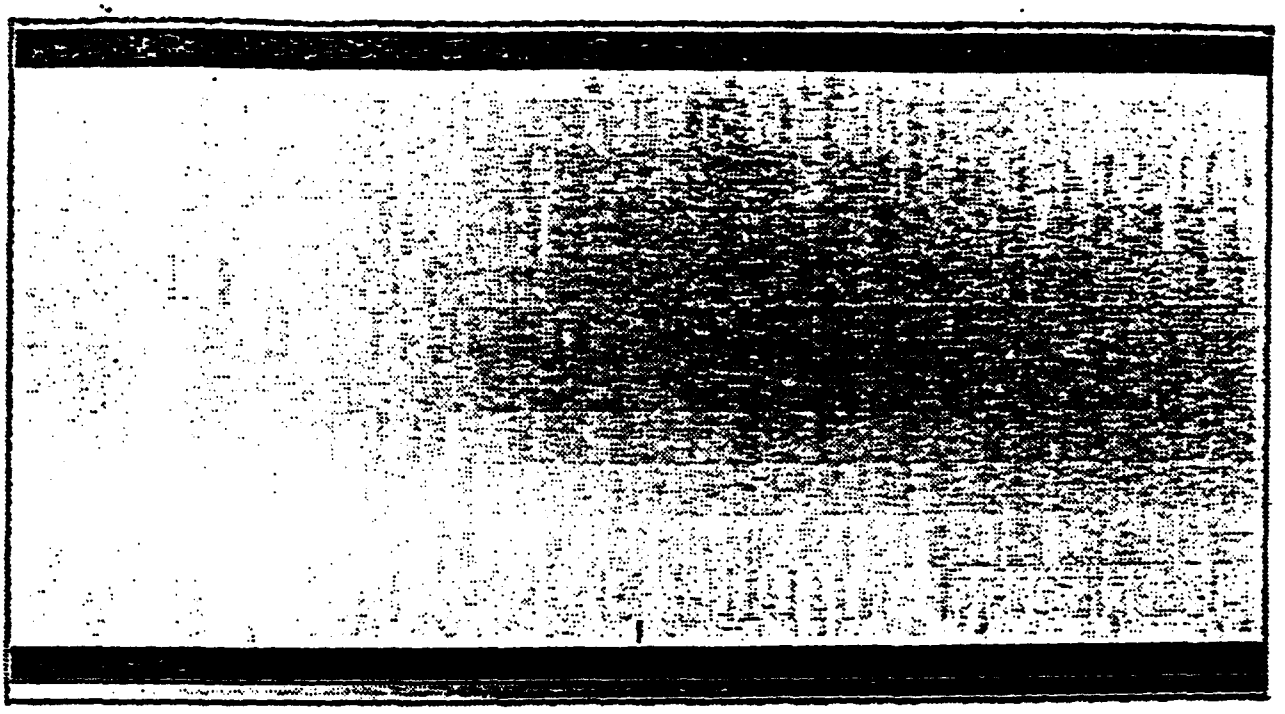

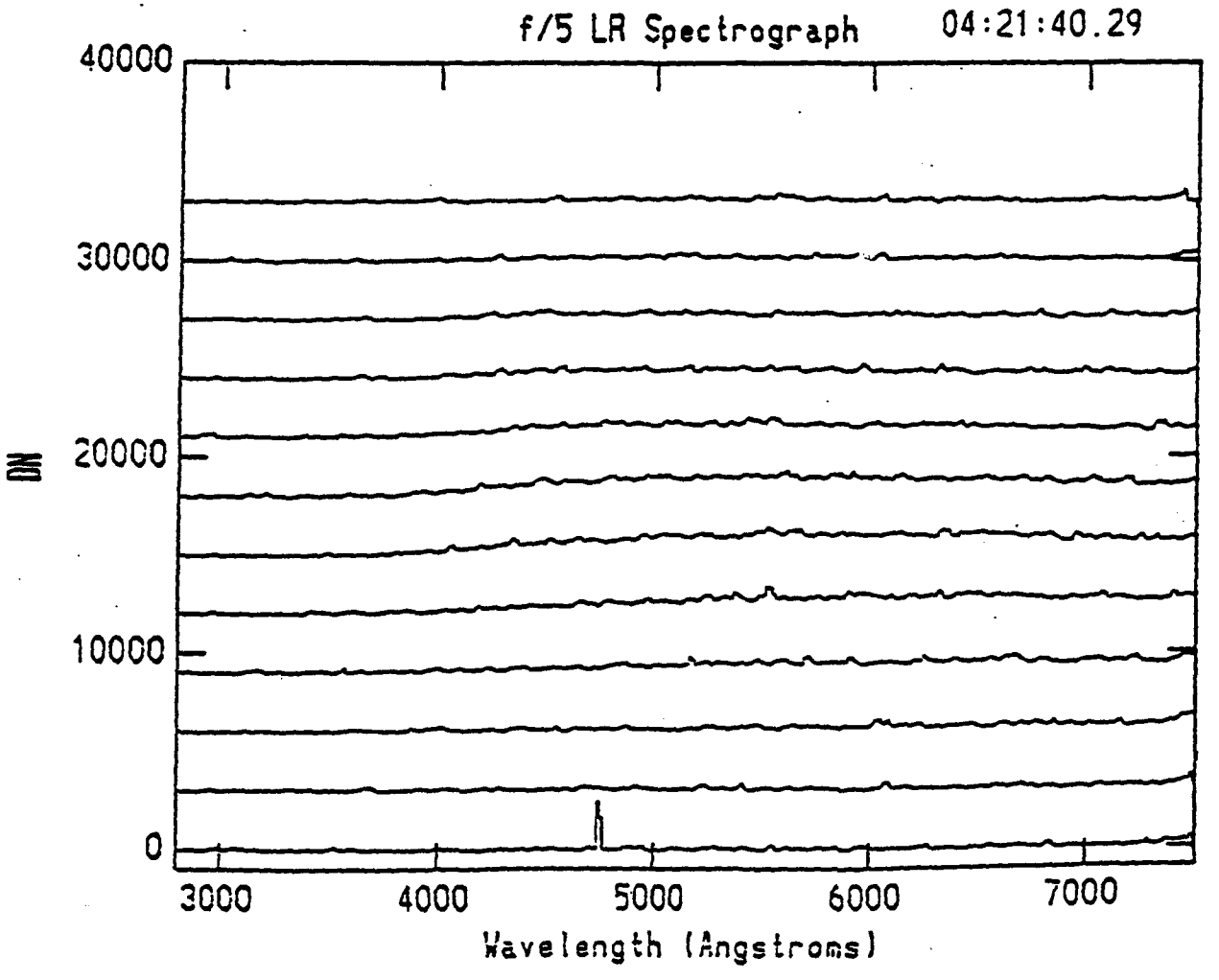
f/5 LR Spectrograph
04:21:40.29
40000
30000
20000
10000
0
DN
3000
4000
5000
6000
7000
Wavelength (Angstroms)

Figure 14

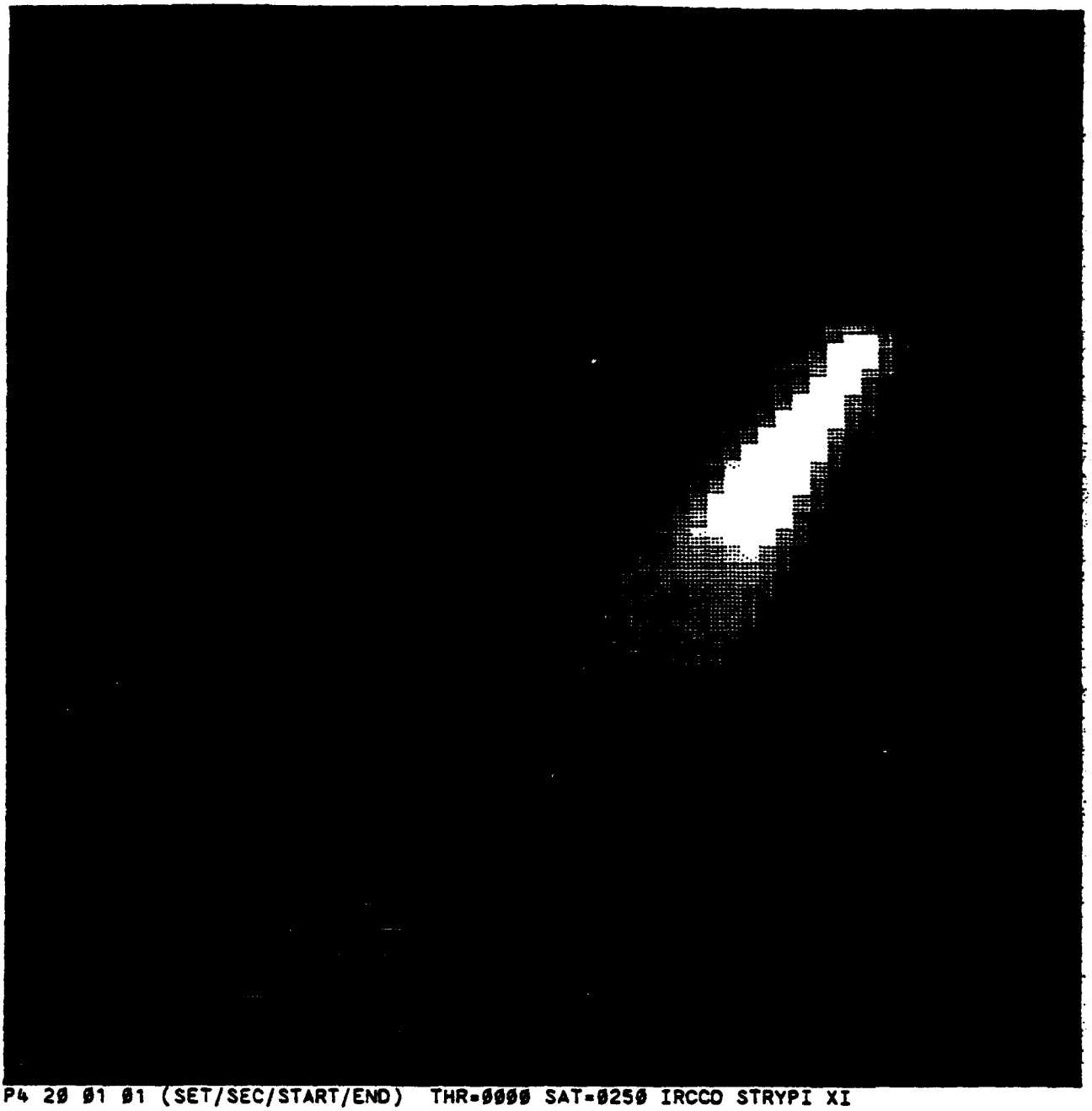

Figure 15

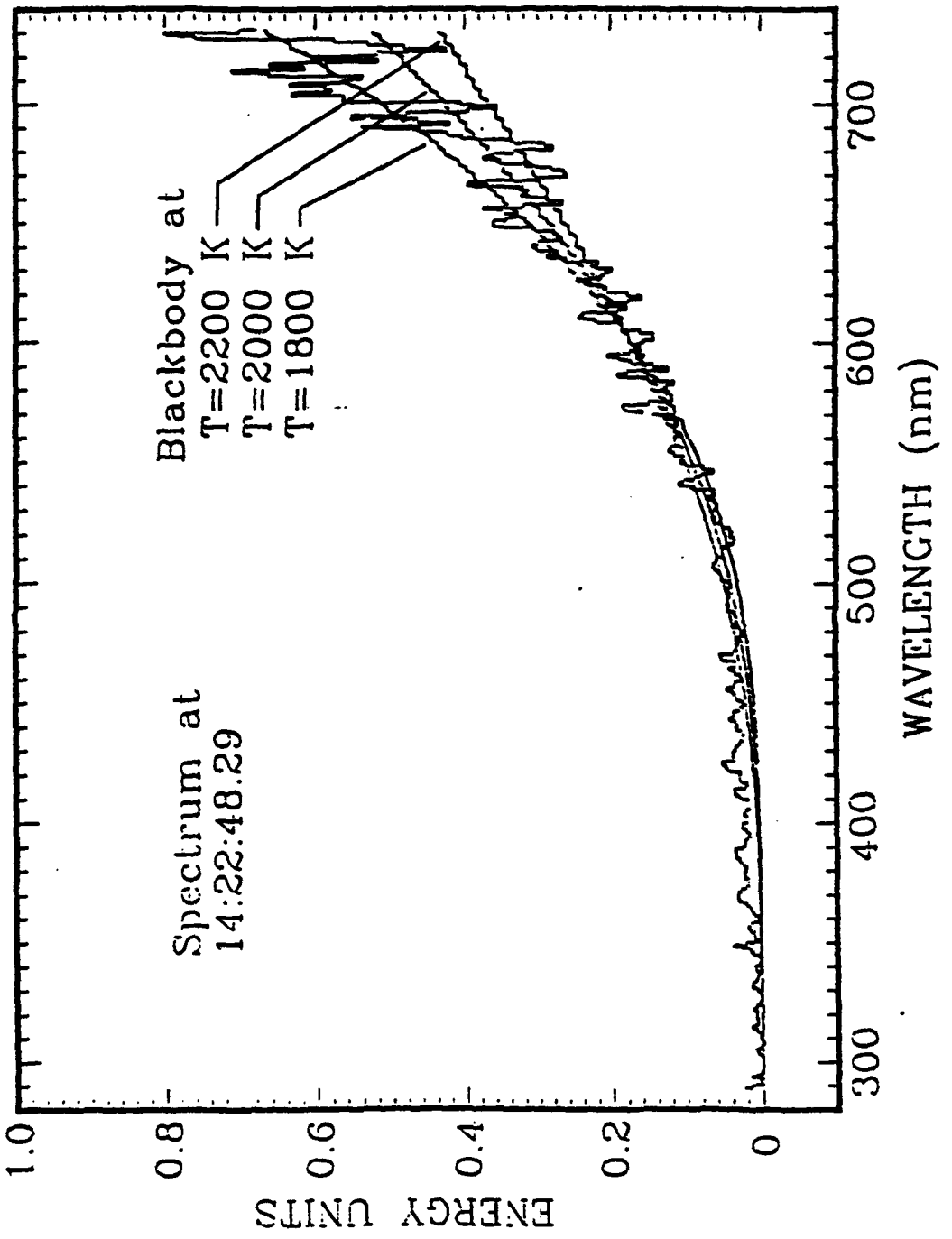
Spectrum at
14:22:48.29
Blackbody at
T=2200 K
T=2000 K
T=1800 K
ENERGY UNITS
1.0
0.8
0.6
0.4
0.2
0
300
400
500
600
700
WAVELENGTH (nm)

Figure 16